IOP Publishing Journal of Physics: Condensed Matter
J. Phys.: Condens. Matter **32** (2020) 143001 (33pp) https://doi.org/10.1088/1361-648X/ab5488

## Topical Review

# Skyrmion-electronics: writing, deleting, reading and processing magnetic skyrmions toward spintronic applications

**Xichao Zhang[1], Yan Zhou[1], Kyung Mee Song[2], Tae-Eon Park[2], Jing Xia[1], Motohiko Ezawa[3], Xiaoxi Liu[4], Weisheng Zhao[5], Guoping Zhao[6] and Seonghoon Woo[7]**

[1] School of Science and Engineering, The Chinese University of Hong Kong, Shenzhen, Guangdong 518172, People's Republic of China
[2] Center for Spintronics, Korea Institute of Science and Technology (KIST), Seoul 02792, Republic of Korea
[3] Department of Applied Physics, University of Tokyo, Hongo 7-3-1, Tokyo 113-8656, Japan
[4] Department of Electrical and Computer Engineering, Shinshu University, Wakasato 4-17-1, Nagano 380-8553, Japan
[5] Fert Beijing Institute, BDBC, and School of Microelectronics, Beihang University, Beijing 100191, People's Republic of China
[6] College of Physics and Electronic Engineering, Sichuan Normal University, Chengdu 610101, People's Republic of China
[7] IBM Thomas J. Watson Research Center, Yorktown Heights, New York 10598, United States of America

E-mail: shwoo@ibm.com

Received 6 December 2018, revised 27 September 2019
Accepted for publication 5 November 2019
Published 6 January 2020

**Abstract**

The field of magnetic skyrmions has been actively investigated across a wide range of topics during the last decades. In this topical review, we mainly review and discuss key results and findings in skyrmion research since the first experimental observation of magnetic skyrmions in 2009. We particularly focus on the theoretical, computational and experimental findings and advances that are directly relevant to the spintronic applications based on magnetic skyrmions, i.e. their writing, deleting, reading and processing driven by magnetic field, electric current and thermal energy. We then review several potential applications including information storage, logic computing gates and non-conventional devices such as neuromorphic computing devices. Finally, we discuss possible future research directions on magnetic skyrmions, which also cover rich topics on other topological textures such as antiskyrmions and bimerons in antiferromagnets and frustrated magnets.

Keywords: spintronics, magnetism, magnetic skyrmion, magnetic antiskyrmion, logic gates, bio-inspired computing, racetrack memory

(Some figures may appear in colour only in the online journal)

 

## Contents



## 1. Background

### *1.1. Topological spin textures*

Topology is an important discipline of pure and applied mathematics, which also plays a significant role in the understanding of many real-world physical phenomena. In the field of magnetism and spintronics, the concept of topology is particularly important to the physics of some exotic magnetic spin textures (i.e. the so-called magnetic solitons) [1–7], including different types of magnetic skyrmions and vortex-like spin textures, where the behaviors of textures are determined or affected by their topological characteristics. These topologically non-trivial spin textures can be one-dimensional (1D), two-dimensional (2D) and three-dimensional (3D) in real space, and usually carry integer or half-integer topological charges determined by their spin textures in the topological space [1–22]. For most cases, the well-studied topological spin textures are those localized in 2D or quasi-2D magnetic thin films and multilayers [11, 19, 21, 23–36], because that magnetic thin films and multilayers are better understood and preferred for building nanoscale spintronic applications. Several recent works have also demonstrated promising properties of 3D topological spin textures [10, 37–50], leading to the prediction that 3D spin textures might be used in combination with 2D textures in the future. Indeed, the 1D magnetic solitons have also been investigated in the field [9, 12–17, 51, 52], which revealed many fundamental properties of topologically non-trivial objects. For example, the chiral helicoidal soliton lattice was experimentally observed in a chiral helimagnet in 2012 [52], which was theoretically envisioned by I E Dzyaloshinskii in 1964 [15]. In this review, however, we will focus on and limit our discussion to 2D topological spin textures in magnetic materials. Figure 1 shows various exemplary topological spin textures that can be found in such 2D or quasi-2D magnetic materials. Note that quasi-2D system means the variation of spin texture along the thickness direction can be ignored, such as in the thin film with a finite thickness.

The concept of skyrmion model was first proposed in the field of nuclear physics by Skyrme [53] in 1962. In 1989, Bogdanov and Yablonskiĭ for the first time predicted that chiral magnetic skyrmions can also be found in magnetic materials [16]. Then in 1994, Bogdanov and Hubert theoretically studied skyrmion structures in easy-axis magnetic materials with the Dzyaloshinskii–Moriya (DM) interaction [23, 54], where the DM interaction was found to be an important energy term to stabilize skyrmions, which will be discussed below. In 2001, Bogdanov and Rößler developed a phenomenological theory of chiral symmetry breaking in magnetic thin films and multilayers, and also predicted the existence of skyrmions in magnetic thin films and multilayers stabilized by induced DM interactions [18]. In 2006, Rößler and coworkers further theoretically demonstrated that skyrmion structures can be formed as spontaneous ground states in magnetic metals with DM interactions without the assistance of external fields or the proliferation of defects [20].

Due to the topological nature, spin textures including chiral magnetic skyrmions can be regarded as localized quasi-particles in magnetic materials and show topology-dependent static and dynamic properties [1–7, 55]. In the context of 2D and quasi-2D systems, the topological structure of a spin texture is generally characterized by the topological charge [55–57], which is also referred to as the Pontryagin number [2, 3]:

$$Q = \int d^2\boldsymbol{r}\rho(\boldsymbol{r}), \tag{1}$$

where the topological charge density $\rho(\boldsymbol{r})$ reads

$$\rho\left(\boldsymbol{r}\right) = \frac{1}{4\pi}\boldsymbol{m}(\boldsymbol{r}) \cdot \left(\partial_x \boldsymbol{m}\left(\boldsymbol{r}\right) \times \partial_y \boldsymbol{m}\left(\boldsymbol{r}\right)\right). \tag{2}$$

Thus, the topological charge can be calculated based on the exact spin texture configuration according to

$$Q = \frac{1}{4\pi}\int d^2\boldsymbol{r} \cdot \boldsymbol{m}(\boldsymbol{r}) \cdot \left(\partial_x \boldsymbol{m}\left(\boldsymbol{r}\right) \times \partial_y \boldsymbol{m}\left(\boldsymbol{r}\right)\right). \tag{3}$$

The topological charge basically counts how many times the reduced local magnetization (i.e. the spin) $\boldsymbol{m}\left(\boldsymbol{r}\right)$ wraps the

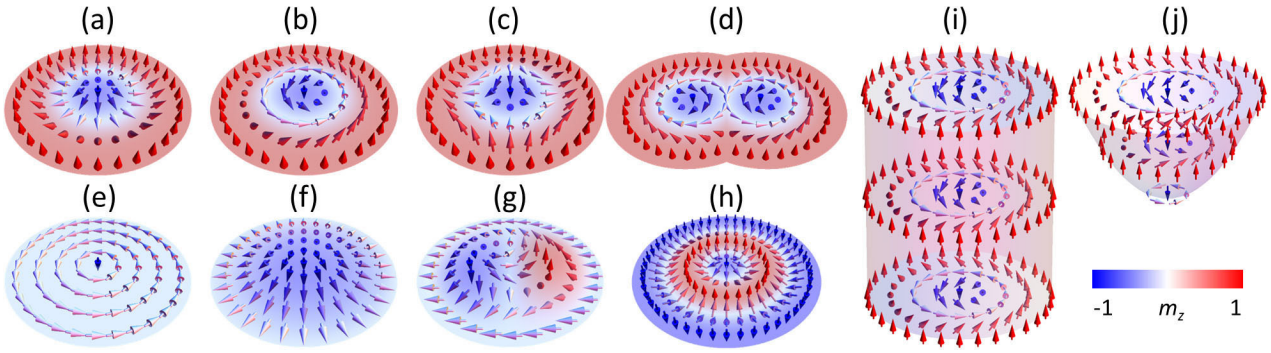


**Figure 1.** Illustrations of a series of 2D and 3D topological spin textures in magnetic materials. (a) Néel-type skyrmion ($Q = -1$), (b) Bloch-type skyrmion ($Q = -1$), (c) antiskyrmion ($Q = +1$), (d) biskyrmion ($Q = -2$), (e) vortex ($Q = -0.5$), (f) meron ($Q = -0.5$), (g) bimeron ($Q = -1$), (h) skyrmionium ($Q = 0$), (i) skyrmion tube, and (j) magnetic bobber. The arrow denotes the spin direction and the out-of-plane spin component ($m_z$) is represented by the color: red is out of the plane, white is in-plane, and blue is into the plane.

2D surface of a 3D ball in 3D space (i.e. the 2-sphere) as the coordinate $(x, y)$ spans the whole planar space. For example, as shown in figure 1, the Néel-type and Bloch-type skyrmions have topological charges of $Q = -1$ (for the core magnetization of $-m_z$), while the antiskyrmion of the same core magnetization has the opposite topological charge of $Q = +1$ (often referred as the antiparticle of skyrmions with $Q = -1$). It is also called '*the skyrmion number*' [2, 55] for a series of skyrmion-like spin textures that will be discussed throughout this review.

In fact, chiral magnetic skyrmions are not limited to the case of topological charges $|Q| = 1$, and could be of any topological charge [24, 58–60]. For example, the skyrmionium can be regarded as a topological combination of a skyrmion with $Q = +1$ and a skyrmion with $Q = -1$, which carries a net topological charge of $Q = 0$. The skyrmionium structure was first studied in a theoretical work by Bogdanov and Hubert in 1999 [24]. It is also referred to as the target skyrmion [61]. The topological charge difference between the skyrmionium with $Q = 0$ and skyrmion with $Q = +1$ originates from their out-of-plane spin textures. A serious of theoretical works have suggested that skyrmioniums in magnetic materials can be manipulated by different external stimuli [11, 58, 62–73]. As other examples, the biskyrmion has a topological charge of $Q = -2$, which can be formed in some materials such as chiral bulk or frustrated magnets when two skyrmions with the same topological number ($Q = -1$ in this case) are approaching to each other. The meron and bimeron have topological charges of $Q = -0.5$ and $Q = -1$, respectively, where the bimeron consists of a meron with $Q = -0.5$ and an antimeron with $Q = -0.5$. The bimeron with $Q = -1$ can be regarded as a counterpart of skyrmions with $Q = -1$ in magnetic materials with easy-plane magnetic anisotropy, where magnetization prefer to lie in the plane [74]. We will discuss these skyrmion-like structures in detail in section 5.2.

Obviously, these multifarious topological spin textures cannot be fully distinguished only using the topological charge $Q$, because there might be some degenerate states for a given value of the topological charge. Taking the skyrmion with $Q = -1$ as an example, there are additional degrees of freedom in the in-plane spin configuration. Therefore, one could calculate the vorticity number $Q_v$ and the helicity number $Q_h$, which completely characterize the topological spin texture accompanying the topological charge $Q$.

First, a point of the $x$-$y$ space is parameterized as

$$x = r\cos\varphi, y = r\sin\varphi. \tag{4}$$

By applying the mapping $r = 0$ as $z \to -1$, $r = 1$ as $z = 0$, $r \to \infty$ as $z \to 1$, and $\lim_{r\to\infty} \boldsymbol{m}(x, y) = \lim_{z\to 1} \boldsymbol{m}(z, \phi)$ [56], we map the $x$-$y$ space onto the 2D surface of a 3D ball parameterized by

$$x = \sqrt{1-\cos^2\theta}\cos\phi, y = \sqrt{1-\cos^2\theta}\sin\phi, z = z = \cos\theta, \tag{5}$$

with $z$ being defined as $r = (1+z)/(1-z) = (1+\cos\theta)/(1-\cos\theta)$. Therefore, we can re-write the local magnetization direction as

$$\boldsymbol{m}(\boldsymbol{r}) = \boldsymbol{m}(\theta, \phi) = (\sin\theta\cos\phi, \sin\theta\sin\phi, \cos\theta). \tag{6}$$

By substituting equation (6) into (3), we obtain the topological charge determined by $\theta$ and $\phi$, given as

$$Q = \frac{1}{4\pi}\int_{\pi}^{0}\sin\theta \mathrm{d}\theta\int_{0}^{2\pi}d\phi = -\frac{1}{4\pi}\left[\cos\theta\right]_{\pi}^{0}\left[\phi\right]_{0}^{2\pi}. \tag{7}$$

From equation (7), it can be seen that the topological charge is actually determined by both the out-of-plane ($\theta$) and in-plane ($\phi$) spin textures. It should be noted that here we only consider the skyrmion solution where $\theta$ rotates $\pi$ when $r$ goes from zero to infinity. For the skyrmionium solution, $\theta$ rotates $2\pi$ when $r$ goes from zero to infinity [24]. Hence, in order to describe the in-plane spin texture, we define the vorticity number as

$$Q_v = \frac{1}{2\pi}\oint_C d\phi = \frac{1}{2\pi}\left[\phi\right]_{\varphi=0}^{\varphi=2\pi}. \tag{8}$$

One also needs to introduce the helicity number, which is the phase appearing in

$$\phi = Q_v\varphi + Q_h. \tag{9}$$

Therefore, equation (6) can be rewritten as

$$\boldsymbol{m}(\theta, \varphi) = \left[\sin\theta\cos\left(Q_v\varphi + Q_h\right), \sin\theta\sin\left(Q_v\varphi + Q_h\right), \cos\theta\right]. \tag{10}$$

Therefore, topological spin textures can be fully characterized by the three distinct numbers ($Q$, $Q_v$, $Q_h$). Here it is worth

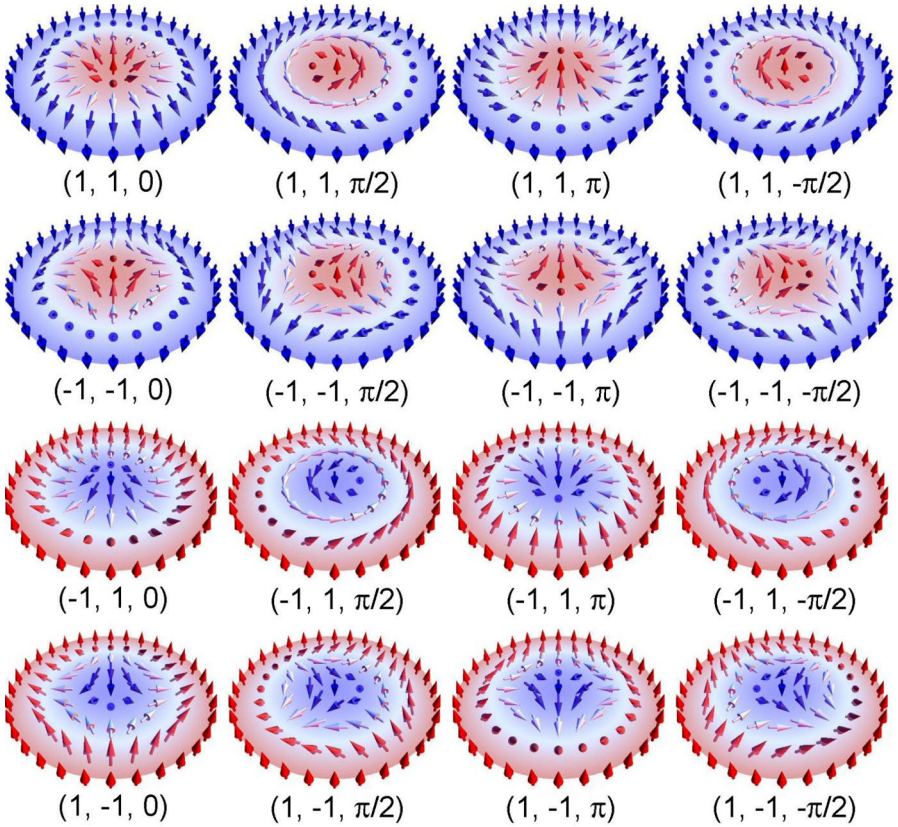


**Figure 2.** Illustrations of 2D magnetic skyrmions with different topological charge, vorticity number and helicity number, i.e. ($Q$, $Q_v$, $Q_h$). The arrow denotes the spin direction and the out-of-plane spin component ($m_z$) is represented by the color: red is out of the plane, white is in-plane, and blue is into the plane.

mentioning that the spin structures of chiral spin textures can also be described and observed in reciprocal or momentum space [8, 75–77], which allows diffraction-based techniques using e.g. neutrons to be effectively used to characterize the crystal of magnetic textures [75, 78, 79]. For example, the hexagonal chiral magnetic skyrmion lattice in real space can be described in reciprocal space as a superposition of three helical modulations (meaning three basis vectors of the crystalline structure) [77], which can be observed as six-fold scattering patterns in reciprocal space [75, 78, 80].

Figure 2 depicts some examples of degenerate skyrmion textures with varying $Q_v$ and $Q_h$, where the basic skyrmion textures with the topological charge $|Q| = 1$ with different in-plane magnetization rotational senses are shown. For example, for the Néel-type skyrmion with a spin-up (i.e. pointing along the $+z$ direction) and spin-down edge (i.e. pointing along the $-z$ direction), its in-plane spins can point toward or away from the skyrmion core. For the Bloch-type skyrmion, its in-plane spins can form a circle in either a clockwise or counterclockwise fashion. However, for the antiskyrmion with $|Q| = 1$, although its helicity number can vary between 0 and $2\pi$, the spin texture actually has a two-fold rotational symmetry with respect to the skyrmion core. So, the antiskyrmion structure is effectively determined by its vorticity number [81]. It is noteworthy that skyrmions and antiskyrmions carry positive and negative $Q_v$, respectively. The topological spin textures with different topological structures build a large family and lead to the emerging field of *topological magnetism*, which promises new opportunities for magnetic and spintronic applications.

As the topological spin textures are non-collinear spin textures, their existence in magnetic materials is usually a result of delicate interplay among different energy terms. From the viewpoint of micromagnetism at zero temperature, the energy terms for common magnetic materials include the Heisenberg exchange interaction, dipolar interaction energy terms as well as magnetic anisotropy and Zeeman energy terms. The dominated Heisenberg exchange interaction favors the parallel or antiparallel alignment of the adjacent magnetic spins in most cases, so that it does not stabilize any non-collinear spin texture. However, the strong emergence of various other energy terms that may naturally exist in or be introduced to the magnetic materials can lead to the stabilization of non-collinear topological spin textures. In particular, the most important energy term, which has been studied for many years, is the asymmetric exchange interaction, i.e. the above mentioned DM interaction [82, 83]. The DM interaction favors a right angle between the adjacent magnetic spins, thus a delicate competition between the Heisenberg exchange and DM interactions could result in the formation of non-collinear domain wall structures and topological spin textures with a fixed rotation fashion (called '*chirality*'), such as the chiral magnetic skyrmion and magnetic helical state. It is noteworthy that the spin-helix length in magnetic materials with DM interactions is determined by $4\pi A/|D|$, where $A$ is the Heisenberg ferromagnetic exchange constant.

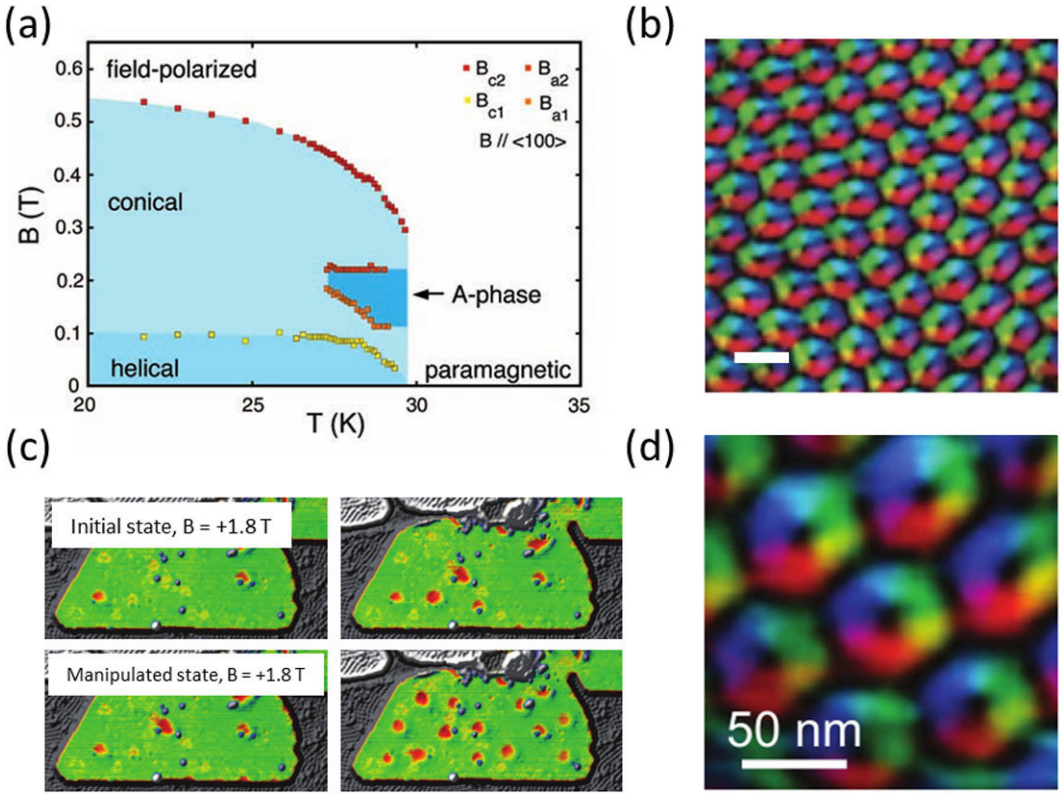


**Figure 3.** Observation of magnetic skyrmions at low temperature. (a) Magnetic phase diagram of MnSi. For $B = 0$, helimagnetic order develops below $T_c = 29.5$ K. From [75]. Reprinted with permission from AAAS. (b) A hexagonal skyrmion crystal observed using Lorentz TEM in a thin film of crystalline $Fe_{0.5}Co_{0.5}Si$ at a low temperature of 25 K. Scale bar, 100 nm. Reprinted from [102]. Copyright © 2010 Macmillan Publishers Limited. With permission of Springer. (c) Successive population of the island with skyrmions by injecting higher-energy electrons through local voltage sweeps. From [106]. Reprinted with permission from AAAS. (d) Skyrmion crystal in $Cu_2OSeO_3$ thin film obtained through the analysis of Lorentz TEM data taken at 5 K. From [109]. Reprinted with permission from AAAS.

The homogeneous DM interaction can exist in bulk materials lacking inversion symmetry and is expressed as

$$E_{\mathrm{bDM}} = d_{\mathrm{bDM}} \sum_{\langle i,j \rangle} u_{ij} \cdot (\boldsymbol{m}_i \times \boldsymbol{m}_j), \tag{11}$$

where $\langle i, j \rangle$ denotes the nearest-neighbor sites, $\boldsymbol{m}_i$ and $\boldsymbol{m}_j$ are the reduced magnetic spin vectors at sites $i$ and $j$, respectively. $d_{\mathrm{bDM}}$ is the bulk DM interaction coupling energy, $u_{ij}$ is the unit vector between $\boldsymbol{m}_i$ and $\boldsymbol{m}_j$. In the micromagnetic model [11], the bulk DM interaction reads

$$E_{\mathrm{bDM}} = b \iint D_{\mathrm{bDM}} \left[\boldsymbol{m} \cdot (\nabla \times \boldsymbol{m})\right] d^2\boldsymbol{r}, \tag{12}$$

with $D_{\mathrm{bDM}}$ being the continuous effective bulk DM interaction constant, and $b$ being the magnetic film thickness. The bulk DM interaction could result in the stabilization of Bloch-type skyrmions with $(Q = +1,\ Q_{\mathrm{v}} = +1,\ Q_{\mathrm{h}} = \pi)$ and $(Q = -1,\ Q_{\mathrm{v}} = +1,\ Q_{\mathrm{h}} = 0)$.

On the other hand, the DM interaction can also be induced at the interface between an ultrathin magnetic film and a non-magnetic film with a large spin–orbit coupling (SOC), given as

$$E_{\mathrm{iDM}} = d_{\mathrm{iDM}} \sum_{\langle i,j \rangle} (u_{ij} \times \hat{z}) \cdot (\boldsymbol{m}_i \times \boldsymbol{m}_j), \tag{13}$$

where $d_{\mathrm{iDM}}$ is the interface-induced DM interaction coupling energy, and $\hat{z}$ is the normal to the interface determined by Moriya's rule [83], oriented from the large SOC material to the magnetic film. In the micromagnetic model [11], the interface-induced DM interaction reads

$$E_{\mathrm{iDM}} = b \iint D_{\mathrm{iDM}} \left[m_z (\boldsymbol{m} \cdot \nabla) - (\nabla \cdot \boldsymbol{m}) m_z\right] d^2\boldsymbol{r}, \tag{14}$$

with $D_{\mathrm{iDM}}$ being the continuous effective interface-induced DM interaction constant. The interface-induced DM interaction could result in the stabilization of Néel-type skyrmions with $(Q = +1,\ Q_{\mathrm{v}} = +1,\ Q_{\mathrm{h}} = \pi)$ and $(Q = -1,\ Q_{\mathrm{v}} = +1,\ Q_{\mathrm{h}} = 0)$.

Note that the structures of skyrmions stabilized by DM interactions are not only limited to Bloch- and Néel-types, as recent reports have reported the presence of intermediate type of skyrmions [84–87] stabilized by other DM interactions. Also, the Dresselhaus SOC in materials with bulk inversion asymmetry can generate a type of DM interactions, which stabilizes antiskyrmions instead of skyrmions [88].

Indeed, the topological spin textures can also be stabilized by other mechanisms such as the frustrated exchange interactions [89], four-spin exchange interactions [8] as well as the long-range dipolar interactions [90–93]. However, most theoretical and experimental studies in the field focused on the systems with DM interactions during the last decade, as the DM interaction can be induced and adjusted by using modern interface engineering and multilayer fabrication techniques

[2, 3, 5–7, 94–101]. As such, for the rest of this review, we will focus on the magnetic skyrmion textures stabilized by DM interactions, while other mechanisms will also be briefly reviewed in the last section. It is worth mentioning that, although conventional magnetic bubbles can be stabilized by the competition between ferromagnetic Heisenberg exchange and long-range dipolar interactions. The in-plane spin texture (i.e. helicity and chirality) of these common bubbles are not fixed, so that they cannot be treated as a topological object in the strict context of topological magnetism.

For the last decade, these topological spin textures have been significantly highlighted, mainly inspired by their potential to handle information in devices at low energy consumption and/or high processing speed. In particular, the study of magnetic skyrmions for the purpose of designing novel spintronic applications has led to an emerging research field called *skyrmion-electronics* [1–3], which is also referred to as *skyrmionics* in some contexts [5]. It is an important task to study and understand how to stabilize and manipulate these topological spin textures, to eventually realize spin texture-based spintronic applications, such as memories, logic computing elements and transistor-like functional devices. In the following, we will review the representative topological spin texture—the magnetic skyrmion, from the points of views of writing, deleting, reading and processing magnetic skyrmions toward spintronic applications.

### 1.2. Magnetic skyrmions at low temperature

In the history of magnetism, many new phenomena and magnetic structures were first discovered at low temperature due to the low transition temperature of magnetic materials, where the thermal fluctuations are largely reduced. Likely, ten years ago in 2009, Mühlbauer *et al* for the first time experimentally observed the lattice structure of magnetic skyrmions in the chiral itinerant-electron magnet MnSi at a low temperature about 29 K [75] using a neutron scattering measurement (see figure 3(a)). The lattice of magnetic skyrmions, so-called the *skyrmion lattice*, is a hexagonal ordered array of skyrmions and often referred to as the *skyrmion crystal*. As shown in figure 3(b), in 2010, such a hexagonal skyrmion crystal was directly observed in a thin film of crystalline $Fe_{0.5}Co_{0.5}Si$ at a low temperature of 25 K by Yu *et al* [102], where the real-space imaging of magnetic spin textures was acquired by using the Lorentz transmission electron microscopy (LTEM). Using the same technique, in 2011, Yu *et al* reported the formation of the skyrmion crystal in FeGe over a wide range of temperature ranging from 60 K to 260 K [103], which is very close to room temperature. In 2012, Yu *et al* further demonstrated the current-induced motion of the skyrmion crystal in a FeGe thin film at a near room temperature, ranging from 250 K to 270 K [104]. In 2013, the transition of a skyrmion crystal phases to other magnetic textures (including helimagnetic, conical and ferromagnetic phases) in $Fe_{1-x}Co_xSi$ ($x = 0.5$) was also observed by using the magnetic force microscopy (MFM) at a very low temperature of 10 K [105]. Stabilization of skyrmions in such non-centrosymmetric crystalline materials is known to originate from the bulk-form DM interaction due to the broken inversion symmetry as discussed in section 1.1.

However, as was discussed in earlier section 1.1 of this article, the existence of magnetic skyrmions turns out to be possible not only in ferromagnetic bulk metals, but also ultrathin films where the interface-oriented DM interaction is harnessed. In 2011, Heinze *et al* experimentally revealed the 2D square skyrmion crystal in a hexagonal monolayer crystalline Fe film grown on the Ir surface using the spin-polarized scanning tunnelling microscopy (SP-STM) at a low temperature of 11 K [8]. Such a topological spin texture stems from the interplay among the Heisenberg exchange, four-spin and DM interactions. In such interface-oriented DM interaction-governed system, Romming *et al* for the first time experimentally realized both the writing and deleting of individual skyrmions in a PdFe bilayer on Ir(1 1 1) at a low temperature of 4.2 K (see figure 3(c)), where skyrmions are controlled by local spin-polarized currents from a STM. At the time, an out-of-plane magnetic field of several Tesla (e.g. $B = \sim 3$ T) is required to stabilize individual skyrmions at low temperatures [106]. It is worth to mention that Jonietz *et al* [78] and Schulz *et al* [107] also reported the ultralow threshold current, $10^6$ A m$^{-2}$, for depinning magnetic skyrmions at ~26 K, which is 4–5 orders smaller than the depinning threshold of ferromagnetic domain walls, and these demonstrations excited great interest on using skyrmions for low power spintronic applications together with earlier findings. However, as skyrmions driven by the extremely low depinning current were displaced at a relatively low velocity [1, 107, 108], the required current density for actual devices may be increased as skyrmions need to move with a fast velocity.

At low temperatures, the hosting materials of skyrmions are not limited to conventional metallic ferromagnets, and other kinds of topological magnetic textures can also be stabilized. In 2012, Seki and colleagues [109] for the first time identified skyrmions in an insulating multiferroic magnet $Cu_2OSeO_3$ through LTEM and magnetic susceptibility measurements below the temperature of 60 K (see figure 3(d)). By utilizing the small-angle neutron scattering (SANS), Seki *et al* also found a triangular skyrmion lattice in multiferroic insulator $Cu_2OSeO_3$ [110].

In 2016, Matsumoto *et al* directly observed skyrmion domain boundaries in $FeGe_{1-x}Si_x$ ($x \sim 0.25$) using the differential phase contrast scanning transmission electron microscopy (DPC STEM) equipped with a segmented annular all-field detector at a temperature of 95 K [111], where they found that individual skyrmions at the domain boundary cores can flexibly change their size and shape to stabilize their core structures. The flexibility of the skyrmion structure at domain boundaries could be a basis for creating twisted skyrmion [112] that can be used for applications. Here it is worth mentioning that the DPC STEM technique can directly and precisely observe electromagnetic structures at an ultra-high resolution down to 1 nm. In 2016, McGrouther *et al* revealed the internal spin structures of skyrmions in a freestanding nanowedge specimen of cubic B20 structured FeGe by using the DPC STEM technique but equipped with a pixelated detector [113]. In 2018, also by using the DPC STEM with a pixelated detector, McVitie *et al* imaged the Néel-type domain wall structure and precisely measured the domain wall width [114].

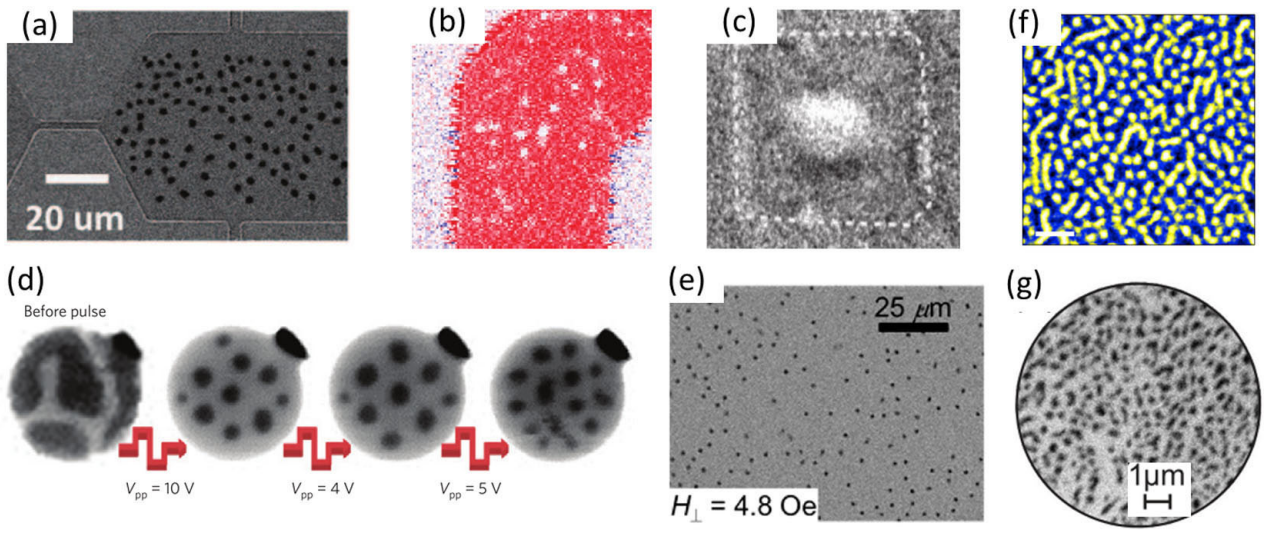


**Figure 4.** Observation of magnetic skyrmions at room temperature. (a) The current-induced generation of skyrmion bubbles in Ta (5 nm)/$Co_{20}Fe_{60}B_{20}$ (1.1 nm)/$TaO_x$ (3 nm). From [116]. Reprinted with permission from AAAS. (b) A 1.5 × 1.5 $\mu m^2$ out-of-plane magnetization ($m_z$) map obtained by STXM on a $(Ir/Co/Pt)_{10}$ multilayer with applying out-of-plane magnetic field of 68 mT. Reprinted from [29]. Copyright © 2016 Macmillan Publishers Limited. With permission of Springer. (c) XMCD-PEEM image of a 420 nm square dot (indicated by the dotted line) which is patterned with Ta (3 nm)/Pt (3 nm)/Co (0.5–1 nm)/$MgO_x$/Ta (2 nm) thin film. Reprinted from [120], Copyright © 2016 Macmillan Publishers Limited. With permission of Springer. (d) An initial labyrinth domain state was generated by static field (first image) and then transformed into a hexagonal skyrmion lattice in a 2 $\mu$m Pt/Co/Ta disc by applying a bipolar pulse train with $V_{pp} = 10$ V (second image). The last two images were acquired after applying $V_{pp} = 4$ V and $V_{pp} = 5$ V, respectively. Dark (light) contrast corresponds to up (down) magnetization in all STXM images except for the last three, where the x-ray magnetic circular dichroism (XMCD) contrast was inverted. Reprinted from [121]. Copyright © 2016, Springer Nature. With permission of Springer. (e) Polar-MOKE images of CoFeB thin film with PMA field of $H_k \approx 1.1$ kOe for 4.8 Oe out-of-plane external magnetic field. Reprinted with permission from [122]. Copyright © 2016 American Chemical Society. (f) Microscopic imaging (scale bar, 0.5 $\mu$m) of sample Fe (3)/Co (6) (number of atomic layers in braces) with MFM at ~ −100 mT of applied field. Reprinted from [31]. Copyright © 2016 Macmillan Publishers Limited. With permission of Springer. (g) The out-of-plane SPLEEM images of Fe (2.6 ML)/Ni (2 ML)/Cu (8.6 ML)/Ni (15 ML)/Cu (0 0 1) multilayer structures (1 ML ~ 1.8 Å). Reprinted from [125], with the permission of AIP Publishing.

These early stage experimental observations of skyrmions at low temperatures mainly focused on the existence of skyrmion crystals, skyrmion chain, skyrmion cluster, and individual isolated skyrmions in diverse material platforms stabilized by either bulk or interfacial DM interactions. Although these findings have proved fascinating physical properties of skyrmions and provided in-depth physical understanding behind their topological characteristics, from the viewpoint of practical applications, most commercial electronic devices based on skyrmions would require their room-temperature stabilization (or at even higher temperature). In the following, we will review the discovery of skyrmions and relevant topological spin textures at room temperature.

### *1.3. Discovery of room-temperature skyrmions*

Between 2015 and 2016, there have been several reports of room-temperature stabilized magnetic skyrmions. The most notable demonstration was the stabilization of room-temperature skyrmions in the industry-relevant sputter-grown non-crystalline ferromagnetic heterostructures. This approach was motivated by the theoretical suggestion [9] and the experimental confirmation [13, 115] of homochiral Néel-type domain walls in such ultrathin ferromagnet-based asymmetric heterostructures at room temperature. In 2015, Jiang *et al* not only observed stable room-temperature individual skyrmion bubbles in a Ta (5 nm)/CoFeB (1.1 nm)/$TaO_x$ (3 nm) trilayer grown by magnetron sputtering (see figure 4(a)), but also demonstrated the current-driven transformation of skyrmion bubbles from strip domains in such a trilayer device via a geometrical constriction [116]. It should be noted that the term '*skyrmion bubble*' studied in this report is a topologically non-trivial object with a skyrmion number of $|Q| = 1$ and a fixed Néel-type chirality induced by the DM interaction. However, unlike the compact skyrmion with 1–100 nm diameter, the skyrmion bubble has a larger size (~1 $\mu$m) comparable to trivial achiral bubbles stabilized by dipolar fields [91, 117–119]. Both skyrmion bubble and compact skyrmion are topological spin textures and turned out to be equivalent in the topological definition (see equation (3)), but they are often differentiated with two different names—skyrmion bubble or compact skyrmion—in some contexts due to their significant size difference. Soon after this report, in 2016, some other groups subsequently reported the observation of room-temperature skyrmions in similar ultrathin ferromagnetic asymmetric heterostructures.

Moreau-Luchaire *et al* fabricated the Ir/Co/Pt asymmetric multilayers [29], where an additive interface-induced DM interaction of about 2 mJ $m^{-2}$ was achieved, and using the scanning x-ray transmission microscopy (SXTM), sub-100 nm individual skyrmions were imaged in the asymmetric multilayers at room temperature and low magnetic fields (e.g. $B_z = 58$ mT) (see figure 4(b)). As the thermal stability of magnetization increases with the volume of the magnet, the

skyrmions in the ten repetitions of the Ir/Co/Pt films are stable against thermal fluctuations at room temperature [29]. As shown in figure 4(c), Boulle *et al* also observed stable skyrmions in sputtered ultrathin Pt/Co/MgO nanostructures at room temperature and zero external magnetic field [120]. Based on the in-plane magnetization sensitive x-ray magnetic circular dichroism photoemission electron microscopy (XMCD-PEEM) experiments, it was found that the skyrmions in the Pt/Co/MgO thin films have the left-handed chiral Néel structure [120], which indicates they are stabilized by interface-induced DM interactions.

In the same year, Woo *et al* reported the observation of stable room-temperature skyrmions and their current-induced motion in [Pt (3 nm)/Co (0.9 nm)/Ta (4 nm)]$_{15}$ and [Pt (4.5 nm)/CoFeB (0.7 nm)/MgO (1.4 nm)]$_{15}$ multilayer stacks by using both the full-field magnetic transmission soft x-ray microscopy (MTXM) and STXM [121]. Woo *et al* demonstrated the stabilization of skyrmion lattice in a confined circular magnetic disk of about 2 $\mu$m diameter (see figure 4(d)), and further reported the motion of a train of individual skyrmions at a speed up to 100 m s$^{-1}$ driven by a current density of $j \sim 5 \times 10^{11}$ A m$^{-2}$ [121]. This is a direct experimental evidence that suggests skyrmions can be used for real-world high-speed spintronic applications. Later in 2016, as shown in figure 4(e), Yu *et al* also experimentally demonstrated the creation of room-temperature skyrmion bubbles in ultrathin CoFeB films [122], where skyrmion bubbles are stabilized by a delicate competition among the Heisenberg exchange interaction, dipolar interaction, and perpendicular magnetic anisotropy (PMA). The skyrmion bubbles found in this work have a skyrmion number of $|Q| = 1$ and typical size close to 1 micrometer. Yu *et al* reported that, although the DM interaction strength is only of 0.25 mJ m$^{-2}$ in the CoFeB films, it is strong enough to fix the Néel-type chirality of skyrmion bubbles, leading to the Néel-type chiral nature. In 2017, Soumyanarayanan *et al* [31] found a tunable room-temperature skyrmion platform in the Ir/Fe/Co/Pt multilayer stacks for studying sub-50 nm skyrmions (see figure 4(f)), where one can adjust the magnetic interactions governing skyrmions by varying the ferromagnetic layer composition. In 2018, Zhang *et al* experimentally realized the control of skyrmion density in Pt/Co/Ta multilayer stacks by varying temperature [123] or in-plane magnetic field [124].

The existence of room-temperature magnetic skyrmions were also demonstrated using non-centrosymmetric crystalline interfaces and bulk materials. As shown in figure 4(g), Chen *et al* imaged the room-temperature magnetic skyrmions in the Fe/Ni/Cu/Ni/Cu(0 0 1) multilayers using the spin-polarized low-energy electron microscopy (SPLEEM) [125], where the exchange coupling across non-magnetic spacer layers is responsible for the stabilization of skyrmions. A new class of cubic chiral magnets hosting room-temperature skyrmion crystals—$\beta$-Mn-type Co–Zn–Mn alloys, was found by Tokunaga and colleagues [126]. The room-temperature magnetic skyrmion crystal was also realized in an artificial manner, as demonstrated by Gilbert *et al* via patterning asymmetric magnetic nanodots with controlled circularity on an underlayer with PMA [127]. Such an approach is theoretically predicted by Sun *et al* [128], which will be discussed in section 2 as a possible method for writing skyrmions.

As mentioned in section 1.1, magnetic skyrmions can be stabilized in different materials by different mechanisms. The room-temperature skyrmions in asymmetric ferromagnetic multilayer stacks are usually stabilized by enhanced interface-induced DM interactions. In 2017, Hou *et al* [129] for the first time observed the skyrmion bubbles with variable topological charges at room temperature in the frustrated kagome $Fe_3Sn_2$ magnet with uniaxial magnetic anisotropy, by using *in situ* LTEM. In the same year, antiskyrmions with $Q_v = -1$ were experimentally identified in acentric tetragonal Heusler compounds $Mn_{1.4}Pt_{0.9}Pd_{0.1}Sn$ by Nayak *et al* [88]. These two works not only provide more material platforms for hosting magnetic skyrmions and other topological spin textures, but also prove that topological spin textures with different topological charges can be stabilized at room temperature, shedding light on possible future applications based on different topological spin textures.

### 1.4. Potential applications

The field of *skyrmion-electronics* mainly focuses on the design and development of information storage and processing devices [2, 3, 5–7, 130]. The most highlighted skyrmionic information storage device—skyrmionic racetrack memory is proposed by Fert *et al* in 2013 [1], which is an improved design based on the domain-wall racetrack memory proposed by Parkin *et al* in 2008 [131]. Later in 2013, Iwasaki *et al* [108, 132] and Sampaio *et al* [133] independently studied the current-induced dynamics of isolated skyrmions in ferromagnetic racetracks, which provided fundamental insight into the design of skyrmion-based racetrack memory. Since 2013, a number of theoretical and experimental works were carried out on the skyrmion-based racetrack memory and its derived applications, however, the experimental demonstration of such fully functional electrically operating skyrmion-based memory device is awaiting its demonstration.

In 2013, the magnetoelectric resonance effect of magnetic skyrmions was found by Mochizuki *et al* [134] and Okamura *et al* [135], which suggests an opportunity for building the skyrmion-based microwave applications, such as microwave detector [136]. Besides, the skyrmion-based nano-oscillators [137–139] can be built using the oscillation characteristics induced by currents.

In 2015, Zhang *et al* [140] theoretically proposed the prototype of skyrmion-based logic computing gates, which can perform the logic AND and OR operations. Zhang *et al* [141] also proposed a transistor-like functional device based on skyrmions, where the current-induced motion of skyrmions is controlled by a gate voltage. Note that a similar idea on the control of skyrmion dynamics by a gate voltage was also proposed by Upadhyaya *et al* [142] in the same year. These potential skyrmion-based information computing devices can be combined with the skyrmion-based racetrack memory devices, which may lead to the invention of an in-memory logic computing circuit based on skyrmions.

Some bio-inspired applications based on skyrmions were also proposed in the last few years. Huang *et al* [143]

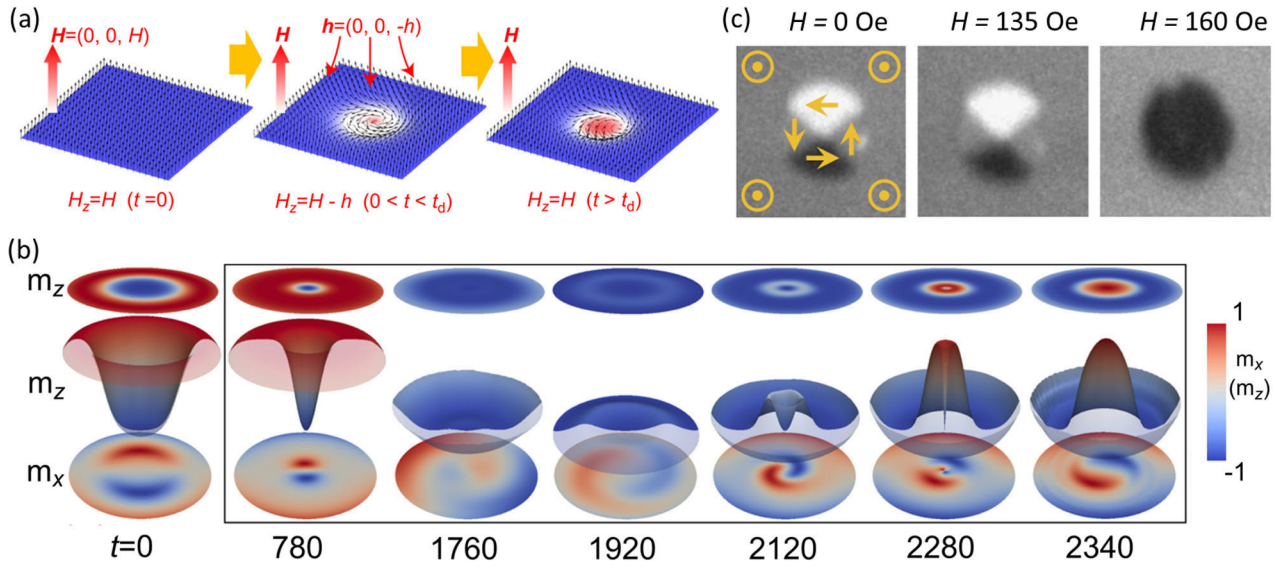


**Figure 5.** Writing, deleting and switching of skyrmions using magnetic fields. (a) Schematic of skyrmion creation in a magnetic field application. Reprinted from [167]. With the permission of AIP Publishing. (b) The skyrmion core reversal induced by an AC magnetic field pulse. Reprinted with permission from [173]. With the permission of AIP Publishing. (c) The skyrmion core annihilation process with applying an in-plane magnetic field pulse. The yellow symbols indicate the out-of-plane spins. Reprinted from [174]. Copyright © 2014 Macmillan Publishers Limited. With the permission of Springer.

designed a skyrmion-based artificial synapse device for neuromorphic computing systems in 2017, which was recently experimentally realized by Song *et al* [144]. Li *et al* [145] also proposed a skyrmion-based artificial neuron that mimics the leaky-integrate-fire function of a biological neuron. In 2018, Bourianoff *et al* [146] and Prychynenko *et al* [147] proposed the first reservoir computing model based on magnetic skyrmions. Most recently, the thermally activated dynamics of skyrmions was investigated by several groups and found to be useful for computing [148–159]. For example, the thermal skyrmion diffusion-based signal reshuffling device operation was experimentally realized by Zázvorka *et al* [160], which could be used in future skyrmion-based probabilistic computing devices. Besides, Nozaki *et al* experimentally realized the control of the thermal diffusion of skyrmions by applying a pure voltage [149].

For the successful demonstration of any skyrmion-based potential applications, the energy-efficient writing, deleting, reading and processing processes of skyrmions are prerequisites. In the following, we review the progresses that have been made over the last 10 years in the writing, deleting, and reading of magnetic skyrmions. We will also review several representative skyrmion-based applications in detail, including the skyrmion-based racetrack memory, logic computing gate, transistor-like device and bio-inspired applications.

## 2. Writing and deleting skyrmions

Magnetic skyrmion is a promising block for building future spintronic applications, as it can be employed as a non-volatile information carrier in magnetic media. The simplest method to encode binary information using magnetic skyrmions in magnetic materials is based on the writing and deleting of individual isolated skyrmions. Namely, the presence of a skyrmion can stand for the binary information digit '1' or '0'. Hence, the controllable and reliable creation and annihilation of skyrmions are prerequisites for any skyrmion-based information storage applications. It is a vital task to find the best method to write and delete skyrmions.

### 2.1. Magnetic field

Magnetic field is one of the most important and controllable external stimuli that can be rather easily realized in most laboratories. In the early stage of skyrmion research, a number of theoretical and experimental studies were carried out on the magnetic phase diagram, where skyrmion crystals and isolated skyrmions usually form in chiral magnets within the range of certain out-of-plane magnetic fields and temperature [54, 75, 78, 102, 103, 105, 109, 161–163]. That is to say, by applying an external magnetic field perpendicularly to the magnetic film with DM interactions, it is possible to control the formation of skyrmion textures [106]. Some of the initial demonstrations of room-temperature skyrmions introduced in section 1.1 were also realized by shrinking maze stripe domains into circular bubble-shaped domains by applying magnetic field.

On the other hand, once the skyrmion is created in a magnetic film, its size also depends on the strength of the external out-of-plane magnetic field [11, 164, 165] that interplays with other energetic contributions e.g. DM interaction, magnetic anisotropy, demagnetization energy and exchange interaction. Namely, a small out-of-plane magnetic field is usually required for the formation of skyrmions, while a large out-of-plane magnetic field could lead to the collapse and annihilation of skyrmions. In 2016, Müller *et al* predicted and numerically demonstrated that, by applying magnetic field pulses, skyrmions can be created close to the edge of a chiral magnet due to

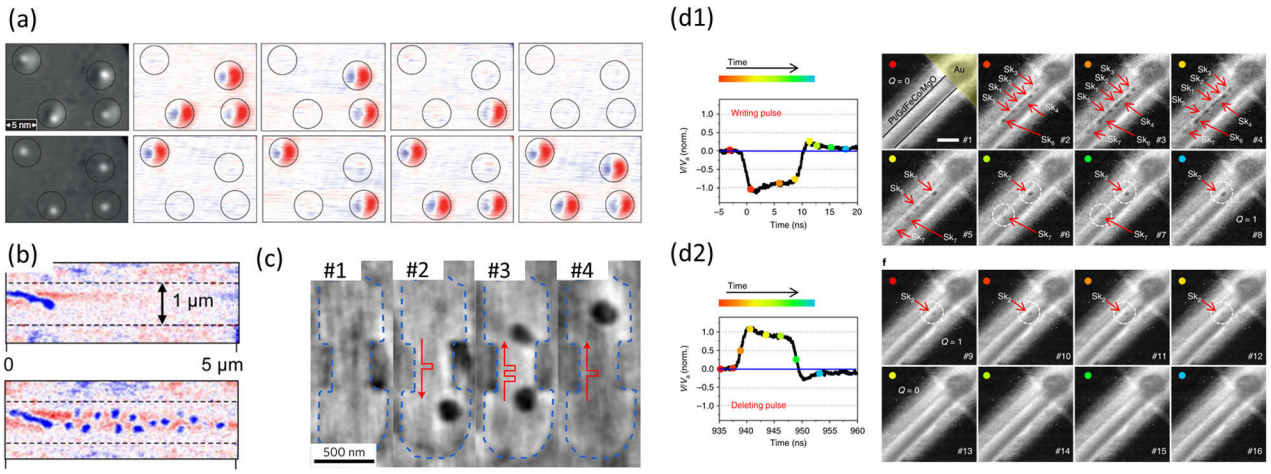


**Figure 6.** Writing and deleting of skyrmions using spin-polarized electric currents. (a) Creation and annihilation of single skyrmions with local spin-polarized currents at $T = 4.2$ K in the PdFe bilayer. Reprinted from [106] with permission from AAAS. (b) MFM images of the 1 $\mu$m wide tracks before any pulses and after the injection of 1000 current pulses of 200 ns in 0.6 nm thick Co multilayers. Reprinted with permission from [32]. Copyright © 2017, American Chemical Society. (c) Single-skyrmion generation and subsequent motion in Pt/CoFeB/MgO multilayers. From [35]. Copyright © 2017 Macmillan Publishers Limited. With permission of Springer. (d) Magnetic skyrmion configuration for writing (d1) and deleting (d2). Scale bar, 500 nm. From [36]. Copyright © 2018, Springer Nature. With permission of Springer.

the edge instability [166]. In 2017, Mochizuki [167] demonstrated that in a magnetic film with a fabricated hole or notch, individual skyrmions can be created by an external magnetic field in a controlled manner (see figure 5(a)). Most recently, the writing of skyrmions in a uniformly magnetized film by a magnetic dipole was theoretically investigated by Garanin *et al* [168], which can be seen as the creation of skyrmions by a localized magnetic field. In 2018, such a creation method of writing skyrmions was experimentally demonstrated by Zhang *et al* using a scanning local magnetic field provided by MFM tips [169].

Once the magnetic skyrmion is created, it can also be manipulated or even deleted by magnetic fields, similar to the magnetic vortices in magnetic disks [170, 171]. For example, Büttner *et al* showed that the gigahertz gyrotropic eigenmode dynamics of a single skyrmion bubble can be excited by an external magnetic field pulse and corresponding magnetic field gradient [172]. Magnetic skyrmions in nanostructures with confined geometries can also be switched by microwave magnetic fields (see figure 5(b)) [173] or magnetic field pulses (see figure 5(c)) [174, 175]. Note that the microwave magnetic field can also excited other dynamics of skyrmions [176, 177]. Indeed, when the strength of magnetic field is larger than certain threshold, it is destructive for skyrmions and may ultimately lead to the fully polarized magnetic state, i.e. the ferromagnetic state. Hence, the application of a strong magnetic field, either in-plane or out-of-plane, is also the easiest way to delete skyrmions from magnetic media.

### 2.2. Spin-polarized electric current

Spin-polarized electric current could provide spin-transfer torques (STTs) or spin–orbit torques (SOTs) on magnetic moments, which is an important driving force for magnetization dynamics in modern spintronic devices [97, 178, 179]. In 2011, the interaction between STTs and skyrmion lattices in chiral magnets was theoretically studied by Everschor *et al* [180]. Then, the writing of a magnetic skyrmion using the spin-polarized electric current was theoretically predicted by Tchoe *et al* in 2012, where skyrmions can be nucleated from a ferromagnetic background by a vertical current injection with the current density of the estimated order of $j \sim 10^{10}$–$10^{11}$ A m$^{-2}$ [181]. In 2013, Iwasaki *et al* [132] and Sampaio *et al* [133] independently studied the current-induced skyrmion creation in confined geometries using theoretical and numerical approaches. In particular, Iwasaki *et al* numerically demonstrated that skyrmions can be nucleated and created from the notch in a nanotrack [132], which is an effective method to write skyrmions at a certain location. In the same year, as was noted in section 2.1, Romming *et al* [106] for the first time experimentally realized both the writing and deleting of single isolated magnetic skyrmions by using the local tunneling spin-polarized currents (~1 nA) from a STM at low temperature (see figure 6(a)).

In 2014, Zhou and Ezawa theoretically predicted that a magnetic skyrmion can be converted from a domain-wall pair in a junction geometry ($j \sim 1.8 \times 10^{12}$ A m$^{-2}$) [182]. In a similar manner, in 2015, Jiang *et al* demonstrated in a room-temperature MOKE experiments that magnetic skyrmion bubbles can be created by utilizing the spin current-driven ($j \sim 0.5 \times 10^{10}$ A m$^{-2}$) transformation between strip domains and skyrmion bubbles in a Ta/$Co_{20}Fe_{60}B_{20}$/$TaO_x$ trilayer with a junction constriction [116]. The creation of skyrmion bubbles in such a junction constriction driven by inhomogeneous spin currents was further theoretically studied independently by Heinonen *et al* [183], Lin [184], and Liu *et al* [185], confirming its efficient mechanism and device compatibility suitable for future applications.

The spin-polarized current can also result in the creation of skyrmions or skyrmion bubbles by other different mechanisms. In 2016, Yuan and Wang theoretically demonstrated that a skyrmion can be created in a ferromagnetic nanodisk by applying a nano-second current pulse ($j \sim 2.0 \times 10^{12}$ A m$^{-2}$) [186]. Yin *et al* also suggested in a theoretical study that it

**Table 1.** Writing and deleting of skyrmions using spin-polarized electric currents with different current densities in both theoretical and experimental works.

| Materials | Current density | Pulse width | $T$ (K) | B (mT) | Reference |
|---|---|---|---|---|---|
| | | Experimental writing | | | |
| PdFe bilayer | 1–200 nA | | 4.2 | 1800 | [106] |
| $Ta/Co_{20}Fe_{60}B_{20}/TaO$ | $0.5 \times 10^{10}$ A m$^{-2}$ | 1 $\mu$s (single) | RT | 0.5 | [116] |
| $Ta/Co/[Pt/Ir/Co/]_{10}/Pt$ | $2.38 \times 10^{11}$ A m$^{-2}$ | 200 ns (1000 pulses) | RT | 20.5 | [32] |
| $[Pt/Co_4Fe_4B_2/MgO]_{20}$ | $1.6 \times 10^{11}$ A m$^{-2}$ | 20 ns (3.33 MHz, 5s) | RT | 0 | [33] |
| $[Pt/CoFeB/MgO]_{15}$ | $3.0 \times 10^{11}$ A m$^{-2}$ | 7.5 ns (10 000 pulses) | RT | 40 | [34] |
| Pt/Ni/Co/Ni/Au/Ni/Co/Ni/Pt | $2.8 \times 10^{11}$ A m$^{-2}$ | 7 ns (single) | RT | 6 | [188] |
| $[Pt/Co_{60}Fe_{20}B_{20}/MgO]_{15}$ | $2.6 \times 10^{11}$ A m$^{-2}$ | 12 ns (single) | RT | 6.1 | [35] |
| $[Pt/Gd_{25}Fe_{65.6}Co_{9.4}/MgO]_{20}$ | $2.5 \times 10^{10}$ A m$^{-2}$ | 10 ns (single) | RT | 130 | [36] |
| | | Experimental deleting | | | |
| $[Pt/Gd_{25}Fe_{65.6}Co_{9.4}/MgO]_{20}$ | $2.5 \times 10^{10}$ A m$^{-2}$ | 10 ns (single) | RT | 130 | [36] |
| | | Theoretical writing | | | |
| CoPt | $1.8 \times 10^{12}$ A m$^{-2}$ | | 0 | 0 | [182] |
| CoFeB | $1.0 \times 10^{12}$ A m$^{-2}$ | 40 ns (single) | 0 | 0.5 | [183] |
| $Co_{20}Fe_{60}B_{20}$ | $1.5–3.0 \times 10^{10}$ A m$^{-2}$ | | 0 | 70 | [185] |
| CoPt | $2.0 \times 10^{12}$ A m$^{-2}$ | 0.7 ns (single) | 0 | 0 | [186] |
| | $1.7 \times 10^{11}$ A m$^{-2}$ | | 50 | | [187] |
| | $3.6 \times 10^{11}$ A m$^{-2}$ | | 0 | | [132] |
| | | Theoretical deleting | | | |
| CoFeB | $5–20 \times 10^{12}$ A m$^{-2}$ | | 0 | 0 | [190] |

RT, room temperature.

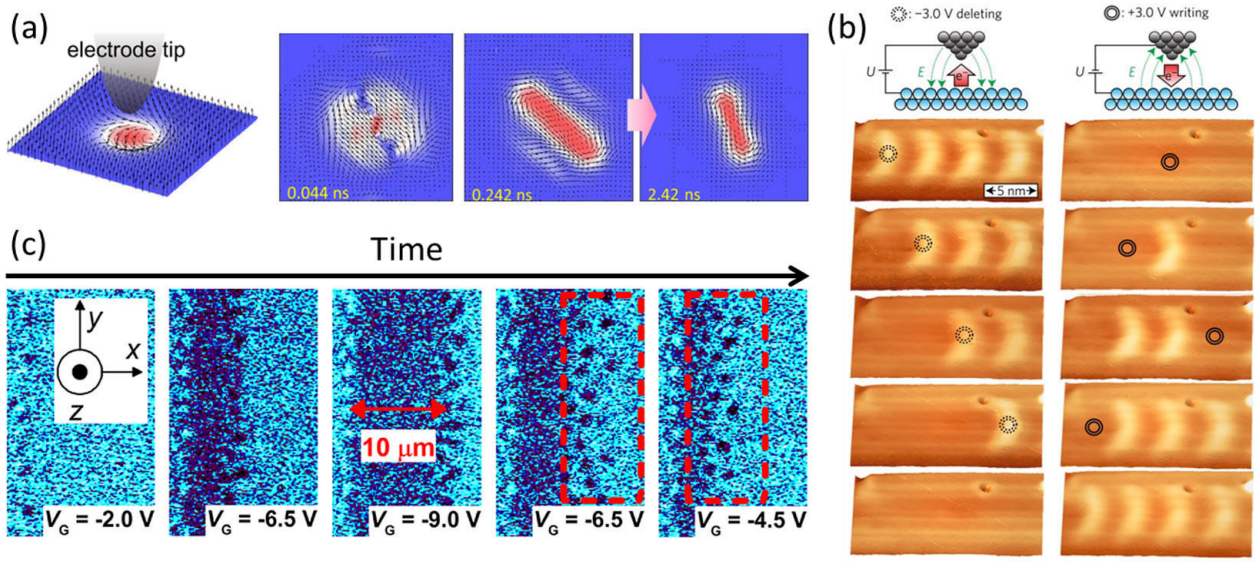


**Figure 7.** Writing and deleting of skyrmions by electric fields. (a) Schematic of skyrmion creation via local application of an electric field using an electrode tip and simulated spatiotemporal dynamics of the magnetizations for the electrical skyrmion creation process in the $Cu_2OSeO_3$ thin film. Reprinted from [193], with the permission of AIP Publishing. (b) Perspective views of subsequent SP–STM constant-current images of the same Fe triple layer area showing the writing and deleting of individual magnetic skyrmions. Reprinted from [195]. Copyright © 2017 Macmillan Publishers Limited. With permission of Springer. (c) MOKE microscopy images of the EF-induced creation and motion of a chiral domain wall accompanied by the creation of skyrmion bubbles in Pt/CoNi/Pt/CoNi/Pt multilayer with the thickness gradient at $H_z = -0.2$ mT. Reprinted with permission from [198]. Copyright © 2019, American Chemical Society.

is possible to create a single skyrmion in helimagnetic thin films using the dynamical excitations induced by the Oersted field and the STT given by a vertically injected spin-polarized current ($j \sim 1.7 \times 10^{11}$ A m$^{-2}$) [187]. In 2017, as shown in figure 6(b), Legrand *et al* experimentally realized the creation of magnetic skyrmions by applying a uniform spin current directly into nanotracks ($j \sim 2.38 \times 10^{11}$ A m$^{-2}$) [32]. Latter in 2017, Woo *et al* experimentally demonstrated the creation of skyrmions at room temperature and zero external magnetic field by applying bipolar spin current pulses ($j \sim 1.6 \times 10^{11}$ A m$^{-2}$) directly into a Pt/CoFeB/MgO multilayer [33], which turned out to be thermally-induced skyrmion generation as systematically studied recently by Lemesh *et al* [34]. Hrabec *et al* also reported the experimental creation of skyrmions induced by applying electric current ($j \sim 2.8 \times 10^{11}$ A m$^{-2}$) through an electric contact placed upon a symmetric magnetic bilayer

system [188]. The spin-polarized current-induced generation of skyrmions can be deterministic and systematic when pinning sites or patterned notches, where PMA is locally reduced, are used as the source of skyrmion generation as reported by Buttner *et al* [35] in 2017 ($j \sim 2.6 \times 10^{11}$ A m$^{-2}$) (see figure 6(c)) and Woo *et al* [36] in 2018 ($j \sim 2.5 \times 10^{10}$ A m$^{-2}$) (figure 6(d)). More recently, Finizio *et al* reported that localized strong thermal fluctuation could also introduce systematic skyrmion generation at a designed location [189].

On the other hand, the spin-polarized current can delete skyrmions in nanostructures. For example, in 2017, De Lucia *et al* theoretically studied the annihilation of skyrmions induced by spin current pulses ($j \sim 5 \times 10^{12}$ A m$^{-2}$) and suggested that skyrmions can be reliably deleted by designing the pulse shape [190]. In 2018, Woo *et al* experimentally demonstrated such deterministic deletion of a single skyrmion in ferrimagnetic GdFeCo films with the application of designed current pulses ($j \sim 2.5 \times 10^{10}$ A m$^{-2}$) [36]. In table 1, we summarized the typical current density applied to create and delete skyrmions in the above mentioned theoretical and experimental works for the purposes of reference and comparison.

### 2.3. Local electric field

In the last decade, a number of studies have been performed to explore skyrmion dynamics induced by electric current, however, the electric current often accompanies Joule heating that leads to energy losses or even permanent damages to metallic devices. Therefore, it may be necessary to find more reliable ways to drive skyrmion dynamics, and in this context, the pure electric field is one of the desired ways to drive skyrmion dynamics because of its ultralow power consumption with negligible Joule heating. A number of reports [109, 134, 135, 191, 192] had shown the possibility to control skyrmions in magnetoelectric materials, such as the chiral magnetic insulator $Cu_2OSeO_3$, using a pure electric field (due to the magnetoelectric coupling). In 2015, Mochizuki and Watanabe [193] theoretically proposed the writing of isolated skyrmions in a multiferroic thin film by applying a local electric field (see figure 7(a)), which is realized through the magnetoelectric coupling effect in multiferroic compounds. In 2016, the electric-field-controlled transition between the skyrmion lattice phase and conical phase was experimentally realized in magnetoelectric chiral magnet $Cu_2OSeO_3$ [194].

In ferromagnetic materials, the writing and deleting of magnetic skyrmions can also be induced by a pure electric field, usually based on the effect of voltage control of magnetic anisotropy (VCMA) [142]. In 2017, as shown in figure 7(b), Hsu *et al* experimentally demonstrated the reversible transition between the ferromagnetic texture and the magnetic skyrmion by applying a local electric field to the Fe triple layer on Ir(1 1 1) [195]. Such a local electric field, which can induce the writing and deleting of magnetic skyrmions, were realized by using the SP-STM. In the same year, the writing and deleting of skyrmion bubbles controlled by electric field in a Pt/Co/oxide trilayer was realized in an efficient and reproducible manner by Schott *et al* at room temperature [196].

In 2018, Srivastava *et al* experimentally demonstrated the electric field turning of DM interactions in a Ta/FeCoB/$TaO_x$ trilayer [197], which can be used as a method to further control the skyrmion chirality. Huang *et al* also experimentally realized the writing of skyrmions in the magnetoelectric compound $Cu_2OSeO_3$ [192].

In 2019, Ma *et al* designed and fabricated a Pt/CoNi/Pt/CoNi/Pt multilayer, which is sandwiched between the indium tin oxide (ITO)/$SiO_2$ bilayer and the glass substrate, in the form of racetracks where the thickness of the films had a slope [198]. In such a nanostructure, Ma *et al* demonstrated that many skyrmion bubbles can be created (i.e. corresponding to the skyrmion writing) and directionally displaced about 10 micrometres by applying a pure electric field (see figure 7(c)). When the electric field is removed, the skyrmion bubbles will be annihilated, which can be regarded as the deleting of skyrmion bubbles.

Similar to the manipulations of skyrmions by magnetic field and electric current, the polarity of skyrmions can also be switched by a pure electric field, in principle. For example, Bhattacharya *et al* numerically demonstrated the electric-field-induced switching of a magnetic skyrmion in a magnetic tunnel junction (MTJ) structure [199]. On the other hand, the dynamics of skyrmions can also be controlled by a pure electric field, as experimentally demonstrated by Nozaki *et al* in a W/FeB/Ir/MgO multilayer structure recently [149], the thermal motion of skyrmion bubbles can be controlled by a pure voltage.

### 2.4. Laser

The magnetization dynamics can also be driven by (ultrafast) laser pulses, and laser pulse-induced magnetization excitation has been of great interest for many years. Such excitation enabled the observation of ultrafast demagnetization [200] and all-optical switching [201–204], which could enable the integration of optical spintronics devices. Single laser shot-induced *deterministic* magnetization switching was also demonstrated using ferrimagnetic thin films, where the ultrafast last-induced heating could lead to the angular momentum transfer between two sublattices [202]. Unlike ferrimagnetic materials, the injected laser-induced local heating in ferromagnetic materials *probabilistically* lead to the switching of magnetization within the heated area due to the thermal perturbation and its interactions with e.g. local dipolar field [130, 205, 206]. In detail, the switching field (i.e. coercive field) of ferromagnets generally decreases with increasing temperature, therefore, the dipolar interactions that favor the formation of multi-domains overcome the switching field threshold, leading to the local magnetization switching. Nevertheless, in chiral magnetic materials, such laser-induced magnetization switching results in the local generation of a single or multiple chiral magnetic textures, including skyrmions. In 2009, Ogasawara *et al* experimentally studied the magnetization reversal dynamics in a TbFeCo film induced by a femtosecond laser pulse in the presence of a small external magnetic field [207], where the laser-induced reversed magnetic domain has

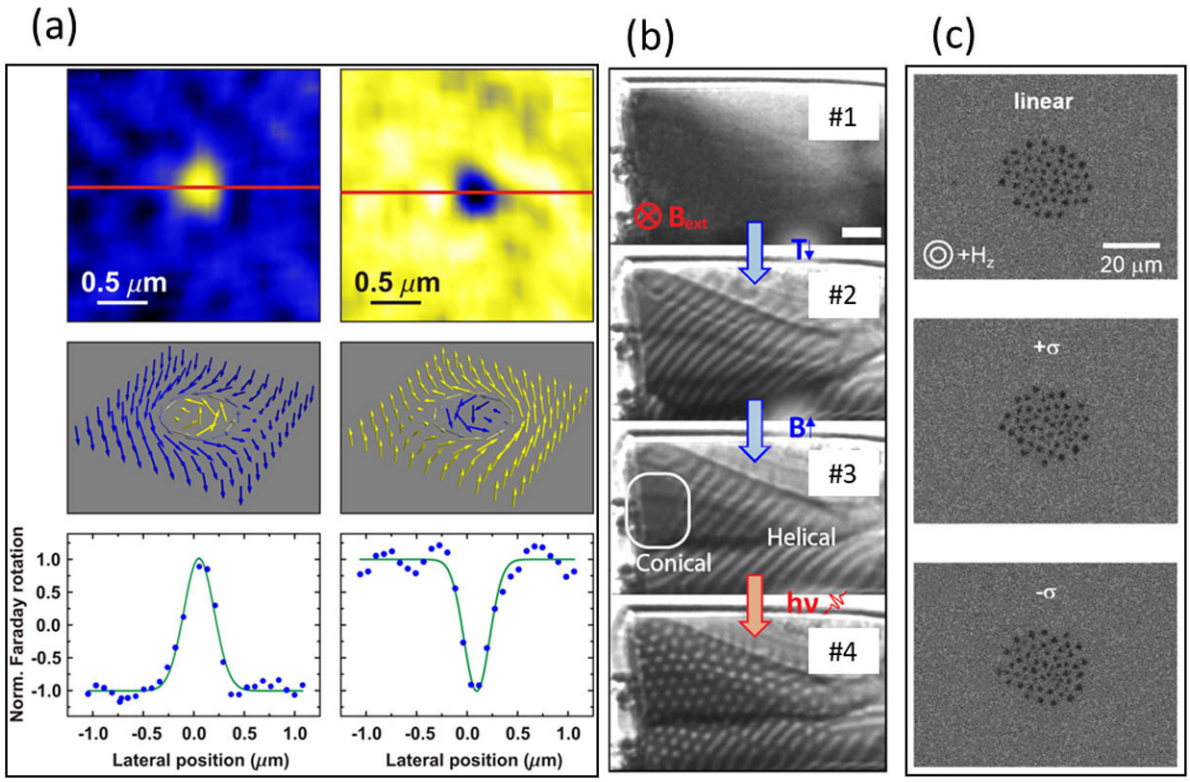


**Figure 8.** Writing of skyrmions by lasers. (a) Near-field Faraday rotation map showing magnetic domains induced in a thin TbFeCo film after single laser pulse irradiation, corresponding skyrmion spin textures, and profile (dots) of the Faraday rotation measured along the red lines. Reprinted with permission from [209], © 2013 American Physical Society. (b) Lorentz-Fresnel micrographs of the FeGe nanoslab. The skyrmion lattice in #4 is created by near-IR fs laser pulses. Scale bar is 250 nm. Reprinted with permission from [211], © 2018 by the American Physical Society. (c) Nucleated skyrmion bubbles from a saturated state ($+z$) by a 35 fs single laser pulse with a laser with linear polarization, right-handed $\sigma^+$ polarization, and left-handed $\sigma^-$ polarization. Reprinted with permission from [206]. Copyright © 2018, American Chemical Society.

a size of about 1 $\mu$m. Such a circular magnetic domain, which is stabilized by the dipolar interaction, can be seen as a achiral skyrmion bubble [208]. In 2013, Finazzi *et al* reported the creation of topological spin textures induced by ultrashort single laser pulses in an amorphous thin alloy film of $Tb_{22}Fe_{69}Co_9$ without the help of an external magnetic field [209], where both skyrmion and skyrmionium textures are created (see figure 8(a)). The lateral size of the laser-created magnetic skyrmions can be as small as 150 nm [209].

In 2017, Fujita and Sato theoretically studied the ultrafast creation of skyrmion and skyrmionium textures by applying a vortex laser beam [68], where the switching of magnetization in either a ferromagnetic or antiferromagnetic background is a result of the laser-induced non-uniform temperature. In 2018, Yang *et al* numerically studied the manipulation of skyrmions by an all-photonic orbital angular momentum transfer mechanism [210]. In the same year, as shown in figure 8(b), the laser-induced writing and deleting of skyrmions in the prototypical itinerant chiral magnet FeGe was experimentally realized by Berruto *et al* [211], where the writing and deleting speed was found to be controlled by the cooling rate following the laser-induced temperature increase. Je *et al* also experimentally demonstrated the laser-induced creation of disordered hexagonal skyrmion bubble lattices from a ferromagnetic background in an ultrathin $Ta/Fe_{72}Co_8B_{20}/TaO_x$ trilayer film at room temperature (see figure 8(c)), where the density of skyrmion bubbles was controlled by the laser fluence [206]. Such an experiment suggests that the skyrmion bubbles and bubble lattices can possibly be manipulated by lasers in a controlled manner.

Apart from the writing and deleting of skyrmions, magnetic skyrmions can be excited to different modes by optical methods. For example, Ogawa *et al* reported the laser-induced collective excitation modes of the skyrmion phase in an insulating chiral magnet $Cu_2OSeO_3$ [212], including the rotation mode, breathing mode, and several additional spin precession modes.

### 2.5. Imprinting

Skyrmion-like magnetic vortex domains, which is stabilized by geometrical constrains, can also be created by means of nanoimprinting even in the absence of DM interactions. As shown in figure 9(a), in 2013, Sun *et al* proposed a method for the creation of a skyrmion lattice based on a combination of a perpendicularly magnetized CoPt film and nanopatterned arrays of magnetic vortices that are geometrically confined within Co nanodisks [128]. Such a method is similar to the exchange spring model [213], where the spin textures in a soft phase (i.e. corresponding to the magnetic vortex in Co nanodisk) can be imprinted into the hard phase (i.e. corresponding to the CoPt film) due to the interlayer exchange coupling between the soft and hard phases. In principle, the created skyrmion lattice (see figure 9(b)) can be stabilized in

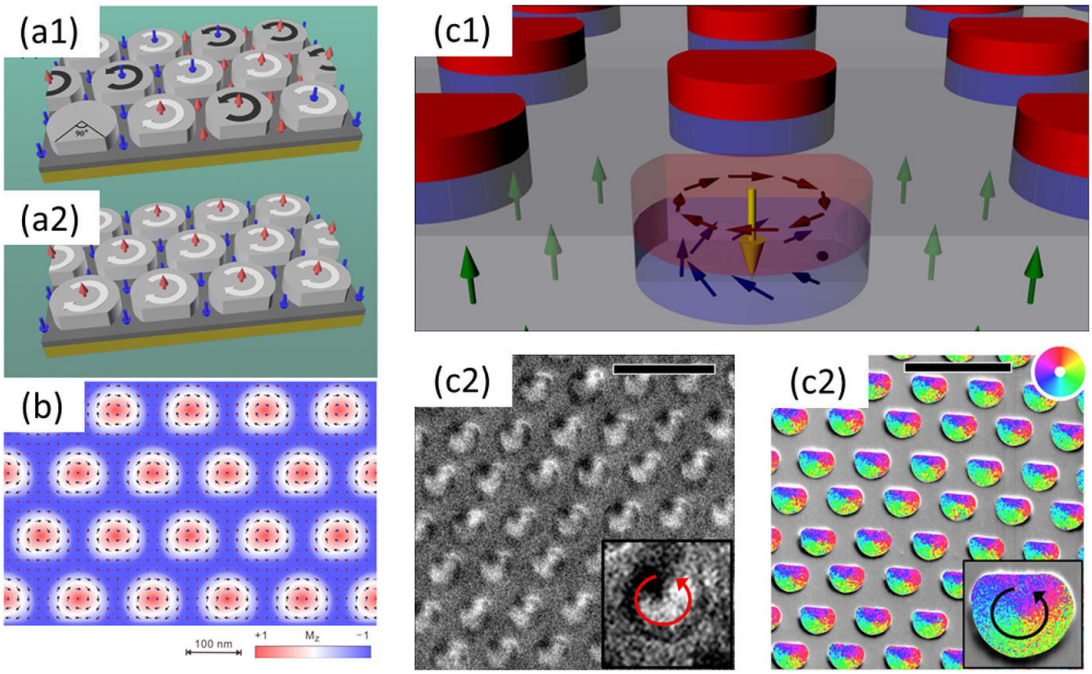


**Figure 9.** Writing of skyrmions by imprinting. (a) and (b) The theoretical proposal for creating the 2D skyrmion crystal. (a1) Ordered arrays of magnetic submicron disks are prepared on top of a film with perpendicular anisotropy. The arrows represent the magnetization orientation of the local moments. (a2) Skyrmion lattice creation with the field treatment. (b) Top view of magnetic configuration of the CoPt layer in a calculated artificial skyrmion crystal. (a) and (b) are reprinted with permission from [128], © 2013 American Physical Society. (c) Imprinted artificial skyrmion lattices at room temperature. (c1) Illustration of the hybrid structure consists of Co dots (red) on top of Co/Pd PMA underlayer (grey) where the in-plane spin texture of the Co dots (purple arrows) is imprinted into an irradiated Co/Pd region (light blue) underneath the dots (tilted blue arrows). Remanent-state (c1) MFM and (c2) SEMPA (superimposed onto a scanning electron microscopy image of the dots) images, after saturating the dots in an in-plane field parallel to the flat edge of the dots to the right, indicate circularity control. Scale bar, 2 mm. A key to the magnetization winding direction is shown in the insets. Reprinted with permission from [127]. CC BY 4.0.

a wide temperature and field range, even at room temperature, zero magnetic field, and in the absence of the DM interaction.

In 2015, Fraerman *et al* experimentally observed the creation of skyrmions in a perpendicularly magnetized Co/Pt multilayer film via the imprinting method [214], where the Co/Pt multilayer film is exchange-coupled with a Co nanodisk with the vortex state. In the same year, by using the transmission soft x-ray microscopy, Streubel *et al* experimentally studied the dynamics of imprinted skyrmion textures and found that skyrmionium textures can also be created by imprinting a magnetic vortex from the soft Py layer into the hard Co/Pd layer in the presence of reasonable interlayer exchange coupling [215]. The imprinting skyrmion lattice with controlled circularity and polarity as ground state at room temperature was also experimentally realized by Gilbert *et al* [127], where the magnetic vortex state in Co nanodots were imprinted into the Co/Pd underlayer with PMA (see figure 9(c)). On the other hand, Del-Valle *et al* theoretically demonstrated the possibility to imprint skyrmions in thin films by superconducting vortices [216].

In 2018, Sun *et al* numerically studied the stability and skyrmion Hall effect (SkHE) of magnetic skyrmions in the exchange-coupled system [217], which was used for the creation of skyrmions via imprinting effect in previous reports. They found that the stability of the skyrmion state can be enhanced due to the coupling between skyrmions in the thin film and the vortices in the capping nanodisks. At the same time, the capping nanodisks also act as attracting centers so that the SkHE can be effectively suppressed. The SkHE is a phenomenon related to the topology of skyrmion structures [26, 218, 219], which may be detrimental for the in-line motion of skyrmions. We will discuss the SkHE in detail in section 4.

In this section, we have reviewed a series of methods for writing and deleting skyrmions in magnetic materials. From the viewpoint of practical applications, it is desirable to use the spin-polarized electric current to control the generation/deletion of skyrmions, which can be integrated into transistor-based conventional complimentary metal-oxide semiconductor (CMOS) scheme. Spin currents can be rather easily generated either by using a polarizer layer via spin-filtering effect or by using high spin–orbit coupling material with relatively large spin Hall effect (or interfaces with large Rashba effect), which have been extensively explored for the last few years. Such a heavy metal/ferromagnet heterostructure are also known to generate certain DM interaction and PMA to stabilize skyrmions. However, the method utilizing electric excitation often suffers from inevitable current-induced Joule heating and leads to a large power consumption, therefore the electric field and laser could also be alternative methods for writing and deleting skyrmions in a low-energy manner in the future.

**Table 2.** List of the representative imaging techniques for the observation of magnetic skyrmions.

| Methods | Spatial resolution | Advantages | Best used for | Reference |
|---|---|---|---|---|
| LTEM | ~1 nm | High resolution<br>Easy access | Thin chiral magnets with nanoscale Bloch-type skyrmions | [102, 109, 220–225] |
| DPC-STEM | ~1 nm | High resolution<br>No post imaging process | Thin chiral magnets with nanoscale Néel/Bloch-type skyrmions | [111, 113] |
| SP-STM | Single atom | Ultrahigh resolution down to atomic scale | Crystalline chiral magnets with extremely small skyrmions | [106, 195, 226] |
| XMCD-PEEM | ~25 nm | In-plane spin resolution | Surface magnetic skyrmions | [120, 174] |
| STXM | ~25 nm | Easy magnetic/electric excitation<br>Dynamics imaging (~70 ps) | Skyrmions in buried magnetic multilayers accompanying excitations | [29, 36, 227] |
| SPLEEM | ~10 nm | In-plane spin resolution<br>High surface sensitivity | *In situ* deposited surface magnetic skyrmions | [125] |
| X-ray holography | ~10 nm | Drift-free technique<br>Dynamics imaging (~70 ps) | Nanoscale skyrmions in buried magnetic multilayers | [35] |
| MOKE | ~1 $\mu$m | Easy access and custom modification | >1 $\mu$m skyrmions | [116, 148, 160, 197, 228] |

LTEM, Lorentz transmission electron microscopy; DPC-STEM, differential phase contrast scanning transmission electron microscopy; SP-STM, spin-polarized scanning tunneling microscopy; XMCD-PEEM, photoemission electron microscopy combined with x-ray magnetic circular dichroism; STXM, scanning transmission x-ray microscopy; SPLEEM, spin polarized low-energy electron microscopy; MOKE, magneto-optical Kerr effect microscopy

## 3. Reading skyrmions

### *3.1. Microscopy imaging of magnetic skyrmions: x-ray, TEM, SPM, MOKE*

The manipulation of magnetic skyrmions as information carriers in device applications requires the precise tracking of their locations and dynamic behaviors. Hence, the efficient reading of skyrmions in real space is an important task that needs to be realized in a reliable manner with high enough on/off ratio. A lot of state-of-art microscopy magnetic imaging techniques have been used to observe the real-space profiles of skyrmions in laboratories for the purpose of studying their static and dynamic properties (see table 2) [29, 33, 35, 36, 102, 106, 109, 111, 116, 120, 121, 125, 148, 160, 174, 195, 197, 220–233]. However, as a part of the information write-in/read-out system, electrical reading scheme is a prerequisite for any skyrmion-based information storage and computing device applications. Some methods were purposed to read and detect skyrmions in device applications, such as by using the MTJ or reading skyrmion-induced Hall voltages. In this section, we first review recent progress on the real-space imaging/reading of skyrmions in laboratories.

The microscopy imaging of magnetic skyrmions in real space is very important for both theoretical and applied reasons. From the theoretical point of view, the imaging of the in-plane and out-of-plane spin textures in real space can directly identify the topological nature of a skyrmion. For example, one may calculate the topological charge based on the detailed in-plane spin texture of a skyrmion, including the vorticity number $Q_v$ and helicity number $Q_h$. Moreover, some of techniques offer sub-ns temporal resolution along with real-space magnetization imaging, which plays an important role to understand the ultrafast dynamic properties of skyrmions, e.g. excitation modes.

The real-space imaging of a 2D skyrmion lattice, which consists of many Bloch-type skyrmions, was first realized in a thin film of $Fe_{0.5}Co_{0.5}Si$ by using the LTEM in 2010 [102]. Later, skyrmion lattices in thin films of FeGe [41, 103, 220–222], $Cu_2OSeO_3$ [109, 192, 234], MnSi [223, 235], $Mn_{1-x}Fe_xGe$ [224], and Fe-Gd alloy [225] were also observed by using the LTEM as discussed in section 1.2. The LTEM is a particularly useful tool for observing the magnetization lying in the film plane, e.g. Bloch-type skyrmions, as the Lorentz interaction is non-vanishing when the magnetic induction component is perpendicular to the electron beam, which will deflect the electron beam [236]. Although typical Frensel-mode LTEM measurement cannot directly observe Néel-type magnetic configurations at zone-axis mode due to the cancellation of magnetic inductions, the observation of Néel-type magnetic domains and skyrmions has also been demonstrated using LTEM by tilting sample plane against beam direction or using off-focused images [237, 238]. More recently, as noted in section 1.2. aberration-corrected DPC-STEM imaging technique has also been introduced [111, 239, 240] and used to directly image magnetic textures including skyrmions [111, 113].

The SP-STM can also be used to measure nanometer-scale magnetic textures (see table 2). In 2013, Romming *et al* observed nanoscale isolated skyrmions in a PdFe bilayer on Ir(1 1 1) by using SP-STM [106]. The field-dependent size and shape of single isolated skyrmions were then also identified by using the SP-STM [226]. The magnetic properties of nanoscale isolated skyrmions discovered in PdFe/Ir bilayers were also experimentally and theoretically investigated by Leonov *et al* in 2016 [230]. In 2017, Hsu *et al* further realized

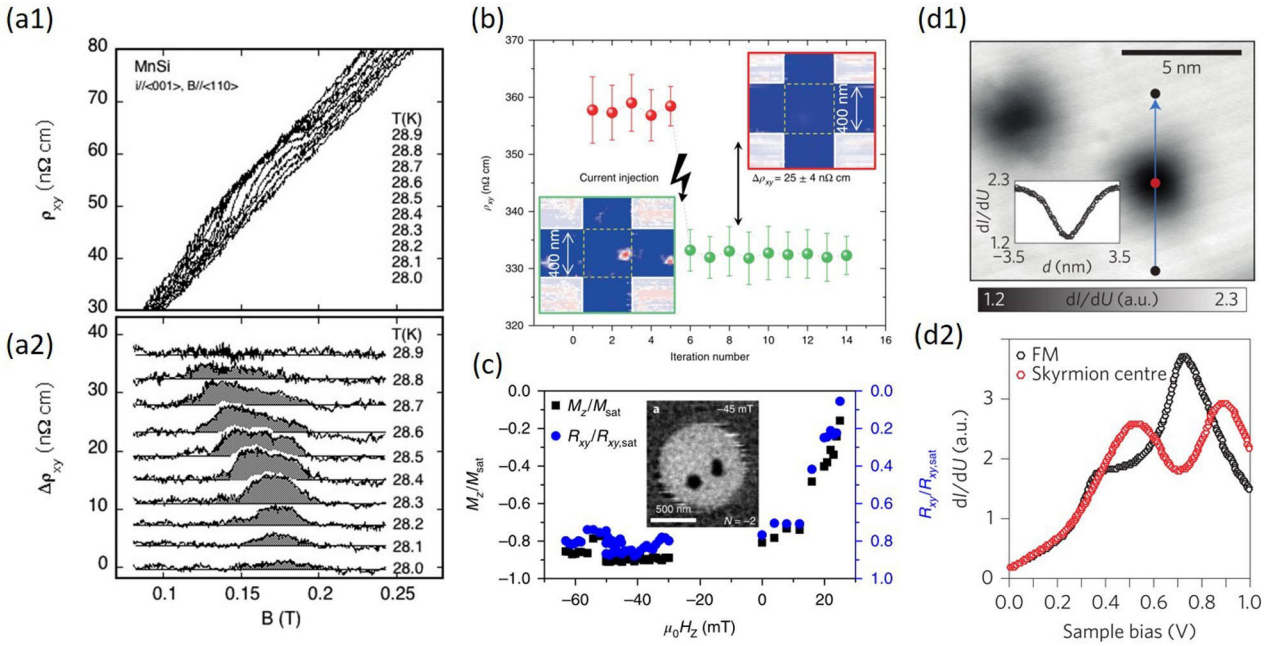


**Figure 10.** Electrical reading of magnetic skyrmions by using the THE and MTJ. (a) THE in the A phase of MnSi. (a1) Hall resistivity $\rho_{xy}$ near Tc in the temperature and field range of the A phase. (a2) Additional Hall contribution $\rho_{xy}$ in the A phase. Data are shifted vertically for better visibility. Reprinted with permission from [242]. Copyright © 2009 The American Physical Society. (b) THE in skyrmion phase of MnSi. (b) Variation in Hall due to a single skyrmion. Hall resistivity shows a change of 25 nΩ cm associated with the single-skyrmion formation. The insets are MFM images. Reprinted from [253]. Copyright © 2018 Macmillan Publishers Limited, part of Springer Nature. With permission of Springer. (c) The normalized Hall resistance $R_{xy}/R_{xy,sat}$ and the extracted $M_z/M_{sat}$. The inset is the XMCD image of two skyrmions at −45 mT. Reprinted from [254]. Copyright © 2018 Macmillan Publishers Limited, part of Springer Nature. With permission of Springer. (d) Electrical detection of magnetic skyrmions by tunnelling non-collinear magnetoresistance. (d1) The signal change caused by the non-collinear magnetoresistance d*I*/d*U* map of two skyrmions in PdFe/Ir(1 1 1); the inset presents a profile along the arrow. (d2) The d*I*/d*U* tunnel spectra in the centre of a skyrmion (red) and outside the skyrmion in the FM background (black). a.u., arbitrary units. Reprinted from [256]. © 2015 Macmillan Publishers Limited. With permission of Springer.

and observed the electric-field-induced switching of single isolated skyrmions in a Fe triple layer on Ir(1 1 1) using the SP-STM [195].

Recently years, various microscopy methods using x-ray radiation were used to as a powerful tool to image ultra-small spin textures and ultra-fast spin dynamics (see table 2). In 2014, Li *et al* observed the imprinted skyrmions by using the element-specific XMCD and PEEM measurements [174]. In 2016, Moreau-Luchaire *et al* realized additive DM interaction in Ir/Co/Pt multilayers at room temperature, where isolated skyrmions with dimeters below 100 nm were directly observed by using the STXM [29]. In the same year, Boulle *et al* observed room-temperature skyrmions in sputtered ultrathin Pt/Co/MgO multilayers by using the photoemission electron microscopy combined with XMCD-PEEM [120], which identified the Néel-type nature of the skyrmion chirality. Woo *et al* also observed room-temperature skyrmions and revealed their current-driven dynamics in Pt/Co/Ta and Pt/CoFeB/MgO multilayers by using the high-resolution STXM [33, 121]. More recently, Woo *et al* directly imaged ferrimagnetic skyrmions in GdFeCo films [227] and observed the writing and deleting dynamics of a ferrimagnetic skyrmion by using the time-resolved x-ray microscopy [36].

Indeed, skyrmion textures can also be directly observed by other methods. For example, by using the SPLEEM, Chen *et al* imaged magnetic skyrmions in *in situ* grown Fe/Ni bilayers in 2015 [125]. Moreover, x-ray holography offers a unique drift-free diffractive magnetic imaging characteristic with sub-10 nm spatial resolution (see table 2), and was used to demonstrate ultra-small skyrmions and their current-driven dynamics [35, 241]. Recently, mainly inspired by easy accessibility, a number of experimental studies reported the direct observation of skyrmions by using the polar magneto-optical Kerr effect (MOKE) microscopy [116, 148, 160, 197, 228]. For example, the first observation of room temperature skyrmions and the creation of skyrmions from stripe domain walls was directly imaged by using the MOKE microscopy [116]. The spatial resolution of MOKE microscopy is rather limited by the wavelength of the light used for the observation, which usually lead to a resolution of a micrometer (see table 2).

### *3.2. Electrical reading 1: topological Hall resistivity measurements*

The realization of reading skyrmions in an electrical manner is a crucial step toward the device applications based on skyrmions. A promising method to read skyrmions electrically is by harnessing the topological Hall effect (THE) of magnetic skyrmions [162, 242–244]. The THE arises from the Berry phase in a magnet with smoothly varying magnetization [245–247], which can occur due to the Berry curvature induced by magnetic skyrmions [162, 244], because conduction electrons must adiabatically obey the unique spin textures of magnetic skyrmions when the *s-d* coupling is strong [2].

Namely, a prominent feature of a skyrmion is that it produces emergent magnetic field, which originates from the solid angle subtended by the spins called scalar spin chirality. The topological property of skyrmion guarantees that the total flux generated by one skyrmion is one flux quantum, $h/e$. The size of a skyrmion is ~1 nm for atomic Fe layer on Ir(1 1 1) surface [8], ~3 nm for MnGe [244], ~18 nm for MnSi [243], and ~70 nm for FeGe [103]. The corresponding emergent magnetic field is ~4000 T, 1100 T, 28 T, and 1 T, respectively. In fact, the THE is a manifestation of emergent magnetic field, where the Hall effect occurs in the presence of skyrmions [107, 242–244]. Moreover, the quantized THE has been theoretically proposed [248].

In 2009, Neubauer *et al* [242] experimentally studied the THE of the skyrmion crystal phase in MnSi, where a district anomalous contribution to the Hall effect in the skyrmion crystal phases was identified (see figure 10(a)). Such a topological Hall contribution has an opposite sign to the normal Hall effect, and its prefactor is consistent with the skyrmion density in a quantitative manner. In 2012, Schulz *et al* experimentally measured the temperature-dependent the Hall resistivity in MnSi under different strengths of applied electric current [107], where the depinning and motion of skyrmions were confirmed by direct observation of the emergent electric field of skyrmions. In the same year, magnetic skyrmions in epitaxial B20 FeGe(1 1 1) thin films was also identified by measuring the topological Hall resistivity due to the skyrmion textures [162].

In 2014, Yokouchi *et al* studied the stability of skyrmions in epitaxial thin films of $Mn_{1-x}Fe_xSi$ with various thicknesses and compositions by measuring the topological Hall resistivity as functions of temperature and applied field [249]. The topological and thermodynamic stability of skyrmions in MnSi was also studied by measuring topological Hall resistivity [250]. In 2016, Matsuno *et al* studied the interface DM interaction in epitaxial bilayers consisting of ferromagnetic $SrRuO_3$ and paramagnetic $SrIrO_3$ by measuring the THE [251], which demonstrated that the skyrmion phase is stabilized by interface-induced DM interaction. In 2017, Liu *et al* demonstrated the creation and annihilation of skyrmion-induced THE in Mn-doped $Bi_2Te_3$ topological insulator films [252].

Although the electrical measurements induced by THE were mostly conducted with crystalline materials where the existence of skyrmion lattice provides large collective electrical signal, recent reports by Maccariello *et al* [253] (see figure 10(b)) and Zeissler *et al* [254] (see figure 10(c)) demonstrated the electrical Hall measurements of individual room temperature skyrmion in sputter-grown films and nanostructures. However, the two demonstrations report large difference in the effective magnitude of topological Hall contribution from a single room-temperature skyrmion, which may need further investigations. In 2019, Shao *et al* also experimentally observed the THE at above room temperature in a bilayer heterostructure composed of a magnetic insulator (thulium iron garnet, $Tm_3Fe_5O_{12}$) in contact with a metal (Pt).

On the other hand, it is noteworthy that, in 2016, Hamamoto *et al* theoretically proposed a method to detect the skyrmion position in a pure electrical way by measuring the Hall conductance in a constricted geometry [255], where the Hall conductance is found to have a peak when a skyrmion is located at the lead position, while it reduces when a skyrmion is away from the lead.

### 3.3. Electrical reading 2: MTJ

Recently, theoretical and experimental studies suggest the efficient large on/off ratio detection of skyrmions by measuring the magnetoresistance [256–259], i.e. by using and embedding MTJ sensors in skyrmion-based devices and circuits.

In 2015, Du *et al* experimentally identified the formation of clusters of individual skyrmions by measuring the magnetoresistance in MnSi nanowires [229, 257], where the number of skyrmions was revealed by quantized jumps in the magnetoresistance curves. In the same year, Hanneken *et al* [256] proposed a pure electrical reading scheme of nanoscale skyrmions by measuring the tunnelling non-collinear magnetoresistance (see figure 10(d)). The electric conductance signal due to the non-collinear magnetoresistance is sensitive to the local magnetic environment, and can directly detect and distinguish the collinear and non-collinear magnetic states without using a magnetic electrode [256, 259]. Such a mechanism is different from the well-known giant magnetoresistance (GMR) [260], and tunnel magnetoresistance (TMR) effect [261], which are dependent of local magnetization directions in two magnetic layers. On the other hand, the electric reading of single isolated skyrmions in a current-perpendicular-to-plane geometry was also studied by Crum *et al* from first principles [262], which is based on the effect of tunnelling spin-mixing magnetoresistance.

In 2017, Tomasello *et al* theoretically proposed a protocol for the electrical reading of a magnetic skyrmion by measuring the change of the TMR signal via a point-contact MTJ in a three-terminal device [258]. Similar method can also be used to read other magnetic solitons, such as magnetic bubbles, in racetrack-type devices [263]. Most recently, numerical simulations suggested that skyrmions can be directly created and detected in a MTJ with DM interaction in a pure electrical manner [264], which shows the possibility of designing the skyrmion-MTJ-based multibit storage and artificial neural network computation. In 2019, Penthorn *et al* found that a single skyrmion with a diameter smaller than 100 nm can lead to a change in MTJ resistance of almost 10% [265], which is enough for electrical detection. In the same year, Kasai *et al* also experimentally realized the electrical detection of skyrmions in MTJ [266], where the skyrmion diameter is about 200 nm.

## 4. Processing skyrmions

### 4.1. Current-driven dynamics of magnetic skyrmions

As briefly mentioned in section 1.2, Jonietz *et al* [78] observed the rotation of skyrmions arising from the interplay of current-induced spin-torque effects and thermal gradients. They found that the current density required to create observable STTs in skyrmion lattice phase of MnSi exceeds an ultralow threshold of ~$10^6$ A $m^{-2}$, which

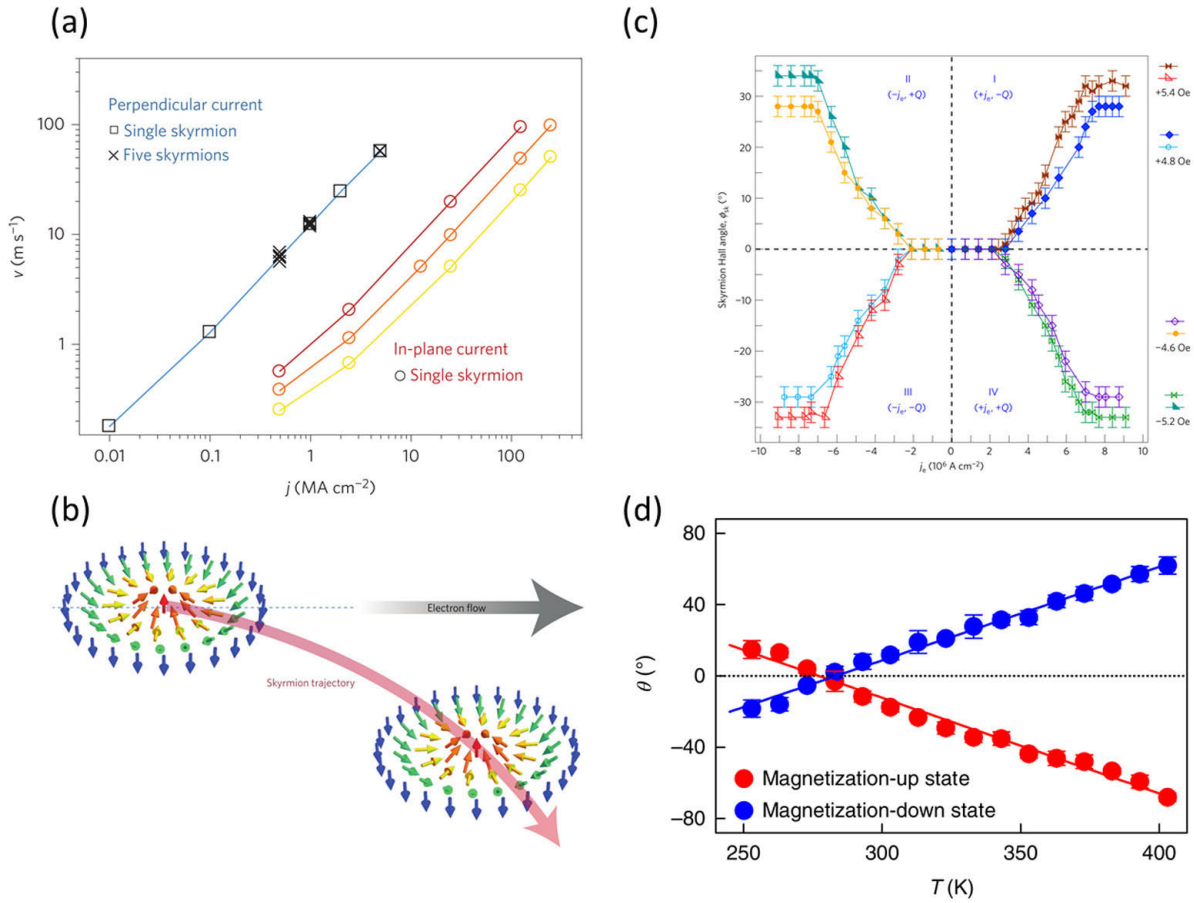


**Figure 11.** (a) Skyrmion velocity $v$ as a function of current density $j$ for in-plane currents with different values of the non-adiabaticity parameter $\beta$ (0.15, 0.30 and 0.60 in yellow, orange and brown lines and circles, respectively) and for vertical currents (blue line, squares for isolated skyrmion). Reprinted from [133]. © 2013 Macmillan Publishers Limited. All rights reserved. With permission of Springer. (b) Schematic of the skyrmion Hall effect. The spin textures of skyrmions are indicated by the arrows. Reprinted from [218]. © 2016, Springer Nature. With permission of Springer. (c) Phase diagram of the skyrmion Hall angle as a function of current density/sign of topological charge obtained by tracking the motion of several tens of skyrmions. Reprinted from [270]. © 2017 Macmillan Publishers Limited. All rights reserved. With permission of Springer. (d) Current-driven elongation of magnetic bubble in GdFeCo/Pt films as a function of temperature. Reprinted from [269]. © 2019 Springer Nature Limited. With permission of Springer.

is over five orders of magnitude smaller than those typically applied in experimental studies on current-driven magnetization dynamics in nanostructures (~$10^{11}$ A $m^{-2}$). These results indicate that the current-driven motion of magnetic skyrmions could be of low-energy consumption. Therefore, the spin-polarized current serves as an effective method for driving and processing skyrmions. However, it should be noted here that the skyrmion velocity is proportional to the driving current density, and practical skyrmion-based applications may require a skyrmion speed much larger than that induced by the very low depinning current density. At the same time, the energy consumption of skyrmion-based application will increase with increasing magnitude of the current.

In 2011, Everschor *et al* [180] theoretically proposed that skyrmions can be driven by the spin-polarized current via STTs. The translational mode and rotational mode can be induced by STTs. Using the method of Thiele [267], they projected the magnetization dynamics equation, i.e. the Landau–Lifshitz–Gilbert (LLG) equation onto the translational mode to derive an effective equation of motion—Thiele equation,

$$\boldsymbol{G} \times (\boldsymbol{v}_{\mathrm{s}} - \boldsymbol{v}_{\mathrm{d}}) + \mathcal{D}\,(\beta \boldsymbol{v}_{\mathrm{s}} - \alpha \boldsymbol{v}_{\mathrm{d}}) = \boldsymbol{0}, \tag{15}$$

where $\boldsymbol{G}$ is the gyrocoupling vector and $\mathcal{D}$ is the dissipative tensor. $\boldsymbol{v}_{\mathrm{s}}$ is the velocity of the conduction electrons and $\boldsymbol{v}_{\mathrm{d}}$ is the drift velocity of skyrmions.

In 2011, Zang *et al* [26] considered the additional damping term in the LLG equation and theoretically proposed the skyrmion Hall effect, where the skyrmion shows a transverse velocity when it is driven by the spin current. In 2013, the current-induced creation and motion of skyrmions are numerically demonstrated by Iwasaki *et al* [108, 132] and Sampaio *et al* [133] (see figure 11(a)). Iwasaki *et al* investigated the current-induced motion of skyrmions in the presence of geometrical boundaries [108, 132]. In a channel with a finite width, the transverse confinement results in steady-state characteristics of the skyrmion velocity as a function of current density, which are similar to those of domain walls in ferromagnets. Sampaio *et al* [133] considered two cases. One is the case of spin-polarized current injected under a current-in-plane geometry. The skyrmion is driven by the adiabatic and non-adiabatic STTs,

$$\boldsymbol{\tau}_{\mathrm{adiab}} = u\boldsymbol{m} \times \left(\frac{\partial \boldsymbol{m}}{\partial x} \times \boldsymbol{m}\right), \boldsymbol{\tau}_{\text{non-adiab}} = \beta u \left(\boldsymbol{m} \times \frac{\partial \boldsymbol{m}}{\partial x}\right), \tag{16}$$

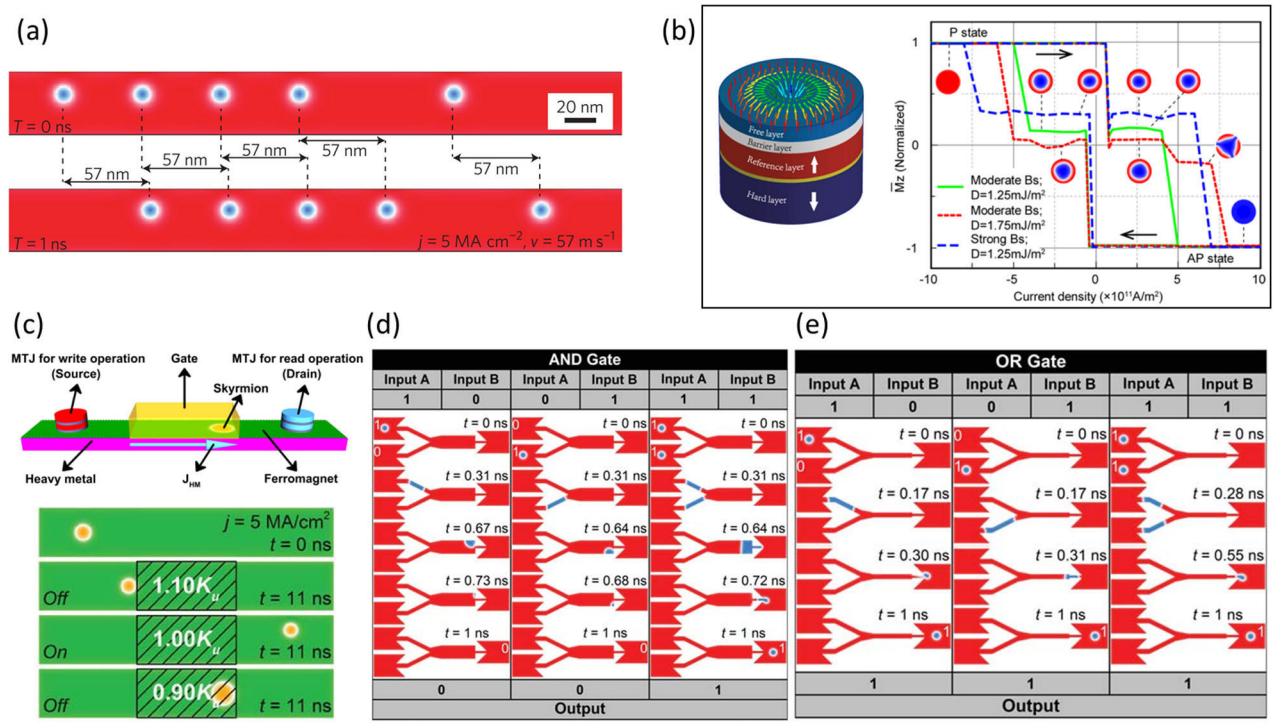


**Figure 12.** (a) The illustration of skyrmionic racetrack memory, in which the skyrmions exhibit the same velocity. The colour scale shows the out-of-plane component of magnetization, $m_z$. Reprinted from [1] © 2013 Macmillan Publishers Limited. All rights reserved. With permission of Springer. (b) Illustration of a skyrmion-based MTJ and magnetization–current hysteresis loops obtained by simulating the switching of $R = 60$ nm MTJs with different $D$ and stray field $B_S$. Reprinted with permission from [264]. Copyright © 2018, American Chemical Society. (c) The top-view of the nanotracks under different spin current density $j$ as well as different voltage-controlled PMA $K_{uv}$. Initial state: both the electric field and spin current are turned off; the skyrmion keeps its position on the left side of the nanotrack. Off state: both the electric field and spin current are turned on. The spin current drives the skyrmion moving toward the right, while the electric field, which results in the change of PMA in the voltage-gated region, leads to the termination of the skyrmion when it approaches the voltage-gated region. On state: the electric field is turned off but the spin current is turned on. The skyrmion driven by the spin current passes the voltage-gated region and reaches the right side of the nanotrack. Reprinted with permission from [141]. CC BY 4.0. (d) Skyrmion logical AND operation. The skyrmion represents logical 1, and the ferromagnetic ground state represents logical 0. Left panel, the basic operation of AND gate $1 + 0 = 0$. Middle panel, the basic operation of the AND gate $0 + 1 = 0$. Right panel, the basic operation of the AND gate $1 + 1 = 1$. (e) Skyrmion logical OR operation. The skyrmion represents logical 1, and the ferromagnetic ground state represents logical 0. Left panel, the basic operation of OR gate $1 + 0 = 1$. Middle panel, the basic operation of the OR gate $0 + 1 = 1$. Right panel, the basic operation of the OR gate $1 + 1 = 1$. (d) and (e) are reprinted with permission from [140]. CC BY 4.0.

where $u = \left|\frac{\gamma_0 \hbar}{\mu_0 e}\right| \frac{jP}{2M_S}$ with the reduced Planck constant $\hbar$, the electron charge $e$, the applied current density $j$, the spin polarization rate $P$, and the saturation magnetization $M_S$. is the electron velocity and $\beta$ is the non-adiabaticity factor. The other is the case driven by a vertical spin current, which can be obtained either by using a MTJ or by utilizing the spin Hall effect. The skyrmion is driven by the induced in-plane and out-of-plane torques,

$$\boldsymbol{\tau}_{\mathrm{IP}} = \frac{u}{t}\boldsymbol{m} \times (\boldsymbol{m}_{\mathrm{p}} \times \boldsymbol{m}), \tau_{\mathrm{OOP}} = -\xi\frac{u}{t}(\boldsymbol{m} \times \boldsymbol{m}_{\mathrm{p}}), \quad (17)$$

where $t$ is the film thickness and $\xi$ is the amplitude of the out-of-plane torque relative to the in-plane one and $\boldsymbol{m}_{\mathrm{p}}$ is the current polarization vector. The numerical results obtained by Sampaio *et al* [133] demonstrated that the efficiency of the vertical spin current to drive skyrmions is much higher than that of the in-plane current.

In 2016, Woo *et al* [121] experimentally demonstrated the stabilization of magnetic skyrmions and their current-driven motion in thin transition metal ferromagnets at room temperature, where a train of individual skyrmions can be driven into motion at speeds exceeding 100 m $s^{-1}$ by current pulses ($5 \times 10^{11}$ A $m^{-2}$) in the Pt/CoFeB/MgO multilayers track. In 2017, Jiang *et al* [218] and Litzius *et al* [219] directly observed the SkHE (see figure 11(b)) in room-temperature experiments where skyrmions are driven by the current-induced SOTs. Like the charged particles in the conventional Hall effect, current-driven skyrmions acquire a transverse velocity component. As shown in figure 11(c), Jiang *et al* observed a linear dependence of the skyrmion Hall angle on the driving current density, which is possibly resulted by the pinning of skyrmions. They also changed the sign of the topological charge $Q$ and the electric current, and thus, a strong similarity between the conventional Hall effect of the electronic charge was found. Litzius *et al* also experimentally observed the dependency of the skyrmion Hall angle on the driving current density, while they suggested that this dependency is induced by the additional effect of the skyrmion deformation as well as the effect of the field-like SOT.

In 2017, Legrand *et al* [32] investigated the nucleation and spin-torque-induced motion of sub-100 nm skyrmions in Pt/Co/Ir trilayers, which enable additive DM interactions at the Pt/Co and Co/Ir interfaces [29]. In particular, they showed that

such small compact skyrmions can be nucleated by applying a uniform current directly into tracks and subsequently be driven into motion via SOTs.

In 2016, theoretical studies [155, 268] have predicted enhanced current-driven behaviors of antiferromagnetic skyrmions due to the elimination of SkHE. In 2018, Woo *et al* [36] experimentally investigated the skyrmion in ferrimagnetic GdFeCo multilayers, where the stabilization of ferrimagnetic skyrmions and their current-driven dynamics were demonstrated. The distinctive nature is that the SkHE is not totally eliminated in the ferrimagnetic system since the magnetization are different between two antiferromagnetically coupled underlying sub-lattices. Indeed, they demonstrated that the current-driven ferrimagnetic skyrmion shows a small, but non-zero SkHE. They further confirmed that ferrimagnetic skyrmions can move at a velocity of ~50 m $s^{-1}$ with reduced skyrmion Hall angle, $|\theta_{SkHE}|$ ~20°. In 2019, Hirata *et al* [269] experimentally demonstrated that the SkHE can be totally vanished at the angular momentum compensation temperature of a ferrimagnet (see figure 11(d)), i.e. when the ferrimagnet becomes antiferromagnet.

### 4.2. Information storage: racetrack memory and skyrmion-MTJ

In 2013, Fert *et al* [1] proposed that the skyrmion can be used to build the racetrack memory, which is based on the design of domain wall-based racetrack memory [271]. In the skyrmion-based racetrack memory, the information can be coded by the presence and absence of skyrmions, as shown in figure 12(a). In 2014, Tomasello *et al* [272] showed the technological advantages and limitations of the manipulation of Bloch-type and Néel-type skyrmions by spin currents generated in the ferromagnetic layer or in the heavy-metal substrate arising from the spin Hall effect. They found that the Néel-type skyrmion driven by the spin torques due to the spin Hall effect is a promising strategy for technological implementation of next-generation of skyrmion racetrack memories. In 2017, Yu *et al* experimentally demonstrated a room-temperature skyrmion shift device [273], which could serve as a basis for building a fully functional skyrmion-based racetrack memory.

In 2014, Zhou *et al* numerically demonstrated a current-driven reversible conversion between a skyrmion and a domain-wall pair in a junction geometry [182]. The information encoded in domain walls can be transformed into skyrmions, and then read out by transforming skyrmions back to domain walls after a functional control of the skyrmions. Such a hybrid device has the potential to outperform domain-wall racetrack memory because that it combined advantages of domain walls and skyrmions for spintronic applications.

In 2015, Zhang *et al* [274] numerically investigated the effects of skyrmion–skyrmion and skyrmion-edge repulsions on the feasibility of skyrmion-based racetrack memory. They suggested that the practicable spacing between consecutive skyrmionic bits is determined by the DM interaction helix length, i.e. $4\pi A/|D|$, where $A$ is the exchange constant and $D$ is the DM interaction constant. Further, they demonstrated that by fabricating a notched tip at the end of the nanotrack is an effective and simple method to avoid the clogging of skyrmionic bits, which also enables the elimination of useless skyrmionic bits beyond the reading element.

As discussed in section 4.1, when the skyrmion is driven into motion by a spin current, the trajectory of skyrmion bends away from the driving current direction due to the topological Magnus force [108, 155, 275], which is always perpendicular to the velocity. Such a SkHE may create an obstacle for the transportation of skyrmions. Consequently, the skyrmions may be destroyed by touching the nanotrack edges. In 2016, Zhang *et al* [276] theoretically proposed a antiferromagnetically exchange-coupled bilayer system, i.e. a synthetic antiferromagnetic bilayer nanotrack, in which the SkHE can be suppressed as the Magnus forces in the top and bottom layers are exactly cancelled. This system serves as a promising platform where skyrmions can move in a perfectly straight trajectory even at an ultra-fast processing speed. In 2017, Tomasello *et al* [277] investigated the performance of synthetic antiferromagnetic racetrack memory. They pointed out that two adjacent racetracks can be more closer as compared with the with single heavy metal/ferromagnet bilayer since the dipole interactions of the two antiferromagnetically coupled layers cancel each other and the disturbance is thus reduced significantly.

In 2016, Kang *et al* [278] also proposed a complementary skyrmion racetrack memory structure, in which the skyrmions can be selectively driven into two different nanotracks by using a voltage-controlled Y-junction. In such proposed structure, both data bits '0' or '1' are represented with the presence of a skyrmion, therefore improving the data robustness and clock synchronization. In 2018, a skyrmion-based multilevel device with tunneling magnetoresistance was proposed [264], in which a MTJ with stable intermediate states can be realized based on the skyrmionic states in the free layer (see figure 12(b)). This design may also facilitate the electrical detection of skyrmions. Most recently, the deterministic electrical switching from a ferromagnetic state to a skyrmion spin texture in the free layer of a MTJ was experimentally realized by Penthorn *et al* [265]. Kasai *et al* also experimentally realized the electrical detection of skyrmions in MTJ [266]. Although fully functional skyrmion-based racetrack memory has not been experimentally demonstrated yet, integrating above mentioned findings in a single device scheme may enable the realization of such skyrmion-based information storage devices.

### 4.3. Information computing: transistor-like devices and skyrmionic logic

In 2015, Zhang *et al* [141] proposed a skyrmion-based transistor-like functional device (see figure 12(c)), where a gate voltage can be used to switch on/off a circuit. The PMA in the gate region is locally controlled by an applied electric field due to the charge accumulations. For the ON state: the spin current is turned on but the electric field is turned off. The skyrmion driven by the spin current passes the voltage-gated region. For the OFF state: both the electric field and the spin current are turned on; the electric field changes the PMA in the voltage-gated region and creates an energy barrier, leading to the

termination of the skyrmion when it approaches the voltage-gated region. Zhang *et al* numerically demonstrated that the working conditions can be controlled by tuning the amplitude of applied electric field and spin current, while proving the scalability of this transistor-like device. In the same year, a similar idea on the control of skyrmion dynamics by a gate voltage was also proposed by Upadhyaya *et al* [142], which also suggests the transistor-like function of skyrmions. In 2017, Xia *et al* [279] numerically demonstrated the skyrmion-based transistor-like functional device also can be driven by spin waves and the working conditions can be adjusted by the amplitude and frequency of spin waves, as well as the applied voltage on the gated region. Later in 2018, Zhao *et al* [280] also numerically demonstrated the antiferromagnetic skyrmion transistor-like device based on strain manipulation.

In 2015, Zhang *et al* [140] theoretically proposed that skyrmions can be reproduced and merged in junction geometries based on the reversible conversion between skyrmions and domain walls [182]. They demonstrated that the logic AND (see figure 12(d)) and OR (see figure 12(e)) operations can be realized based on the duplication and merging of skyrmions. In their proposed skyrmionic logic devices, binary digit '0' corresponds to the absence of a skyrmion and binary digit '1' corresponds to the presence of a skyrmion. There are two input branches and one output branch in the device. The logic AND operations, '0' + '0' = '0', '0' + '1' = '0', '0' + '1' = '0', '1' + '1' = '1', can be implemented in the designed geometry. For example, '1' + '0' means that there is one skyrmion in input A and no skyrmion in input B. Under the driving force provided by the spin current, the skyrmion in branch A moves toward the output side. The skyrmion is first converted into a domain wall pair and the domain pair fail to convert into skyrmion in the wide Y-junction. Then, no skyrmion exists in the output branch. Thus, the logic operation '1' + '0' = '0' is thus realized. Similarly to the AND operation, the OR operation, '0' + '0' = '0', '0' + '1' = '1', '0' + '1' = '1', and '1' + '1' = '1', can also be implemented in a slightly modified geometry. For example, in the OR operation, '1' + '0' means that there is one skyrmion in input A and no skyrmion in input B. Under the driving force provided by the spin current, the skyrmion in branch A moves toward the output side. The skyrmion is first converted into a domain wall pair and the domain pair is then converted into skyrmion in the narrow Y-junction. Therefore, there is one skyrmion in the output branch finally, and the operation '1' + '0' = '1' is implemented.

Soon after the numerical demonstration of the first prototype of skyrmionic logic computing device, several works on skyrmion logic emerged. For example, in 2015, Zhang *et al* [281] designed the skyrmion-based NIMP, XOR, and IMP gates. In 2016, Xing *et al* [282] numerically demonstrated the NAND and NOR gates by using both domain walls and skyrmions. In 2018, Luo *et al* [283] numerically demonstrated logic functions including AND, OR, NOT, NAND, NOR, XOR, and XNOR in the ferromagnetic nanotrack by virtue of various effects including SOT, SkHE, skyrmion-edge repulsions, and skyrmion-skyrmion collision. However, it should be noted that the skyrmion-based Boolean logic operations have not yet been demonstrated in an experiment. The complex structures and the co-existence of the already proposed skyrmion logic gates as well as the precise control of the dynamic behaviors of skyrmions may be difficult to be realized in nanoscale dimensions at the current stage.

### *4.4. Bio-inspired computing: skyrmions for neuromorphic devices*

In 2017, Huang *et al* proposed that the skyrmion can be used to build a skyrmion-based artificial synapse device for neuromorphic computing. They numerically demonstrated the short-term plasticity and long-term potentiation functions based on skyrmions in a nanotrack. The synaptic weight of the proposed device can be strengthened/weakened by positive/negative stimuli, mimicking the potentiation/depression process of a biological synapse. Also, the resolution of the synaptic weight can be adjusted based on the nanotrack width and the skyrmion size. The merits of using skyrmions for such artificial synaptic device include several aspects. For example, the skyrmion structure can be regarded as a nanoscale rigid object due to its quasi-particle-like nature. Based on this feature, many nanoscale skyrmions can accumulate in a given device and controlled by external stimuli, of which the properties are approximately analogous to those of a biological synapse and could be used to build nanoscale computing devices with good variability and scalability [3, 106]. Moreover, the extremely low-threshold for skyrmion excitation [1, 78, 107, 108] may promise the reduced power consumption of skyrmion synapse-based neuromorphic computing, which is highly desired for such device to be used for massive parallel computations. Later in 2017, Li *et al* [145] presented a magnetic skyrmion-based artificial neuron device concept based on current-induced skyrmion motion in a nanotrack. The neuronal activity of a biologic neuron was realized with the tunable current-driven skyrmion motion dynamics of a single skyrmion. In 2018, Chen *et al* [284] also proposed a magnetic skyrmion-based device to emulate the core functionality of neurons and synapses for an all-spin spiking deep neural network. The synaptic weight can be adjusted by the number of skyrmions under the read MTJs, and the resolution can be improved by having multiple branches with various conductance ranges. Recently, utilizing current-induced skyrmion generation, motion, deletion and detection together in a single device scheme, Song *et al* experimentally demonstrated the basic operations of a magnetic skyrmion-based artificial synapse including *potentiation* and *depression*, and further demonstrated artificial skyrmion synapse-based neuromorphic pattern recognition computing using simulations [144].

Besides, in 2018, Prychynenko *et al* [147] proposed the skyrmion-based reservoir computing applications, in which a single skyrmion is embedded in a ferromagnetic ribbon. The reservoir computing was realized via a two-terminal device with nonlinear voltage characteristics originating from magnetoresistive effects. Most recently in 2019, Zázvorka *et al* experimentally demonstrated a thermal skyrmion diffusion-based signal reshuffling device [160]. In this work, using both experiment and simulation, Zázvorka *et al* uncovered the dynamics of thermally activated skyrmion diffusions

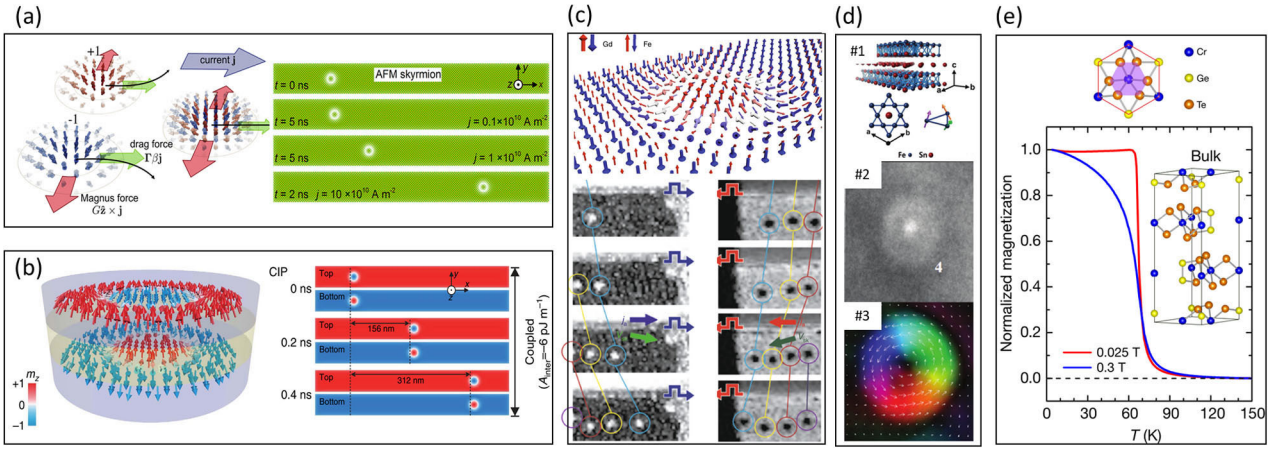


**Figure 13.** Skyrmions in potential novel materials. (a) The AFM Skyrmion is composed of two topological objects with opposite topological charge; hence, the Magnus force acts in opposite directions. The strong coupling between the sublattices leads to a perfect cancellation of the two opposing forces, and so, the AFM Skyrmion has no transverse motion. (a) left hand image reprinted with permission from [155], © 2016 American Physical Society. Right hand image reproduced from [268]. CC BY 4.0. (b) Illustration of a bilayer skyrmion in an AFM-coupled nanodisk and the current-induced motion of skyrmions in the top and bottom FM layers of an AFM-coupled bilayer nanotrack. Reprinted from [276]. CC BY 4.0. (c) Schematic of antiferromagnetically exchange-coupled ferrimagnetic skyrmion on a magnetic track as observed in GdFeCo films and sequential STXM images showing the responses of multiple ferrimagnetic after injecting unipolar current pulses. Reprinted from [227]. Copyright © 2018, Springer Nature. With permission of Springer. (d) Skyrmionic bubbles in a frustrated kagome $Fe_3Sn_2$ magnet imaged using LTEM at 300 K. Reprinted with permission from [129]. John Wiley & Sons. © 2017 WILEY-VCH Verlag GmbH & Co. KGaA, Weinheim. (e) Temperature-dependent magnetization of the bulk crystal $Cr_2Ge_2Te_6$ measured by SQUID under fields of 0.025 T (red) and 0.3 T (blue). The inset shows the crystal structure of $Cr_2Ge_2Te_6$. Bulk $Cr_2Ge_2Te_6$ has a layered structure with interlayer vdW spacing of 3.4 Å. Reprinted from [305]. © 2017 Macmillan Publishers Limited, part of Springer Nature. All rights reserved. With permission of Springer.

using low-pinning multilayer materials, and further analysis revealed the possibility of using skyrmions for an efficient future probabilistic computing device [160].

## 5. Summary and outlook

### *5.1. Potential novel materials: antiferromagnet, synthetic antiferromagnet, ferrimagnet, frustrated magnet and 2D van der Waals magnet*

In this section, we give an outlook on magnetic skyrmions in terms of potential novel materials and other possible topological spin textures. From the viewpoint of possible skyrmion-hosting materials, many previous works have focused on the ferromagnet, which is the most commonly known and important class of magnetic materials that has been employed in commercial products, such as modern hard disk drives. There are also two other technologically promising classes of magnetic materials, namely, the ferrimagnets and antiferromagnets, which can be used to host skyrmions. For example, several theoretical studies have demonstrated that skyrmion textures can be stabilized and manipulated in antiferromagnets [155, 268, 285–287].

For the last few years, antiferromagnetic spintronics has received much attention from the magnetism community as the antiferromagnetic materials have several intrinsic properties that may lead to a better performance of spin dynamics suitable for practical applications [288, 289]. Since 2016, several theoretical works have suggested that the magnetic skyrmions in antiferromagnets may have better mobility in compared to that in ferromagnets [155, 268, 290–293]. In ferromagnets, the magnetic skyrmion driven by an external force, such as the spin current, usually shows an undesired transverse shift, which may result in the destruction of skyrmion at sample edges. Such a phenomenon is referred to as the SkHE as mentioned in section 4, which is attributed to the Magnus force induced by the topological nature of the skyrmion. In antiferromagnets, as shown in figure 13(a), a magnetic skyrmion can be regarded as two coupled sublattice skyrmions with opposite topological charges, which means that the Magnus forces acted on the two sublattice skyrmions can be exactly cancelled and therefore, leading to the straight motion of the antiferromagnetic skyrmion along the direction force direction [155, 268, 290]. Compared to the current-driven skyrmions in ferromagnets, the speed of antiferromagnetic skyrmions can also be significant improved [155, 268, 290]. Similar to the skyrmions in antiferromagnets, the bilayer skyrmions in the synthetic antiferromagnets (see figure 13(b)) also have a zero topological charge and show no SkHE when they are driven by external driving forces [276, 277, 294]. Theoretical works also suggest that the multilayer skyrmions in a synthetic antiferromagnetic multilayer packed with even constituent ferromagnetic layers are also immune from the SkHE [30]. However, the efficient electrical manipulation (in particular—detection) of antiferromagnetic spin textures with zero net magnetization remains as an important challenge for the practical application of antiferromagnetic materials for skyrmion-electronics.

On the other hand, ferrimagnets are also composed of two sublattices which favor antiparallel alignment of spins between each other, where the magnetic moments of the two sublattices are not equal and lead to a net magnetic moment. Therefore, the ferrimagnetic skyrmions (see figure 13(c)) should have intermediate properties between ferromagnetic

and antiferromagnetic ones. Indeed, ferrimagnetic skyrmions have non-zero SkHE, but their SkHE is much reduced in compared to the ferromagnetic skyrmions [227]. Recent reports also demonstrated that compensated ferrimagnets can have zero SkHE [269] as well as largely improved current-driven velocity suggested by the current-driven motion of domain walls in compensated ferrimagnets [241]. Due to the absence or reduction of the SkHE and their inherent fast dynamics, both antiferromagnetic and ferrimagnetic skyrmions can reach a very high speed without being destroyed at sample edges on a racetrack-like device scheme. That is to say, the antiferromagnetic skyrmion can strictly move along the nanotrack without showing a transverse motion toward the edge. For the ferrimagnetic skyrmion, although it still shows a transverse motion (i.e. a shift) toward the edge, the skyrmion-edge interaction becomes very strong only when the skyrmion velocity is extremely large. Therefore, antiferromagnets, synthetic antiferromagnets, and ferrimagnets are considered as possible skyrmion-hosting materials, where the dynamic performance of skyrmions can be remarkably improved in compared with their counterparts in conventional ferromagnetic materials.

Recently, another type of magnetic materials with exotic and particular properties, i.e. the frustrated magnet, has been reported to host magnetic skyrmions. The frustration [295] in magnets can be raised from competing exchange interactions, and usually leads to complex magnetic phase diagrams. In 2012, Okubo *et al* theoretically discovered that the skyrmion lattice can be stabilized in a frustrated magnet by an order-from-disorder mechanism [89]. In 2015, Leonov and Mostovoy theoretically investigated a rich phase diagram of an anisotropic frustrated magnet and properties of frustrated skyrmions with arbitrary vorticity and helicity [296]. Then, many exotic and unique properties of frustrated skyrmions have also been studied theoretically [42, 297–300]. For example, the energy of a skyrmion with a vorticity number of $Q_v = +1$ is identical to that of an antiskyrmion with a vorticity number of $Q_v = -1$. Namely, the skyrmion energy in frustrated magnets can be irrespective to the skyrmion helicity [301]. Also, a frustrated skyrmion may show coupled dynamics of its helicity and center of mass, which can result in the rotational skyrmion motion [301–303]. Indeed, the coupled dynamics of a frustrated skyrmion depends on many factors. In 2017, Zhang *et al* [302] theoretically reported the current-induced helicity locking-unlocking transition phenomenon of a frustrated skyrmion, which suggests the dipolar interaction may also play an important role in the dynamics of skyrmions in the frustrated magnets, especially at low temperature.

Owing to the multiple degrees of freedom of skyrmions in frustrated magnets, it is anticipated that frustrated skyrmions can be used as versatile information carriers to perform information storage and computing. As shown in figure 13(d), in 2017, Hou *et al* successfully observed various and spontaneous skyrmion bubbles in a frustrated kagome magnet $Fe_3Sn_2$ by using the LTEM at room temperature [129]. In 2019, Kurumaji *et al* [304] experimentally found a Bloch-type skyrmion state in a frustrated centrosymmetric triangular-lattice magnet $Gd_2PdSi_3$, where a giant topological Hall response is observed, indicating the field-induced skyrmion phase.

Very recently, it has been reported that 2D van der Waals (vdW) crystals can also have long-range intrinsic ferromagnetism in few materials with strong magnetic anisotropy [305, 306], e.g. $Cr_2Ge_2Te_3$ or $CrI_3$, whereas such magnetic order is usually strongly suppressed by thermal fluctuations (see figure 13(e)), as predicted by the Mermin–Wagner theorem [307]. These studies on 2D magnets opened a whole new door toward 2D heterostructure-based spintronics, as a result, there appeared significant following interests and efforts revealing the possibility of such devices by demonstrating the magnetoresistance effect in 2D magnets [308], gate-tunable room-temperature 2D magnets [309], current-driven magnetization switching [310, 311], skyrmions in 2D magnets [312], and so on. Due to the broken inversion symmetry and expected large SOC (induced by heavy atomic component) of some representative 2D magnets, e.g. $Fe_3GeTe_2$, it was suggested that 2D magnets might permit the presence of DM interaction that could stabilize magnetic skyrmions [313, 314]. Recently, several experimental studies indeed demonstrated the stabilization of Néel-type magnetic skyrmions in a van der Waals ferromagnet such as $Fe_3GeTe_2$ [315–317] and $Cr_3Ge_2Te_6$ [318], which may excite large research efforts on 2D van der Waals magnet-based skyrmions.

Nevertheless, continuous studies on potential novel skyrmion-hosting materials could reveal more unexpected but remarkable properties and features of skyrmions that can be utilized to perform more efficient information processing in the future.

### *5.2. Other topological spin textures: antiskyrmion, skyrmionium, biskyrmion, meron, antimeron, and bimeron*

During extensive studies on magnetic skyrmions since a decade ago, a number of derivative concepts on skyrmion-like objects were created and envisioned for practical applications. As reviewed in section 1, the skyrmion structure and its topological charge are determined by both in-plane and out-of-plane spin configurations. That is to say, there could be a variety of different skyrmion-like objects due to the modification of either the in-plane or out-of-plane spin configuration in principle. For example, most studies have focused on Néel-type and Bloch-type skyrmions with topological charge of $|Q| = 1$, however, several recent theoretical and experimental reports have revealed that antiskyrmions [81, 88, 205, 300, 319–322] and skyrmioniums [58, 61, 71, 72, 209, 323] have special dynamic properties and can be employed as information carriers similar to conventional skyrmions.

In compared to skyrmions with $Q_v = +1$, the antiskyrmion has different in-plane spin textures, which leads to an opposite-sign vorticity of $Q_v = -1$ as well as largely different current-induced motion as reported in several recent studies [301–303, 314, 324]. In 2017, Nayak *et al* [88] for the first time observed the antiskyrmions in tetragonal Heusler materials above room temperate, as shown in figure 14(a). Also, both skyrmions and antiskyrmions are stable or meta-stable solutions in frustrated magnets [301–303]. The skyrmion with $Q_v = +1$ and antiskyrmion with $Q_v = -1$ can be used to carry different binary information bits in the same spintronic device. Namely,

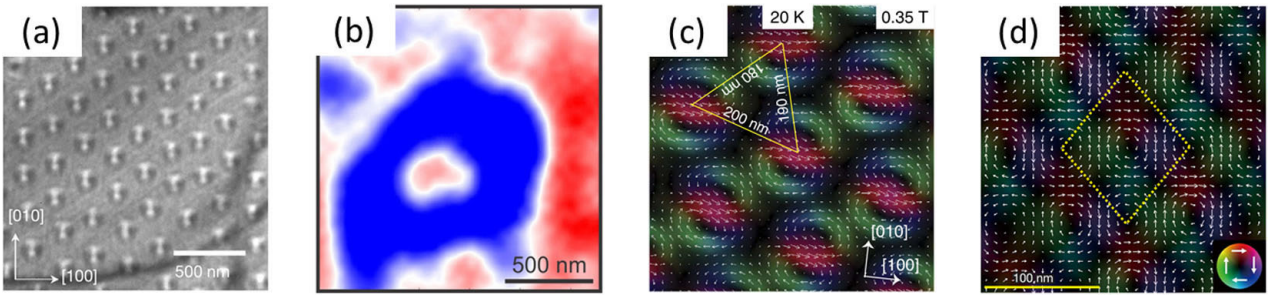


**Figure 14.** Other topological spin textures similar to skyrmions. (a) Under-focused LTEM images of antiskyrmions taken at fields applied along [0 0 1] of 0.29 T for antiskyrmions in $Mn_{1.4}Pt_{0.9}Pd_{0.1}Sn$. Reprinted from [88]. © 2017 Macmillan Publishers Limited, part of Springer Nature. All rights reserved. With permission of Springer. (b) XPEEM image of an isolated skyrmionium obtained at the Fe L3 edge of the NiFe top layer at a temperature of 44 K in zero applied magnetic field. Reprinted with permission from [323]. Copyright © 2018, American Chemical Society. (c) The spin texture of biskyrmion lattice in a bilayered manganese oxide $La_{2-2x}\,Sr_{1+2x}\,Mn_2\,O_7$ with $x = 0.315$. Reprinted from [330]. © 2014 Macmillan Publishers Limited. All rights reserved. With permission of Springer. (d) Real-space magnetization textures of a square lattice of merons and antimerons in a thin plate of the chiral-lattice magnet $Co_8Zn_9Mn_3$. Reprinted from [341]. © 2018 Springer Nature Limited. All rights reserved. With permission of Springer.

the skyrmion stands for digital '1', and the antiskyrmion stands for digital '0'. In such a case, it is expected that information can be computed based on the manipulation of skyrmions and antiskyrmions. Indeed, there should be a detection scheme for the system containing both skyrmions and antiskyrmion. An effective detection method should be sensitive to the variation of in-plane spin textures of skyrmions, such as the electric Hall measurement (see section 3.2). Namely, the skyrmions and antiskyrmions will be differentiated by the sign of the THE since the THE is proportional to the skyrmion number.

As mentioned in section 1.1, the skyrmionium [24] has a topological charge of $Q = 0$. In 2013, the skyrmionium structure was experimentally created by a laser and observed in real space by Finazzi *et al* [209]. Recently, Zhang *et al* [323] also realized the real-space observation of a skyrmionium in ferromagnetic thin films coupled to a magnetic topological insulator (see figure 14(b)). As the skyrmionium has a zero topological charge, it is immune from the SkHE and can be used to reliably delivery information in narrow and long nanotracks. Recently theoretical and simulation works have demonstrated that both spin currents and spin waves are able to drive skyrmioniums into motion in narrow nanotracks [58, 71, 72, 263].

The skyrmion structure with a topological charge of $|Q| = +2$ is referred to as the biskyrmion. Theoretically, the skyrmion with $Q_v = +2$ can be excited from a skyrmion with $Q_v = +1$ by external stimuli, such as the STT [325]. The biskyrmion with $Q_v = +2$ can also be formed by merging two skyrmions with $Q_v = +1$, as theoretically demonstrated in frustrated magnets [302]. Recent years, some experiments revealed the rich static and dynamic properties of biskyrmions in different type of magnetic materials [326–330]. In 2014, Yu *et al* [330] observed biskyrmions in a layered manganite by using the LTEM (see figure 14(c)), and realized the current-driven motion of biskyrmions. However, Loudon *et al* pointed out in a recent report that the images of biskyrmions observed by LTEM can be explained as type-II magnetic bubbles viewed at an angle to their axes [331]. Note that the type-II magnetic bubble has a topological charge of zero and thus is a topologically trivial object. So, future works on biskyrmions could focus on their topology-dependent dynamics, which should be different from that of type-II bubbles.

The above mentioned antiskyrmion, skyrmionium, and biskyrmion are possible solutions in easy-axis magnets. In easy-plane magnets (i.e. magnets in which magnetization favor in-plane configuration), there is also a counterpart of skyrmions, i.e. the so-called bimeron [140]. The bimeron consists of a meron and an antimeron, which forms an asymmetric spin texture carrying a topological charge of $|Q| = 1$. For this reason, the bimeron is also referred to as a meron-antimeron pair [84, 332, 333] or an asymmetric skyrmion in easy-plane magnets [334, 335]. The meron and antimeron were originated in classical field theory [336], of which the concept was then studied in different systems. For example, the bimeron was theoretically studied in quantum Hall systems in 2010 [337, 338], where a skyrmion in the bilayer system with imbalanced the electron density may be deformed into a bimeron when the parallel magnetic field penetrates between the two layers.

As a counterpart of the skyrmions in easy-axis magnets (i.e. magnets where magnetization favor out-of-plane configuration), the bimeron is a localized and compact quasi-particle like spin textures in easy-plane magnets. Recently theoretical works have suggested that an isolated bimeron in either easy-plane ferromagnets or easy-plane antiferromagnets can be driven into motion by STTs [334, 335, 339]. Similar to the transformation from strip magnetic domains to magnetic skyrmions or bubbles via the 'pinching mechanism' [32, 34, 116, 184, 340], the mutual conversion between a skyrmion and a bimeron is also an important issue, which is essential for future spintronic circuits based on different topological spin textures. In 2014, Zhang *et al* numerically demonstrated the possibility that a single isolated skyrmion in an easy-axis magnet can be transformed to a single isolated bimeron in an easy-plane magnet through a bridge-like narrow nanotrack junction connecting the easy-axis and easy-plane magnets [140]. In 2018, as shown in figure 14(d), the magnetic field-driven transformation between meron-antimeron pair lattice and skyrmion lattice was experimentally realized in a chiral magnet by Yu *et al* [341, 342].

### 5.3. Summary

In this review, we have mainly focused on key device application-relevant findings and advances that have been made

in the emerging field of *skyrmion-electronics* since the first experimental identification of skyrmions in 2009, which might indeed enable practical applications in the future. We have reviewed the writing and deleting of skyrmions by using different methods, including magnetic field, electric field, electric current, and laser. The imaging and electrical reading of skyrmions by different state-of-art experimental techniques are also discussed. Moreover, as the processing of skyrmions is fundamental to any skyrmion-based functional device applications, relevant findings have been reviewed with a focus on the implementation of skyrmion-based racetrack memory, logic computing devices and other emerging devices. The *skyrmion-electronics* is a rapidly growing field, in which a number of main topics have been expanded and many promising new topics have been introduced. Therefore, we have also introduced and put forward an overview on recent skyrmion research of different material systems as well as different skyrmion counterparts. We envision that *skyrmion-electronics* will continue to be an active and intriguing field of study, where more theoretical and experimental findings on the manipulation of skyrmions and their counterparts will emerge to support the development of practical applications and products for industry.

Finally, we note that no review articles can cover this topic exhaustively, and therefore, here we refer to other published reviews where some of the aspects of chiral magnetic skyrmions are discussed in more detail [2, 3, 5–7, 94, 98, 100, 157, 163, 295, 343–345].

## Acknowledgments

XZ acknowledges the support by the Presidential Postdoctoral Fellowship of The Chinese University of Hong Kong, Shenzhen (CUHKSZ). YZ acknowledges the support by the President's Fund of CUHKSZ, Longgang Key Laboratory of Applied Spintronics, National Natural Science Foundation of China (Grant Nos. 11974298 and 61961136006), Shenzhen Fundamental Research Fund (Grant No. JCYJ20170410171958839), and Shenzhen Peacock Group Plan (Grant No. KQTD20180413181702403). KMS and T-EP acknowledge the support by KIST Institutional Program (2E29410) and the support from the National Research Council of Science and Technology (NST) (Grant No. CAP-16-01-KIST) by the Korean Government (MSIP). ME acknowledges the support by the Grants-in-Aid for Scientific Research from JSPS KAKENHI (Grant Nos. JP18H03676, JP17K05490, and JP15H05854) and also the support by CREST, JST (Grant Nos. JPMJCR16F1 and JPMJCR1874). WZ acknowledges the support by the National Natural Science Foundation of China (Grant Nos. 61871008, 61571023, 61627813), and the National Key Technology Program of China (Grant No. 2017ZX01032101). GZ acknowledges the support by the National Natural Science Foundation of China (Grant Nos. 51771127, 51571126 and 51772004) of China, the Scientific Research Fund of Sichuan Provincial Education Department (Grant Nos. 18TD0010 and 16CZ0006). XL acknowledges the support by the Grants-in-Aid for Scientific Research from JSPS KAKENHI (Grant Nos. 17K19074, 26600041 and 22360122). SW acknowledges the support from IBM Research and management support from Guohan Hu and Daniel Worledge.

## ORCID iDs

Xichao Zhang https://orcid.org/0000-0001-9656-9696
Yan Zhou https://orcid.org/0000-0001-5641-9191
Motohiko Ezawa https://orcid.org/0000-0002-3629-5643
Seonghoon Woo https://orcid.org/0000-0001-8879-1203

## References

[1] Fert A, Cros V and Sampaio J 2013 Skyrmions on the track *Nat. Nanotechnol.* **8** 152
[2] Nagaosa N and Tokura Y 2013 Topological properties and dynamics of magnetic skyrmions *Nat. Nanotechnol.* **8** 899
[3] Wiesendanger R 2016 Nanoscale magnetic skyrmions in metallic films and multilayers: a new twist for spintronics *Nat. Rev. Mater.* **1** 16044
[4] Seidel J, Vasudevan R K and Valanoor N 2016 Topological structures in multiferroics—domain walls, skyrmions and vortices *Adv. Electron. Mater.* **2** 1500292
[5] Kang W, Huang Y, Zhang X, Zhou Y and Zhao W 2016 Skyrmion-electronics: an overview and outlook *Proc. IEEE* **104** 2040
[6] Finocchio G, Büttner F, Tomasello R, Carpentieri M and Kläui M 2016 Magnetic skyrmions: from fundamental to applications *J. Phys. D: Appl. Phys.* **49** 423001
[7] Fert A, Reyren N and Cros V 2017 Magnetic skyrmions: advances in physics and potential applications *Nat. Rev. Mater.* **2** 17031
[8] Heinze S, von Bergmann K, Menzel M, Brede J, Kubetzka A, Wiesendanger R, Bihlmayer G and Blügel S 2011 Spontaneous atomic-scale magnetic skyrmion lattice in two dimensions *Nat. Phys.* **7** 713
[9] Thiaville A, Rohart S, Jué É, Cros V and Fert A 2012 Dynamics of Dzyaloshinskii domain walls in ultrathin magnetic films *Europhys. Lett.* **100** 57002
[10] Rybakov F N, Borisov A B and Bogdanov A N 2013 Three-dimensional skyrmion states in thin films of cubic helimagnets *Phys. Rev.* B **87** 094424
[11] Rohart S and Thiaville A 2013 Skyrmion confinement in ultrathin film nanostructures in the presence of Dzyaloshinskii–Moriya interaction *Phys. Rev.* B **88** 184422
[12] Wang W, Albert M, Beg M, Bisotti M-A, Chernyshenko D, Cortés-Ortuño D, Hawke I and Fangohr H 2015 Magnon-driven domain-wall motion with the Dzyaloshinskii–Moriya Interaction *Phys. Rev. Lett.* **114** 087203
[13] Ryu K S, Thomas L, Yang S H and Parkin S 2013 Chiral spin torque at magnetic domain walls *Nat. Nanotechnol.* **8** 527
[14] Yang S H, Ryu K S and Parkin S 2015 Domain-wall velocities of up to 750 m $s^{-1}$ driven by exchange-coupling torque in synthetic antiferromagnets *Nat. Nanotechnol.* **10** 221
[15] Dzyaloshinskii I E 1964 Theory of helicoidal structures in antiferromagnets. I. Nonmetals *Sov. Phys. JETP* **19** 960
[16] Bogdanov A N and Yablonskii D A 1989 Thermodynamically stable 'vortices' in magnetically ordered crystals. The mixed state of magnets *Sov. Phys. JETP* **68** 101

[17] Bogdanov A N 1995 New localized solutions of the nonlinear field equations *JETP Lett.* **62** 247

[18] Bogdanov A N and Rossler U K 2001 Chiral symmetry breaking in magnetic thin films and multilayers *Phys. Rev. Lett.* **87** 037203

[19] Bogdanov A N, Rößler U K, Wolf M and Müller K H 2002 Magnetic structures and reorientation transitions in noncentrosymmetric uniaxial antiferromagnets *Phys. Rev.* B **66** 214410

[20] Rossler U K, Bogdanov A N and Pfleiderer C 2006 Spontaneous skyrmion ground states in magnetic metals *Nature* **442** 797

[21] Butenko A B, Leonov A A, Bogdanov A N and Rößler U K 2009 Theory of vortex states in magnetic nanodisks with induced Dzyaloshinskii–Moriya interactions *Phys. Rev.* B **80** 134410

[22] Murakawa H, Onose Y and Tokura Y 2009 Electric-field switching of a magnetic propagation vector in a helimagnet *Phys. Rev. Lett.* **103** 147201

[23] Bogdanov A and Hubert A 1994 Thermodynamically stable magnetic vortex states in magnetic crystals *J. Magn. Magn. Mater.* **138** 255

[24] Bogdanov A and Hubert A 1999 The stability of vortex-like structures in uniaxial ferromagnets *J. Magn. Magn. Mater.* **195** 182

[25] Bogdanov A N, Rössler U K and Pfleiderer C 2005 Modulated and localized structures in cubic helimagnets *Physica* B **359–61** 1162

[26] Zang J, Mostovoy M, Han J H and Nagaosa N 2011 Dynamics of skyrmion crystals in metallic thin films *Phys. Rev. Lett.* **107** 136804

[27] Karhu E A, Rößler U K, Bogdanov A N, Kahwaji S, Kirby B J, Fritzsche H, Robertson M D, Majkrzak C F and Monchesky T L 2012 Chiral modulations and reorientation effects in MnSi thin films *Phys. Rev.* B **85** 094429

[28] Dupé B, Bihlmayer G, Böttcher M, Blügel S and Heinze S 2016 Engineering skyrmions in transition-metal multilayers for spintronics *Nat. Commun.* **7** 11779

[29] Moreau-Luchaire C *et al* 2016 Additive interfacial chiral interaction in multilayers for stabilization of small individual skyrmions at room temperature *Nat. Nanotechnol.* **11** 444

[30] Zhang X, Ezawa M and Zhou Y 2016 Thermally stable magnetic skyrmions in multilayer synthetic antiferromagnetic racetracks *Phys. Rev.* B **94** 064406

[31] Soumyanarayanan A *et al* 2017 Tunable room-temperature magnetic skyrmions in Ir/Fe/Co/Pt multilayers *Nat. Mater.* **16** 898

[32] Legrand W *et al* 2017 Room-temperature current-induced generation and motion of sub-100 nm skyrmions *Nano Lett.* **17** 2703

[33] Woo S *et al* 2017 Spin–orbit torque-driven skyrmion dynamics revealed by time-resolved x-ray microscopy *Nat. Commun.* **8** 15573

[34] Lemesh I *et al* 2018 Current-induced skyrmion generation through morphological thermal transitions in chiral ferromagnetic heterostructures *Adv. Mater.* **30** 1870372

[35] Büttner F *et al* 2017 Field-free deterministic ultrafast creation of magnetic skyrmions by spin–orbit torques *Nat. Nanotechnol.* **12** 1040

[36] Woo S *et al* 2018 Deterministic creation and deletion of a single magnetic skyrmion observed by direct time-resolved x-ray microscopy *Nat. Electron.* **1** 288

[37] Dovzhenko Y, Casola F, Schlotter S, Zhou T X, Büttner F, Walsworth R L, Beach G S D and Yacoby A 2018 Magnetostatic twists in room-temperature skyrmions explored by nitrogen-vacancy center spin texture reconstruction *Nat. Commun.* **9** 2712

[38] Zheng F *et al* 2018 Experimental observation of chiral magnetic bobbers in B20-type FeGe *Nat. Nanotechnol.* **13** 451

[39] Fernandez-Roldan J A, Perez del Real R, Bran C, Vazquez M and Chubykalo-Fesenko O 2018 Magnetization pinning in modulated nanowires: from topological protection to the 'corkscrew' mechanism *Nanoscale* **10** 5923

[40] Redies M, Lux F R, Hanke J P, Buhl P M, Müller G P, Kiselev N S, Blügel S and Mokrousov Y 2019 Distinct magnetotransport and orbital fingerprints of chiral bobbers *Phys. Rev.* B **99** 140407

[41] Ahmed A S, Rowland J, Esser B D, Dunsiger S R, McComb D W, Randeria M and Kawakami R K 2018 Chiral bobbers and skyrmions in epitaxial FeGe/Si(1 1 1) films *Phys. Rev. Mater.* **2** 041401

[42] Sutcliffe P 2017 Skyrmion knots in frustrated magnets *Phys. Rev. Lett.* **118** 247203

[43] Sutcliffe P 2018 Hopfions in chiral magnets *J. Phys. A: Math. Theor.* **51** 375401

[44] Wang X, Qaiumzadeh A and Brataas A 2019 Current-driven dynamics of magnetic hopfions *Phys. Rev. Lett.* **123** 147203

[45] Liu Y, Lake R K and Zang J 2018 Binding a hopfion in a chiral magnet nanodisk *Phys. Rev.* B **98** 174437

[46] Tai J-S B and Smalyukh I I 2018 Static Hopf solitons and knotted emergent fields in solid-state noncentrosymmetric magnetic nanostructures *Phys. Rev. Lett.* **121** 187201

[47] Tai J-S B, Ackerman P J and Smalyukh I I 2018 Topological transformations of Hopf solitons in chiral ferromagnets and liquid crystals *Proc. Natl Acad. Sci.* **115** 921

[48] Shiomi Y, Kanazawa N, Shibata K, Onose Y and Tokura Y 2013 Topological Nernst effect in a three-dimensional skyrmion-lattice phase *Phys. Rev.* B **88** 064409

[49] Rybakov F N, Borisov A B, Blügel S and Kiselev N S 2016 New spiral state and skyrmion lattice in 3D model of chiral magnets *New J. Phys.* **18** 045002

[50] Leonov A O, Monchesky T L, Loudon J C and Bogdanov A N 2016 Three-dimensional chiral skyrmions with attractive interparticle interactions *J. Phys.: Condens. Matter* **28** 35LT01

[51] Cheng R, Li M, Sapkota A, Rai A, Pokhrel A, Mewes T, Mewes C, Xiao D, De Graef M and Sokalski V 2019 Magnetic domain wall skyrmions *Phys. Rev.* B **99** 184412

[52] Togawa Y, Koyama T, Takayanagi K, Mori S, Kousaka Y, Akimitsu J, Nishihara S, Inoue K, Ovchinnikov A S and Kishine J 2012 Chiral magnetic soliton lattice on a chiral helimagnet *Phys. Rev. Lett.* **108** 107202

[53] Skyrme T H R 1962 A unified field theory of mesons and baryons *Nucl. Phys.* **31** 556

[54] Bocdanov A and Hubert A 1994 The properties of isolated magnetic vortices *Phys. Status Solidi* B **186** 527

[55] Brauna H-B 2012 Topological effects in nanomagnetism: from superparamagnetism to chiral quantum solitons *Adv. Phys.* **61** 1

[56] Ezawa Z F 2013 *Quantum Hall Effects* (Singapore: World Scientific) (https://doi.org/10.1142/8210)

[57] Belavin A A and Polyakov A M 1975 Metastable states of two-dimensional isotropic ferromagnets *JETP Lett.* **22** 245

[58] Zhang X, Xia J, Zhou Y, Wang D, Liu X, Zhao W and Ezawa M 2016 Control and manipulation of a magnetic skyrmionium in nanostructures *Phys. Rev.* B **94** 094420

[59] Rybakov F N and Kiselev N S 2019 Chiral magnetic skyrmions with arbitrary topological charge *Phys. Rev.* B **99** 064437

[60] Foster D, Kind C, Ackerman P J, Tai J-S B, Dennis M R and Smalyukh I I 2019 Two-dimensional skyrmion bags in liquid crystals and ferromagnets *Nat. Phys.* **15** 655

[61] Leonov A O, Rößler U K and Mostovoy M 2014 Target-skyrmions and skyrmion clusters in nanowires of chiral magnets *EPJ Web Conf.* **75** 05002

[62] Liu X, Zhu Q, Zhang S, Liu Q and Wang J 2015 Static property and current-driven precession of $2\pi$-vortex in nano-disk with Dzyaloshinskii–Moriya interaction *AIP Adv.* **5** 087137

[63] Komineas S and Papanicolaou N 2015 Skyrmion dynamics in chiral ferromagnets *Phys. Rev.* B **92** 064412

[64] Komineas S and Papanicolaou N 2015 Skyrmion dynamics in chiral ferromagnets under spin-transfer torque *Phys. Rev.* B **92** 174405

[65] Liu Y, Du H, Jia M and Du A 2015 Switching of a target skyrmion by a spin-polarized current *Phys. Rev.* B **91** 094425

[66] Beg M *et al* 2015 Ground state search, hysteretic behaviour, and reversal mechanism of skyrmionic textures in confined helimagnetic nanostructures *Sci. Rep.* **5** 17137

[67] Mulkers J, Miloševic M V and Van Waeyenberge B 2016 Cycloidal versus skyrmionic states in mesoscopic chiral magnets *Phys. Rev.* B **93** 214405

[68] Fujita H and Sato M 2017 Ultrafast generation of skyrmionic defects with vortex beams: printing laser profiles on magnets *Phys. Rev.* B **95** 054421

[69] Fujita H and Sato M 2017 Encoding orbital angular momentum of light in magnets *Phys. Rev.* B **96** 060407

[70] Hagemeister J, Siemens A, Rózsa L, Vedmedenko E Y and Wiesendanger R 2018 Controlled creation and stability of $k\pi$ skyrmions on a discrete lattice *Phys. Rev.* B **97** 174436

[71] Kolesnikov A G, Stebliy M E, Samardak A S and Ognev A V 2018 Skyrmionium—high velocity without the skyrmion Hall effect *Sci. Rep.* **8** 16966

[72] Li S, Xia J, Zhang X, Ezawa M, Kang W, Liu X, Zhou Y and Zhao W 2018 Dynamics of a magnetic skyrmionium driven by spin waves *Appl. Phys. Lett.* **112** 142404

[73] Shen M, Zhang Y, Ou-Yang J, Yang X and You L 2018 Motion of a skyrmionium driven by spin wave *Appl. Phys. Lett.* **112** 062403

[74] Coey J M D 2010 *Magnetism and Magnetic Materials* (Cambridge: Cambridge University Press) (https://doi.org/10.1017/CBO9780511845000.008)

[75] Mühlbauer S, Binz B, Jonietz F, Pfleiderer C, Rosch A, Neubauer A, Georgii R and Böni P 2009 Skyrmion lattice in a chiral magnet *Science* **323** 915

[76] Zhang S, van der Laan G, Müller J, Heinen L, Garst M, Bauer A, Berger H, Pfleiderer C and Hesjedal T 2018 Reciprocal space tomography of 3D skyrmion lattice order in a chiral magnet *Proc. Natl Acad. Sci.* **115** 6386

[77] Fujishiro Y *et al* 2019 Topological transitions among skyrmion- and hedgehog-lattice states in cubic chiral magnets *Nat. Commun.* **10** 1059

[78] Jonietz F *et al* 2014 Spin transfer torques in MnSi at ultralow current densities *Science* **330** 1648

[79] Lovesey S W 1984 *Theory of Neutron Scattering from Condensed Matter* (Oxford: Clarendon)

[80] Kezsmarki I *et al* 2015 Neel-type skyrmion lattice with confined orientation in the polar magnetic semiconductor $GaV_4S_8$ *Nat. Mater.* **14** 1116

[81] Koshibae W and Nagaosa N 2016 Theory of antiskyrmions in magnets *Nat. Commun.* **7** 10542

[82] Dzyaloshinskii I 1958 A thermodynamic theory of 'weak' ferromagnetism of antiferromagnetics *J. Phys. Chem. Solids* **4** 241

[83] Moriya T 1960 Anisotropic superexchange interaction and weak ferromagnetism *Phys. Rev.* **120** 91

[84] Lin S-Z, Saxena A and Batista C D 2015 Skyrmion fractionalization and merons in chiral magnets with easy-plane anisotropy *Phys. Rev.* B **91** 224407

[85] Kim K-W, Moon K-W, Kerber N, Nothhelfer J and Everschor-Sitte K 2018 Asymmetric skyrmion Hall effect in systems with a hybrid Dzyaloshinskii–Moriya interaction *Phys. Rev.* B **97** 224427

[86] Rowland J, Banerjee S and Randeria M 2016 Skyrmions in chiral magnets with Rashba and Dresselhaus spin–orbit coupling *Phys. Rev.* B **93** 020404

[87] Güngördü U, Nepal R, Tretiakov O A, Belashchenko K and Kovalev A A 2016 Stability of skyrmion lattices and symmetries of quasi-two-dimensional chiral magnets *Phys. Rev.* B **93** 064428

[88] Nayak A K, Kumar V, Ma T, Werner P, Pippel E, Sahoo R, Damay F, Rößler U K, Felser C and Parkin S S P 2017 Magnetic antiskyrmions above room temperature in tetragonal Heusler materials *Nature* **548** 561

[89] Okubo T, Chung S and Kawamura H 2012 Multiple-q states and the skyrmion lattice of the triangular-lattice Heisenberg antiferromagnet under magnetic fields *Phys. Rev. Lett.* **108** 017206

[90] Lin Y S, Grundy P J and Giess E A 1973 Bubble domains in magnetostatically coupled garnet films *Appl. Phys. Lett.* **23** 485

[91] Malozemoff A and Slonczewski J 1979 *Magnetic Domain Walls in Bubble Materials* (New York: Academic) (https://doi.org/10.1016/C2013-0-06998-8)

[92] Garel T and Doniach S 1982 Phase transitions with spontaneous modulation-the dipolar Ising ferromagnet *Phys. Rev.* B **26** 325

[93] Suzuki T 1983 A study of magnetization distribution of submicron bubbles in sputtered Ho–Co thin films *J. Magn. Magn. Mater.* **31–34** 1009

[94] Liu Y-H and Li Y-Q 2015 Dynamics of magnetic skyrmions *Chin. Phys.* B **24** 017506

[95] Soumyanarayanan A, Reyren N, Fert A and Panagopoulos C 2016 Emergent phenomena induced by spin–orbit coupling at surfaces and interfaces *Nature* **539** 509

[96] Kanazawa N, Seki S and Tokura Y 2017 Noncentrosymmetric magnets hosting magnetic skyrmions *Adv. Mater.* **29** 1603227

[97] Hellman F *et al* 2017 Interface-induced phenomena in magnetism *Rev. Mod. Phys.* **89** 025006

[98] Jiang W, Chen G, Liu K, Zang J, te Velthuis S G E and Hoffmann A 2017 Skyrmions in magnetic multilayers *Phys. Rep.* **704** 1

[99] Dieny B and Chshiev M 2017 Perpendicular magnetic anisotropy at transition metal/oxide interfaces and applications *Rev. Mod. Phys.* **89** 025008

[100] Everschor-Sitte K, Masell J, Reeve R M and Kläui M 2018 Perspective: magnetic skyrmions—overview of recent progress in an active research field *J. Appl. Phys.* **124** 240901

[101] Zhou Y 2018 Magnetic skyrmions: intriguing physics and new spintronic device concepts *Natl Sci. Rev.* **6** 210

[102] Yu X Z, Onose Y, Kanazawa N, Park J H, Han J H, Matsui Y, Nagaosa N and Tokura Y 2010 Real-space observation of a two-dimensional skyrmion crystal *Nature* **465** 901

[103] Yu X Z, Kanazawa N, Onose Y, Kimoto K, Zhang W Z, Ishiwata S, Matsui Y and Tokura Y 2011 Near room-temperature formation of a skyrmion crystal in thin-films of the helimagnet FeGe *Nat. Mater.* **10** 106

[104] Yu X Z, Kanazawa N, Zhang W Z, Nagai T, Hara T, Kimoto K, Matsui Y, Onose Y and Tokura Y 2012 Skyrmion flow near room temperature in an ultralow current density *Nat. Commun.* **3** 988

[105] Milde P *et al* 2013 Unwinding of a skyrmion lattice by magnetic monopoles *Science* **340** 1076

[106] Romming N, Hanneken C, Menzel M, Bickel J E, Wolter B, von Bergmann K, Kubetzka A and Wiesendanger R 2013 Writing and deleting single magnetic skyrmions *Science* **341** 636

[107] Schulz T, Ritz R, Bauer A, Halder M, Wagner M, Franz C, Pfleiderer C, Everschor K, Garst M and Rosch A 2012 Emergent electrodynamics of skyrmions in a chiral magnet *Nat. Phys.* **8** 301

[108] Iwasaki J, Mochizuki M and Nagaosa N 2013 Universal current-velocity relation of skyrmion motion in chiral magnets *Nat. Commun.* **4** 1463

[109] Seki S, Yu X Z, Ishiwata S and Tokura Y 2012 Observation of skyrmions in a multiferroic material *Science* **336** 198

[110] Seki S, Kim J H, Inosov D S, Georgii R, Keimer B, Ishiwata S and Tokura Y 2012 Formation and rotation of skyrmion crystal in the chiral-lattice insulator $Cu_2OSeO_3$ *Phys. Rev.* B **85** 220406

[111] Matsumoto T, So Y-G, Kohno Y, Sawada H, Ikuhara Y and Shibata N 2016 Direct observation of Σ7 domain boundary core structure in magnetic skyrmion lattice *Sci. Adv.* **2** e1501280

[112] Yang H, Wang C, Wang X, Wang X S, Cao Y and Yan P 2018 Twisted skyrmions at domain boundaries and the method of image skyrmions *Phys. Rev.* B **98** 014433

[113] McGrouther D, Lamb R J, Krajnak M, McFadzean S, McVitie S, Stamps R L, Leonov A O, Bogdanov A N and Togawa Y 2016 Internal structure of hexagonal skyrmion lattices in cubic helimagnets *New J. Phys.* **18** 095004

[114] McVitie S *et al* 2018 A transmission electron microscope study of Néel skyrmion magnetic textures in multilayer thin film systems with large interfacial chiral interaction *Sci. Rep.* **8** 5703

[115] Emori S, Bauer U, Ahn S M, Martinez E and Beach G S 2013 Current-driven dynamics of chiral ferromagnetic domain walls *Nat. Mater.* **12** 611

[116] Jiang W *et al* 2015 Blowing magnetic skyrmion bubbles *Science* **349** 283

[117] Bobeck A H and Della Torre E 1975 *Magnetic Bubbles* (Amsterdam: North-Holland)

[118] Thiele A A 1970 Theory of the static stability of cylindrical domains in uniaxial platelets *J. Appl. Phys.* **41** 1139

[119] Thiaville A and Pátek K 1993 Conical bubbles *J. Magn. Magn. Mater.* **124** 355

[120] Boulle O *et al* 2016 Room-temperature chiral magnetic skyrmions in ultrathin magnetic nanostructures *Nat. Nanotechnol.* **11** 449

[121] Woo S *et al* 2016 Observation of room-temperature magnetic skyrmions and their current-driven dynamics in ultrathin metallic ferromagnets *Nat. Mater.* **15** 501

[122] Yu G, Upadhyaya P, Li X, Li W, Kim S K, Fan Y, Wong K L, Tserkovnyak Y, Amiri P K and Wang K L 2016 Room-temperature creation and spin–orbit torque manipulation of skyrmions in thin films with engineered asymmetry *Nano Lett.* **16** 1981

[123] Zhang S, Zhang J, Wen Y, Chudnovsky E M and Zhang X 2018 Creation of a thermally assisted skyrmion lattice in Pt/Co/Ta multilayer films *Appl. Phys. Lett.* **113** 192403

[124] Zhang S, Zhang J, Wen Y, Chudnovsky E M and Zhang X 2018 Determination of chirality and density control of Néel-type skyrmions with in-plane magnetic field *Commun. Phys.* **1** 36

[125] Chen G, Mascaraque A, N'Diaye A T and Schmid A K 2015 Room temperature skyrmion ground state stabilized through interlayer exchange coupling *Appl. Phys. Lett.* **106** 242404

[126] Tokunaga Y, Yu X Z, White J S, Rønnow H M, Morikawa D, Taguchi Y and Tokura Y 2015 A new class of chiral materials hosting magnetic skyrmions beyond room temperature *Nat. Commun.* **6** 7638

[127] Gilbert D A, Maranville B B, Balk A L, Kirby B J, Fischer P, Pierce D T, Unguris J, Borchers J A and Liu K 2015 Realization of ground-state artificial skyrmion lattices at room temperature *Nat. Commun.* **6** 8462

[128] Sun L, Cao R X, Miao B F, Feng Z, You B, Wu D, Zhang W, Hu A and Ding H F 2013 Creating an artificial two-dimensional skyrmion crystal by nanopatterning *Phys. Rev. Lett.* **110** 167201

[129] Hou Z *et al* 2017 Observation of various and spontaneous magnetic skyrmionic bubbles at room temperature in a frustrated kagome magnet with uniaxial magnetic anisotropy *Adv. Mater.* **29** 1701144

[130] Koshibae W, Kaneko Y, Iwasaki J, Kawasaki M, Tokura Y and Nagaosa N 2015 Memory functions of magnetic skyrmions *Japan. J. Appl. Phys.* **54** 053001

[131] Parkin S S P, Hayashi M and Thomas L 2008 Magnetic domain-wall racetrack memory *Science* **320** 190

[132] Iwasaki J, Mochizuki M and Nagaosa N 2013 Current-induced skyrmion dynamics in constricted geometries *Nat. Nanotechnol.* **8** 742

[133] Sampaio J, Cros V, Rohart S, Thiaville A and Fert A 2013 Nucleation, stability and current-induced motion of isolated magnetic skyrmions in nanostructures *Nat. Nanotechnol.* **8** 839

[134] Mochizuki M and Seki S 2013 Magnetoelectric resonances and predicted microwave diode effect of the skyrmion crystal in a multiferroic chiral-lattice magnet *Phys. Rev.* B **87** 134403

[135] Okamura Y, Kagawa F, Mochizuki M, Kubota M, Seki S, Ishiwata S, Kawasaki M, Onose Y and Tokura Y 2013 Microwave magnetoelectric effect via skyrmion resonance modes in a helimagnetic multiferroic *Nat. Commun.* **4** 2391

[136] Finocchio G, Ricci M, Tomasello R, Giordano A, Lanuzza M, Puliafito V, Burrascano P, Azzerboni B and Carpentieri M 2015 Skyrmion based microwave detectors and harvesting *Appl. Phys. Lett.* **107** 262401

[137] Liu R H, Lim W L and Urazhdin S 2015 Dynamical skyrmion state in a spin current nano-oscillator with perpendicular magnetic anisotropy *Phys. Rev. Lett.* **114** 137201

[138] Zhang S F *et al* 2015 Current-induced magnetic skyrmions oscillator *New J. Phys.* **17** 023061

[139] Navau C, Del-Valle N and Sanchez A 2016 Analytical trajectories of skyrmions in confined geometries: skyrmionic racetracks and nano-oscillators *Phys. Rev.* B **94** 184104

[140] Zhang X, Ezawa M and Zhou Y 2015 Magnetic skyrmion logic gates: conversion, duplication and merging of skyrmions *Sci. Rep.* **5** 9400

[141] Zhang X, Zhou Y, Ezawa M, Zhao G P and Zhao W 2015 Magnetic skyrmion transistor: skyrmion motion in a voltage-gated nanotrack *Sci. Rep.* **5** 11369

[142] Upadhyaya P, Yu G, Amiri P K and Wang K L 2015 Electric-field guiding of magnetic skyrmions *Phys. Rev.* B **92** 134411

[143] Huang Y, Kang W, Zhang X, Zhou Y and Zhao W 2017 Magnetic skyrmion-based synaptic devices *Nanotechnology* **28** 08LT02

[144] Song K M *et al* 2019 Magnetic skyrmion artificial synapse for neuromorphic computing (arXiv:1907.00957)

[145] Li S, Kang W, Huang Y, Zhang X, Zhou Y and Zhao W 2017 Magnetic skyrmion-based artificial neuron device *Nanotechnology* **28** 31LT01

[146] Bourianoff G, Pinna D, Sitte M and Everschor-Sitte K 2018 Potential implementation of reservoir computing models based on magnetic skyrmions *AIP Adv.* **8** 055602

[147] Prychynenko D, Sitte M, Litzius K, Krüger B, Bourianoff G, Kläui M, Sinova J and Everschor-Sitte K 2018 Magnetic skyrmion as a nonlinear resistive element: a potential building block for reservoir computing *Phys. Rev. Appl.* **9** 014034

[148] Zhao L *et al* 2019 Spin-topology dependent Brownian diffusion of skyrmions (arXiv:1901.08206)

[149] Nozaki T, Jibiki Y, Goto M, Tamura E, Nozaki T, Kubota H, Fukushima A, Yuasa S and Suzuki Y 2019 Brownian motion of skyrmion bubbles and its control by voltage applications *Appl. Phys. Lett.* **114** 012402

[150] Reichhardt C and Reichhardt C J O 2018 Thermal creep and the skyrmion Hall angle in driven skyrmion crystals *J. Phys.: Condens. Matter* **31** 07LT01

[151] Troncoso R E and Núñez A S 2014 Thermally assisted current-driven skyrmion motion *Phys. Rev.* B **89** 224403

[152] Troncoso R E and Núñez Á S 2014 Brownian motion of massive skyrmions in magnetic thin films *Ann. Phys., NY* **351** 850

[153] Pinna D, Abreu Araujo F, Kim J V, Cros V, Querlioz D, Bessiere P, Droulez J and Grollier J 2018 Skyrmion gas manipulation for probabilistic computing *Phys. Rev. Appl.* **9** 064018

[154] Miltat J, Rohart S and Thiaville A 2018 Brownian motion of magnetic domain walls and skyrmions, and their diffusion constants *Phys. Rev.* B **97** 214426

[155] Barker J and Tretiakov O A 2016 Static and dynamical properties of antiferromagnetic skyrmions in the presence of applied current and temperature *Phys. Rev. Lett.* **116** 147203

[156] Kong L Y and Zang J D 2013 Dynamics of an insulating skyrmion under a temperature gradient *Phys. Rev. Lett.* **111** 067203

[157] Reichhardt C and Olson Reichhardt C J 2016 Depinning and nonequilibrium dynamic phases of particle assemblies driven over random and ordered substrates: a review *Rep. Prog. Phys.* **80** 026501

[158] Bessarab P F, Müller G P, Lobanov I S, Rybakov F N, Kiselev N S, Jónsson H, Uzdin V M, Blügel S, Bergqvist L and Delin A 2018 Lifetime of racetrack skyrmions *Sci. Rep.* **8** 3433

[159] Lin S Z, Batista C D, Reichhardt C and Saxena A 2014 AC current generation in chiral magnetic insulators and skyrmion motion induced by the spin Seebeck effect *Phys. Rev. Lett.* **112** 187203

[160] Zázvorka J *et al* 2019 Thermal skyrmion diffusion used in a reshuffler device *Nat. Nanotechnol.* **14** 658

[161] Rößler U K, Leonov A A and Bogdanov A N 2011 Chiral Skyrmionic matter in non-centrosymmetric magnets *J. Phys.: Conf. Ser.* **303** 012105

[162] Huang S X and Chien C L 2012 Extended skyrmion phase in epitaxial FeGe(1 1 1) thin films *Phys. Rev. Lett.* **108** 267201

[163] Mochizuki M and Seki S 2015 Dynamical magnetoelectric phenomena of multiferroic skyrmions *J. Phys.: Condens. Matter* **27** 503001

[164] Tomasello R, Guslienko K Y, Ricci M, Giordano A, Barker J, Carpentieri M, Chubykalo-Fesenko O and Finocchio G 2018 Origin of temperature and field dependence of magnetic skyrmion size in ultrathin nanodots *Phys. Rev.* B **97** 060402

[165] Wang X S, Yuan H Y and Wang X R 2018 A theory on skyrmion size *Commun. Phys.* **1** 31

[166] Jan M, Achim R and Markus G 2016 Edge instabilities and skyrmion creation in magnetic layers *New J. Phys.* **18** 065006

[167] Mochizuki M 2017 Controlled creation of nanometric skyrmions using external magnetic fields *Appl. Phys. Lett.* **111** 092403

[168] Garanin D A, Capic D, Zhang S, Zhang X and Chudnovsky E M 2018 Writing skyrmions with a magnetic dipole *J. Appl. Phys.* **124** 113901

[169] Zhang S *et al* 2018 Direct writing of room temperature and zero field skyrmion lattices by a scanning local magnetic field *Appl. Phys. Lett.* **112** 132405

[170] Wachowiak A, Wiebe J, Bode M, Pietzsch O, Morgenstern M and Wiesendanger R 2002 Direct observation of internal spin structure of magnetic vortex cores *Science* **298** 577

[171] Van Waeyenberge B *et al* 2006 Magnetic vortex core reversal by excitation with short bursts of an alternating field *Nature* **444** 461

[172] Buttner F *et al* 2015 Dynamics and inertia of skyrmionic spin structures *Nat. Phys.* **11** 225

[173] Zhang B, Wang W, Beg M, Fangohr H and Kuch W 2015 Microwave-induced dynamic switching of magnetic skyrmion cores in nanodots *Appl. Phys. Lett.* **106** 102401

[174] Li J *et al* 2014 Tailoring the topology of an artificial magnetic skyrmion *Nat. Commun.* **5** 4704

[175] Heo C, Kiselev N S, Nandy A K, Blügel S and Rasing T 2016 Switching of chiral magnetic skyrmions by picosecond magnetic field pulses via transient topological states *Sci. Rep.* **6** 27146

[176] Dai Y, Wang H, Yang T, Ren W and Zhang Z 2014 Flower-like dynamics of coupled Skyrmions with dual resonant modes by a single-frequency microwave magnetic field *Sci. Rep.* **4** 6153

[177] Ikka M, Takeuchi A and Mochizuki M 2018 Resonance modes and microwave-driven translational motion of a skyrmion crystal under an inclined magnetic field *Phys. Rev.* B **98** 184428

[178] Ralph D C and Stiles M D 2008 Spin transfer torques *J. Magn. Magn. Mater.* **320** 1190

[179] Sinova J, Valenzuela S O, Wunderlich J, Back C H and Jungwirth T 2015 Spin Hall effects *Rev. Mod. Phys.* **87** 1213

[180] Everschor K, Garst M, Duine R A and Rosch A 2011 Current-induced rotational torques in the skyrmion lattice phase of chiral magnets *Phys. Rev.* B **84** 064401

[181] Tchoe Y and Han J H 2012 Skyrmion generation by current *Phys. Rev.* B **85** 174416

[182] Zhou Y and Ezawa M 2014 A reversible conversion between a skyrmion and a domain-wall pair in junction geometry *Nat. Commun.* **5** 4652

[183] Heinonen O, Jiang W, Somaily H, te Velthuis S G E and Hoffmann A 2016 Generation of magnetic skyrmion bubbles by inhomogeneous spin Hall currents *Phys. Rev.* B **93** 094407

[184] Lin S-Z 2016 Edge instability in a chiral stripe domain under an electric current and skyrmion generation *Phys. Rev.* B **94** 020402

[185] Liu Y, Yan H, Jia M, Du H and Du A 2016 Topological analysis of spin-torque driven magnetic skyrmion formation *Appl. Phys. Lett.* **109** 102402

[186] Yuan H Y and Wang X R 2016 Skyrmion creation and manipulation by nano-second current pulses *Sci. Rep.* **6** 22638

[187] Yin G, Li Y, Kong L, Lake R K, Chien C L and Zang J 2016 Topological charge analysis of ultrafast single skyrmion creation *Phys. Rev.* B **93** 174403

[188] Hrabec A, Sampaio J, Belmeguenai M, Gross I, Weil R, Chérif S M, Stashkevich A, Jacques V, Thiaville A and Rohart S 2017 Current-induced skyrmion generation

and dynamics in symmetric bilayers *Nat. Commun.* **8** 15765
[189] Finizio S, Zeissler K, Wintz S, Mayr S, Weßels T, Huxtable A J, Burnell G, Marrows C H and Raabe J 2019 Deterministic field-free skyrmion nucleation at a nano-engineered injector device *Nano. Lett.* **19** 7246
[190] De Lucia A, Litzius K, Krüger B, Tretiakov O A and Kläui M 2017 Multiscale simulations of topological transformations in magnetic-skyrmion spin structures *Phys. Rev.* B **96** 020405
[191] Seki S, Ishiwata S and Tokura Y 2012 Magnetoelectric nature of skyrmions in a chiral magnetic insulator $Cu_2OSeO_3$ *Phys. Rev.* B **86** 060403
[192] Huang P, Cantoni M, Kruchkov A, Rajeswari J, Magrez A, Carbone F and Rønnow H M 2018 *In situ* electric field skyrmion creation in magnetoelectric $Cu_2OSeO_3$ *Nano Lett.* **18** 5167
[193] Mochizuki M and Watanabe Y 2015 Writing a skyrmion on multiferroic materials *Appl. Phys. Lett.* **107** 082409
[194] Okamura Y, Kagawa F, Seki S and Tokura Y 2016 Transition to and from the skyrmion lattice phase by electric fields in a magnetoelectric compound *Nat. Commun.* **7** 12669
[195] Hsu P-J, Kubetzka A, Finco A, Romming N, von Bergmann K and Wiesendanger R 2017 Electric-field-driven switching of individual magnetic skyrmions *Nat. Nanotechnol.* **12** 123
[196] Schott M, Bernand-Mantel A, Ranno L, Pizzini S, Vogel J, Béa H, Baraduc C, Auffret S, Gaudin G and Givord D 2017 The skyrmion switch: turning magnetic skyrmion bubbles on and off with an electric field *Nano Lett.* **17** 3006
[197] Srivastava T *et al* 2018 Large-voltage tuning of Dzyaloshinskii–Moriya interactions: a route toward dynamic control of skyrmion chirality *Nano Lett.* **18** 4871
[198] Ma C, Zhang X, Xia J, Ezawa M, Jiang W, Ono T, Piramanayagam S N, Morisako A, Zhou Y and Liu X 2019 Electric field-induced creation and directional motion of domain walls and skyrmion bubbles *Nano Lett.* **19** 353
[199] Bhattacharya D, Al-Rashid M M and Atulasimha J 2016 Voltage controlled core reversal of fixed magnetic skyrmions without a magnetic field *Sci. Rep.* **6** 31272
[200] Beaurepaire E, Merle J C, Daunois A and Bigot J Y 1996 Ultrafast spin dynamics in ferromagnetic nickel *Phys. Rev. Lett.* **76** 4250
[201] Stanciu C D, Hansteen F, Kimel A V, Kirilyuk A, Tsukamoto A, Itoh A and Rasing T 2007 All-optical magnetic recording with circularly polarized light *Phys. Rev. Lett.* **99** 047601
[202] Radu I *et al* 2011 Transient ferromagnetic-like state mediating ultrafast reversal of antiferromagnetically coupled spins *Nature* **472** 205
[203] Lambert C H *et al* 2014 All-optical control of ferromagnetic thin films and nanostructures *Science* **345** 1337
[204] Stupakiewicz A, Szerenos K, Afanasiev D, Kirilyuk A and Kimel A V 2017 Ultrafast nonthermal photo-magnetic recording in a transparent medium *Nature* **542** 71
[205] Koshibae W and Nagaosa N 2014 Creation of skyrmions and antiskyrmions by local heating *Nat. Commun.* **5** 5148
[206] Je S-G *et al* 2018 Creation of magnetic skyrmion bubble lattices by ultrafast laser in ultrathin films *Nano Lett.* **18** 7362
[207] Ogasawara T, Iwata N, Murakami Y, Okamoto H and Tokura Y 2009 Submicron-scale spatial feature of ultrafast photoinduced magnetization reversal in TbFeCo thin film *Appl. Phys. Lett.* **94** 162507
[208] Ezawa M 2010 Giant skyrmions stabilized by dipole–dipole interactions in thin ferromagnetic films *Phys. Rev. Lett.* **105** 197202
[209] Finazzi M, Savoini M, Khorsand A R, Tsukamoto A, Itoh A, Duò L, Kirilyuk A, Rasing T and Ezawa M 2013 Laser-induced magnetic nanostructures with tunable topological properties *Phys. Rev. Lett.* **110** 177205
[210] Yang W, Yang H, Cao Y and Yan P 2018 Photonic orbital angular momentum transfer and magnetic skyrmion rotation *Opt. Express* **26** 8778
[211] Berruto G *et al* 2018 Laser-induced skyrmion writing and erasing in an ultrafast cryo-Lorentz transmission electron microscope *Phys. Rev. Lett.* **120** 117201
[212] Ogawa N, Seki S and Tokura Y 2015 Ultrafast optical excitation of magnetic skyrmions *Sci. Rep.* **5** 9552
[213] Kneller E F and Hawig R 1991 The exchange-spring magnet: a new material principle for permanent magnets *IEEE Trans. Magn.* **27** 3588
[214] Fraerman A A, Ermolaeva O L, Skorohodov E V, Gusev N S, Mironov V L, Vdovichev S N and Demidov E S 2015 Skyrmion states in multilayer exchange coupled ferromagnetic nanostructures with distinct anisotropy directions *J. Magn. Magn. Mater.* **393** 452
[215] Streubel R, Fischer P, Kopte M, Schmidt O G and Makarov D 2015 Magnetization dynamics of imprinted non-collinear spin textures *Appl. Phys. Lett.* **107** 112406
[216] Del-Valle N, Agramunt-Puig S, Sanchez A and Navau C 2015 Imprinting skyrmions in thin films by ferromagnetic and superconducting templates *Appl. Phys. Lett.* **107** 133103
[217] Sun L, Wu H Z, Miao B F, Wu D and Ding H F 2018 Tuning the stability and the skyrmion Hall effect in magnetic skyrmions by adjusting their exchange strengths with magnetic disks *J. Magn. Magn. Mater.* **455** 39
[218] Jiang W *et al* 2017 Direct observation of the skyrmion Hall effect *Nat. Phys.* **13** 162
[219] Litzius K *et al* 2017 Skyrmion Hall effect revealed by direct time-resolved x-ray microscopy *Nat. Phys.* **13** 170
[220] Zhao X, Jin C, Wang C, Du H, Zang J, Tian M, Che R and Zhang Y 2016 Direct imaging of magnetic field-driven transitions of skyrmion cluster states in FeGe nanodisks *Proc. Natl Acad. Sci.* **113** 4918
[221] Du H *et al* 2015 Edge-mediated skyrmion chain and its collective dynamics in a confined geometry *Nat. Commun.* **6** 8504
[222] Wang C, Du H, Zhao X, Jin C, Tian M, Zhang Y and Che R 2017 Enhanced stability of the magnetic skyrmion lattice phase under a tilted magnetic field in a two-dimensional chiral magnet *Nano Lett.* **17** 2921
[223] Yu X Z, DeGrave J P, Hara Y, Hara T, Jin S and Tokura Y 2013 Observation of the magnetic skyrmion lattice in a MnSi nanowire by Lorentz TEM *Nano Lett.* **13** 3755
[224] Shibata K, Yu X Z, Hara T, Morikawa D, Kanazawa N, Kimoto K, Ishiwata S, Matsui Y and Tokura Y 2013 Towards control of the size and helicity of skyrmions in helimagnetic alloys by spin–orbit coupling *Nat. Nanotechnol.* **8** 723
[225] Lee J C T *et al* 2016 Synthesizing skyrmion bound pairs in Fe–Gd thin films *Appl. Phys. Lett.* **109** 022402
[226] Romming N, Kubetzka A, Hanneken C, von Bergmann K and Wiesendanger R 2015 Field-dependent size and shape of single magnetic skyrmions *Phys. Rev. Lett.* **114** 177203
[227] Woo S *et al* 2018 Current-driven dynamics and inhibition of the skyrmion Hall effect of ferrimagnetic skyrmions in GdFeCo films *Nat. Commun.* **9** 959
[228] Tolley R, Montoya S A and Fullerton E E 2018 Room-temperature observation and current control of skyrmions in Pt/Co/Os/Pt thin films *Phys. Rev. Mater.* **2** 044404

[229] Jin C-M and Du H-F 2015 Real-space observation of individual skyrmions in helimagnetic nanostripes *Chin. Phys.* B **24** 128501

[230] Leonov A O, Monchesky T L, Romming N, Kubetzka A, Bogdanov A N and Wiesendanger R 2016 The properties of isolated chiral skyrmions in thin magnetic films *New J. Phys.* **18** 065003

[231] Nakajima T and Arima T-H 2019 Observation of magnetic skyrmions by neutron scattering *J. Phys. Soc. Japan* **88** 081006

[232] Luo H, Xia W, Du H and Liu J P 2016 *Skyrmions* (Boca Raton, FL: CRC Press) p 53

[233] Hopster H and Oepen H P 2005 *Magnetic Microscopy of Nanostructures* (Berlin: Springer)

[234] Müller J, Rajeswari J, Huang P, Murooka Y, Rønnow H M, Carbone F and Rosch A 2017 Magnetic skyrmions and skyrmion clusters in the helical phase of $Cu_2OSeO_3$ *Phys. Rev. Lett.* **119** 137201

[235] Tonomura A, Yu X, Yanagisawa K, Matsuda T, Onose Y, Kanazawa N, Park H S and Tokura Y 2012 Real-space observation of skyrmion lattice in helimagnet MnSi thin samples *Nano Lett.* **12** 1673

[236] McVitie S, McGrouther D, McFadzean S, MacLaren D A, O'Shea K J and Benitez M J 2015 Aberration corrected Lorentz scanning transmission electron microscopy *Ultramicroscopy* **152** 57

[237] Benitez M J, Hrabec A, Mihai A P, Moore T A, Burnell G, McGrouther D, Marrows C H and McVitie S 2015 Magnetic microscopy and topological stability of homochiral Néel domain walls in a Pt/Co/$AlO_x$ trilayer *Nat. Commun.* **6** 8957

[238] Pollard S D, Garlow J A, Yu J, Wang Z, Zhu Y and Yang H 2014 Observation of stable Néel skyrmions in cobalt/palladium multilayers with Lorentz transmission electron microscopy *Nat. Commun.* **8** 14761

[239] Dekkers N and De Lang H 1974 Differential phase contrast in a STEM *Optik* **41** 452

[240] Chapman J N, Batson P E, Waddell E M and Ferrier R P 1978 The direct determination of magnetic domain wall profiles by differential phase contrast electron microscopy *Ultramicroscopy* **3** 203

[241] Caretta L *et al* 2018 Fast current-driven domain walls and small skyrmions in a compensated ferrimagnet *Nat. Nanotechnol.* **13** 1154

[242] Neubauer A, Pfleiderer C, Binz B, Rosch A, Ritz R, Niklowitz P G and Böni P 2009 Topological Hall effect in the APhase of MnSi *Phys. Rev. Lett.* **102** 186602

[243] Lee M, Kang W, Onose Y, Tokura Y and Ong N P 2009 Unusual Hall effect anomaly in MnSi under pressure *Phys. Rev. Lett.* **102** 186601

[244] Kanazawa N, Onose Y, Arima T, Okuyama D, Ohoyama K, Wakimoto S, Kakurai K, Ishiwata S and Tokura Y 2011 Large topological Hall effect in a short-period helimagnet MnGe *Phys. Rev. Lett.* **106** 156603

[245] Bruno P, Dugaev V K and Taillefumier M 2004 Topological Hall effect and berry phase in magnetic nanostructures *Phys. Rev. Lett.* **93** 096806

[246] Binz B, Vishwanath A and Aji V 2006 Theory of the helical spin crystal: a candidate for the partially ordered state of MnSi *Phys. Rev. Lett.* **96** 207202

[247] Binz B and Vishwanath A 2008 Chirality induced anomalous-Hall effect in helical spin crystals *Physica* B **403** 1336

[248] Hamamoto K, Ezawa M and Nagaosa N 2015 Quantized topological Hall effect in skyrmion crystal *Phys. Rev.* B **92** 115417

[249] Yokouchi T, Kanazawa N, Tsukazaki A, Kozuka Y, Kawasaki M, Ichikawa M, Kagawa F and Tokura Y 2014 Stability of two-dimensional skyrmions in thin films of $Mn_{1-x}Fe_xSi$ investigated by the topological Hall effect *Phys. Rev.* B **89** 064416

[250] Oike H, Kikkawa A, Kanazawa N, Taguchi Y, Kawasaki M, Tokura Y and Kagawa F 2015 Interplay between topological and thermodynamic stability in a metastable magnetic skyrmion lattice *Nat. Phys.* **12** 62

[251] Matsuno J, Ogawa N, Yasuda K, Kagawa F, Koshibae W, Nagaosa N, Tokura Y and Kawasaki M 2016 Interface-driven topological Hall effect in $SrRuO_3$–$SrIrO_3$ bilayer *Sci. Adv.* **2** e1600304

[252] Liu C, Zang Y, Ruan W, Gong Y, He K, Ma X, Xue Q-K and Wang Y 2017 Dimensional crossover-induced topological Hall effect in a magnetic topological insulator *Phys. Rev. Lett.* **119** 176809

[253] Maccariello D, Legrand W, Reyren N, Garcia K, Bouzehouane K, Collin S, Cros V and Fert A 2018 Electrical detection of single magnetic skyrmions in metallic multilayers at room temperature *Nat. Nanotechnol.* **13** 233

[254] Zeissler K *et al* 2018 Discrete Hall resistivity contribution from Néel skyrmions in multilayer nanodiscs *Nat. Nanotechnol.* **13** 1161

[255] Hamamoto K, Ezawa M and Nagaosa N 2016 Purely electrical detection of a skyrmion in constricted geometry *Appl. Phys. Lett.* **108** 112401

[256] Hanneken C, Otte F, Kubetzka A, Dupé B, Romming N, von Bergmann K, Wiesendanger R and Heinze S 2015 Electrical detection of magnetic skyrmions by tunnelling non-collinear magnetoresistance *Nat. Nanotechnol.* **10** 1039

[257] Du H *et al* 2015 Electrical probing of field-driven cascading quantized transitions of skyrmion cluster states in MnSi nanowires *Nat. Commun.* **6** 7637

[258] Tomasello R, Ricci M, Burrascano P, Puliafito V, Carpentieri M and Finocchio G 2017 Electrical detection of single magnetic skyrmion at room temperature *AIP Adv.* **7** 056022

[259] Kubetzka A, Hanneken C, Wiesendanger R and von Bergmann K 2017 Impact of the skyrmion spin texture on magnetoresistance *Phys. Rev.* B **95** 104433

[260] Baibich M N, Broto J M, Fert A, Van Dau F N, Petroff F, Etienne P, Creuzet G, Friederich A and Chazelas J 1988 Giant magnetoresistance of (0 0 1)Fe/(0 0 1)Cr magnetic superlattices *Phys. Rev. Lett.* **61** 2472

[261] Ikeda S, Miura K, Yamamoto H, Mizunuma K, Gan H D, Endo M, Kanai S, Hayakawa J, Matsukura F and Ohno H 2010 A perpendicular-anisotropy CoFeB–MgO magnetic tunnel junction *Nat. Mater.* **9** 721

[262] Crum D M, Bouhassoune M, Bouaziz J, Schweflinghaus B, Blugel S and Lounis S 2015 Perpendicular reading of single confined magnetic skyrmions *Nat. Commun.* **6** 8541

[263] Loreto R P, Moura-Melo W A, Pereira A R, Zhang X, Zhou Y, Ezawa M and de Araujo C I L 2018 Creation, transport and detection of imprinted magnetic solitons stabilized by spin-polarized current *J. Magn. Magn. Mater.* **455** 25

[264] Zhang X *et al* 2018 Skyrmions in magnetic tunnel junctions *ACS Appl. Mater. Interfaces* **10** 16887

[265] Penthorn N E, Hao X, Wang Z, Huai Y and Jiang H W 2019 Experimental observation of single skyrmion signatures in a magnetic tunnel junction *Phys. Rev. Lett.* **122** 257201

[266] Kasai S, Sugimoto S, Nakatani Y, Ishikawa R and Takahashi Y K 2019 Voltage-controlled magnetic skyrmions in magnetic tunnel junctions *Appl. Phys. Express* **12** 083001

[267] Thiele A A 1973 Steady-state motion of magnetic domains *Phys. Rev. Lett.* **30** 230

[268] Zhang X, Zhou Y and Ezawa M 2016 Antiferromagnetic skyrmion: stability, creation and manipulation *Sci. Rep.* **6** 24795

[269] Hirata Y *et al* 2019 Vanishing skyrmion Hall effect at the angular momentum compensation temperature of a ferrimagnet *Nat. Nanotechnol.* **14** 232

[270] Chen G 2017 Skyrmion Hall effect *Nat. Phys.* **13** 112

[271] Parkin S and Yang S H 2015 Memory on the racetrack *Nat. Nanotechnol.* **10** 195

[272] Tomasello R, Martinez E, Zivieri R, Torres L, Carpentieri M and Finocchio G 2014 A strategy for the design of skyrmion racetrack memories *Sci. Rep.* **4** 6784

[273] Yu G *et al* 2017 Room-temperature skyrmion shift device for memory application *Nano Lett.* **17** 261

[274] Zhang X, Zhao G P, Fangohr H, Liu J P, Xia W X, Xia J and Morvan F J 2015 Skyrmion-skyrmion and skyrmion-edge repulsions on the skyrmion-based racetrack memory *Sci. Rep.* **5** 7643

[275] Lin S-Z, Reichhardt C, Batista C D and Saxena A 2013 Particle model for skyrmions in metallic chiral magnets: dynamics, pinning, and creep *Phys. Rev.* B **87** 214419

[276] Zhang X, Zhou Y and Ezawa M 2016 Magnetic bilayer-skyrmions without skyrmion Hall effect *Nat. Commun.* **7** 10293

[277] Tomasello R, Puliafito V, Martinez E, Manchon A, Ricci M, Carpentieri M and Finocchio G 2017 Performance of synthetic antiferromagnetic racetrack memory: domain wall versus skyrmion *J. Phys. D: Appl. Phys.* **50** 325302

[278] Kang W, Zheng C, Huang Y, Zhang X, Zhou Y, Lv W and Zhao W 2016 Complementary skyrmion racetrack memory with voltage manipulation *IEEE Electron Device Lett.* **37** 924

[279] Xia J, Huang Y, Zhang X, Kang W, Zheng C, Liu X, Zhao W and Zhou Y 2017 A microwave field-driven transistor-like skyrmionic device with the microwave current-assisted skyrmion creation *J. Appl. Phys.* **122** 153901

[280] Zhao X, Ren R, Xie G and Liu Y 2018 Single antiferromagnetic skyrmion transistor based on strain manipulation *Appl. Phys. Lett.* **112** 252402

[281] Zhang S, Baker A A, Komineas S and Hesjedal T 2015 Topological computation based on direct magnetic logic communication *Sci. Rep.* **5** 15773

[282] Xing X, Pong P W T and Zhou Y 2016 Skyrmion domain wall collision and domain wall-gated skyrmion logic *Phys. Rev.* B **94** 054408

[283] Luo S, Song M, Li X, Zhang Y, Hong J, Yang X, Zou X, Xu N and You L 2018 Reconfigurable skyrmion logic gates *Nano Lett.* **18** 1180

[284] Chen M, Sengupta A and Roy K 2018 Magnetic skyrmion as a spintronic deep learning spiking neuron processor *IEEE Trans. Magn.* **54** 1

[285] Göbel B, Mook A, Henk J and Mertig I 2017 Antiferromagnetic skyrmion crystals: Generation, topological Hall, and topological spin Hall effect *Phys. Rev.* B **96** 060406

[286] Buhl P M, Freimuth F, Blügel S and Mokrousov Y 2017 Topological spin Hall effect in antiferromagnetic skyrmions *Phys. Status Solidi* **11** 1700007

[287] He Q L *et al* 2018 Exchange-biasing topological charges by antiferromagnetism *Nat. Commun.* **9** 2767

[288] Jungwirth T, Marti X, Wadley P and Wunderlich J 2016 Antiferromagnetic spintronics *Nat. Nanotechnol.* **11** 231

[289] Baltz V, Manchon A, Tsoi M, Moriyama T, Ono T and Tserkovnyak Y 2018 Antiferromagnetic spintronics *Rev. Mod. Phys.* **90** 015005

[290] Shen L, Xia J, Zhao G, Zhang X, Ezawa M, Tretiakov O A, Liu X and Zhou Y 2018 Dynamics of the antiferromagnetic skyrmion induced by a magnetic anisotropy gradient *Phys. Rev.* B **98** 134448

[291] Velkov H, Gomonay O, Beens M, Schwiete G, Brataas A, Sinova J and Duine R A 2016 Phenomenology of current-induced skyrmion motion in antiferromagnets *New J. Phys.* **18** 075016

[292] Jin C, Song C, Wang J and Liu Q 2016 Dynamics of antiferromagnetic skyrmion driven by the spin Hall effect *Appl. Phys. Lett.* **109** 182404

[293] Silva R L, Silva R C, Pereira A R and Moura-Melo W A 2019 Antiferromagnetic skyrmions overcoming obstacles in a racetrack *J. Phys.: Condens. Matter* **31** 225802

[294] Sheng Q, Liu X L, Chen W J, Li M Y, Liu L J and Zheng Y 2019 Realization of skyrmion subtracter and diverter in a voltage-gated synthetic antiferromagnetic racetrack *J. Appl. Phys.* **125** 064502

[295] Diep T H 2019 Phase transition in frustrated magnetic thin film—physics at phase boundaries *Entropy* **21** 175

[296] Leonov A O and Mostovoy M 2015 Multiply periodic states and isolated skyrmions in an anisotropic frustrated magnet *Nat. Commun.* **6** 8275

[297] Leonov A O and Mostovoy M 2017 Edge states and skyrmion dynamics in nanostripes of frustrated magnets *Nat. Commun.* **8** 14394

[298] Yuan H Y, Gomonay O and Kläui M 2017 Skyrmions and multisublattice helical states in a frustrated chiral magnet *Phys. Rev.* B **96** 134415

[299] von Malottki S, Dupe B, Bessarab P F, Delin A and Heinze S 2017 Enhanced skyrmion stability due to exchange frustration *Sci. Rep.* **7** 12299

[300] Liang J J, Yu J H, Chen J, Qin M H, Zeng M, Lu X B, Gao X S and Liu J M 2018 Magnetic field gradient driven dynamics of isolated skyrmions and antiskyrmions in frustrated magnets *New J. Phys.* **20** 053037

[301] Lin S-Z and Hayami S 2016 Ginzburg–Landau theory for skyrmions in inversion-symmetric magnets with competing interactions *Phys. Rev.* B **93** 064430

[302] Zhang X, Xia J, Zhou Y, Liu X, Zhang H and Ezawa M 2017 Skyrmion dynamics in a frustrated ferromagnetic film and current-induced helicity locking-unlocking transition *Nat. Commun.* **8** 1717

[303] Xia J, Zhang X, Ezawa M, Hou Z, Wang W, Liu X and Zhou Y 2019 Current-driven dynamics of frustrated skyrmions in a synthetic antiferromagnetic bilayer *Phys. Rev. Appl.* **11** 044046

[304] Kurumaji T, Nakajima T, Hirschberger M, Kikkawa A, Yamasaki Y, Sagayama H, Nakao H, Taguchi Y, Arima T-H and Tokura Y 2019 Skyrmion lattice with a giant topological Hall effect in a frustrated triangular-lattice magnet *Science* **365** 914

[305] Gong C *et al* 2017 Discovery of intrinsic ferromagnetism in two-dimensional van der Waals crystals *Nature* **546** 265

[306] Huang B *et al* 2017 Layer-dependent ferromagnetism in a van der Waals crystal down to the monolayer limit *Nature* **546** 270

[307] Mermin N D and Wagner H 1966 Absence of ferromagnetism or antiferromagnetism in one- or two-dimensional isotropic Heisenberg models *Phys. Rev. Lett.* **17** 1133

[308] Song T *et al* 2018 Giant tunneling magnetoresistance in spin-filter van der Waals heterostructures *Science* **360** 1214

[309] Deng Y *et al* 2018 Gate-tunable room-temperature ferromagnetism in two-dimensional $Fe_3GeTe_2$ *Nature* **563** 94

[310] Wang X *et al* 2019 Current-driven magnetization switching in a van der Waals ferromagnet $Fe_3GeTe_2$ (arXiv:1902.05794)

[311] Alghamdi M, Lohmann M, Li J, Jothi P R, Shao Q, Aldosary M, Su T, Fokwa B P T and Shi J 2019 Highly efficient spin–orbit torque and switching of layered ferromagnet $Fe_3GeTe_2$ *Nano Lett.* **19** 4400

[312] Tong Q, Liu F, Xiao J and Yao W 2018 Skyrmions in the Moiré of van der Waals 2D magnets *Nano Lett.* **18** 7194

[313] Li Q *et al* 2018 Patterning-induced ferromagnetism of $Fe_3GeTe_2$ van der Waals materials beyond room temperature *Nano Lett.* **18** 5974

[314] Gibertini M, Koperski M, Morpurgo A F and Novoselov K S 2019 Magnetic 2D materials and heterostructures *Nat. Nanotechnol.* **14** 408

[315] Park T-E *et al* 2019 Observation of magnetic skyrmion crystals in a van der Waals ferromagnet $Fe_3GeTe_2$ (arXiv:1907.01425)

[316] Wang H, Wang C, Zhu Y, Li Z-A, Zhang H, Tian H, Shi Y, Yang H and Li J 2019 Direct observations of chiral spin textures in van der Waals magnet $Fe_3GeTe_2$ nanolayers (arXiv:1907.08382)

[317] Wu Y *et al* 2019 Néel-type skyrmion in $WTe_2/Fe_3GeTe_2$ van der Waals heterostructure (arXiv:1907.11349)

[318] Han M-G, Garlow J A, Liu Y, Zhang H, Li J, DiMarzio D, Knight M, Petrovic C, Jariwala D and Zhu Y 2019 Topological magnetic-spin textures in two-dimensional van der Waals $Cr_2Ge_2Te_6$ (arXiv:1907.05983)

[319] Zhang S, Petford-Long A K and Phatak C 2016 Creation of artificial skyrmions and antiskyrmions by anisotropy engineering *Sci. Rep.* **6** 31248

[320] Ritzmann U, von Malottki S, Kim J-V, Heinze S, Sinova J and Dupé B 2018 Trochoidal motion and pair generation in skyrmion and antiskyrmion dynamics under spin–orbit torques *Nat. Electron.* **1** 451

[321] Camosi L, Rougemaille N, Fruchart O, Vogel J and Rohart S 2018 Micromagnetics of antiskyrmions in ultrathin films *Phys. Rev.* B **97** 134404

[322] Raeliarijaona A, Nepal R and Kovalev A A 2018 Boundary twists, instabilities, and creation of skyrmions and antiskyrmions *Phys. Rev. Mater.* **2** 124401

[323] Zhang S, Kronast F, van der Laan G and Hesjedal T 2018 Real-space observation of skyrmionium in a ferromagnet-magnetic topological insulator heterostructure *Nano Lett.* **18** 1057

[324] Woo S 2018 Skyrmions learn some new moves *Nat. Electron.* **1** 434

[325] Zhang X, Zhou Y and Ezawa M 2016 High-topological-number magnetic skyrmions and topologically protected dissipative structure *Phys. Rev.* B **93** 024415

[326] Peng L *et al* 2017 Generation of high-density biskyrmions by electric current *npj Quantum Mater.* **2** 30

[327] Peng L *et al* 2017 Real-space observation of nonvolatile zero-field biskyrmion lattice generation in MnNiGa magnet *Nano Lett.* **17** 7075

[328] Wang W *et al* 2016 Centrosymmetric hexagonal magnet with superstable biskyrmion magnetic nanodomains in a wide temperature range of 100–340 K *Adv. Mater.* **28** 6887

[329] Peng L, Zhang Y, He M, Ding B, Wang W, Li J, Cai J, Wang S, Wu G and Shen B 2018 Multiple tuning of magnetic biskyrmions using *in situ* L-TEM in centrosymmetric MnNiGa alloy *J. Phys.: Condens. Matter* **30** 065803

[330] Yu X Z, Tokunaga Y, Kaneko Y, Zhang W Z, Kimoto K, Matsui Y, Taguchi Y and Tokura Y 2014 Biskyrmion states and their current-driven motion in a layered manganite *Nat. Commun.* **5** 3198

[331] Loudon J C *et al* 2019 Do images of biskyrmions show type-II bubbles? *Adv. Mater.* **31** e1806598

[332] Kharkov Y A, Sushkov O P and Mostovoy M 2017 Bound states of skyrmions and merons near the lifshitz point *Phys. Rev. Lett.* **119** 207201

[333] Tan A, Li J, Scholl A, Arenholz E, Young A T, Li Q, Hwang C and Qiu Z Q 2016 Topology of spin meron pairs in coupled Ni/Fe/Co/Cu(0 0 1) disks *Phys. Rev.* B **94** 014433

[334] Leonov A O and Kézsmárki I 2017 Asymmetric isolated skyrmions in polar magnets with easy-plane anisotropy *Phys. Rev.* B **96** 014423

[335] Murooka R, Leonov A O, Inoue K and Ohe J-I 2018 Current-induced shuttlecock-like movement of non-axisymmetric chiral skyrmions (arXiv:1812.02939)

[336] De Alfaro V, Fubini S and Furlan G 1976 A new classical solution of the Yang–Mills field equations *Phys. Lett.* B **65** 163

[337] Ezawa Z F and Tsitsishvili G 2011 Skyrmion and bimeron excitations in imbalanced bilayer quantum Hall systems *AIP Conf. Proc.* **1399** 605

[338] Ezawa Z F and Tsitsishvili G 2010 Skyrmion and bimeron excitations in bilayer quantum Hall systems *Physica* E **42** 1069

[339] Göbel B, Mook A, Henk J, Mertig I and Tretiakov O A 2019 Magnetic bimerons as skyrmion analogues in in-plane magnets *Phys. Rev.* B **99** 060407

[340] Gallagher T J and Humphrey F B 1977 Bubble-collapse and stripe-chop mechanism in magnetic bubble garnet materials *Appl. Phys. Lett.* **31** 235

[341] Yu X Z, Koshibae W, Tokunaga Y, Shibata K, Taguchi Y, Nagaosa N and Tokura Y 2018 Transformation between meron and skyrmion topological spin textures in a chiral magnet *Nature* **564** 95

[342] Woo S 2018 Elusive spin textures discovered *Nature* **564** 43

[343] Garst M, Waizner J and Grundler D 2017 Collective spin excitations of helices and magnetic skyrmions: review and perspectives of magnonics in non-centrosymmetric magnets *J. Phys. D: Appl. Phys.* **50** 293002

[344] Wang J 2019 Mechanical control of magnetic order: from phase transition to skyrmions *Annu. Rev. Mater. Res.* **49** 361

[345] Kovalev A A and Sandhoefner S 2018 Skyrmions and antiskyrmions in quasi-two-dimensional magnets *Frontiers Phys.* **6** 98